Mechanics of Late Stellar Evolution

Chris Sneden

University of Texas

Definitions, Assumptions

$$[A/B] \equiv \log_{10}(N_A/N_B)_* - \log_{10}(N_A/N_B)_\odot$$

$$\log \varepsilon(A) \equiv \log N(A) \equiv \log_{10}(N_A/N_H) + 12$$

The Abundances are perfect!

(that is, details can be discussed informally)

But typically:

(A) Data are high Res, high S/N spectra

$R \equiv \frac{\lambda}{\Delta\lambda} \sim 30K \rightarrow 60K$ $\quad S/N \gtrsim 100$

(B) Full model atmosphere analysis

(C) Spectrum syntheses

(D) Now often pure lab data

Abundance Changes due to First Dredge-Up

(A) Standard Predictions (Iben + Renzini 1983, ARAA)

surface ^{12}C ↓ 30%

^{14}N ↑ 2×

$^{12}C/^{13}C$ goes from ~90 to ~25

Li ↓ 20×

^{16}O → steady

(B) These Changes arise from mixing of H-burning products to surface

(C) The problem of Lithium

- standard predictions
- main sequence ⋆'s have no "normal" Li, except an upper limit of
  $\log N \equiv \log \varepsilon \simeq 3.0$
  for Pop I stars!
- Pop I giants reflect this scatter
- Pop II ms ⋆'s have more uniform Li
  ⇒ Pop II giants may have a cleaner story
- An extra mixing episode part way up the giant branch can be identified

(D) Evidence from C, N, $^{12}C/^{13}C$:

- Pop I giants conform to predictions
- "old disk" giants (mildly metal-poor, high velocity) show significant differences:
  1) lower $^{12}C/^{13}C$
  2) less C/N processing
  3) high O
- halo, metal-poor Pop II giants apparently have CN-cycle run amok:
  1) very low C/N
  2) $^{12}C/^{13}C \simeq 4$ to 10

(E) The Nature of the Extra Mixing

- Not the first dredge-up (that happens just as predicted: less surface abundance changes as M, [Fe/H] decrease)
- The luminosity for "sudden" onset of extra mixing can be identified:

$$L_{\text{extra mixing}} \rightleftharpoons M_{\text{LF "Bump"}}$$

Pop II ⋆'s

globular clusters

- Probable explanation: extra mixing induced when H-burn shell eats through μ-barrier left by first dredge-up

c) it can be partially cured by appropriate T_{eff} choice

So angular diameters are vital for "ordinary" red giants

But they are still few, so alternate methods have been devised:

a) Barnes-Evans relation
b) Infrared Flux Method

more angular diameters needed for "early" spectral types (M II-I stars still dominate current measures); see for example

Dyck, van Belle, Thompson 1998
AJ, 116, 981

Now to the first-ascent of giant branch

But Why do stars become giants at all??

Not a settled issue:

"Advances in Stellar Evolution", 1997, ed Rood + Renzini

Iben (1967) → wildly explosive onset of H shell burning?

thermal instabilities in envelope?
mass ratio between core and shell?
opacity changes in shell? envelope?

see Sugimoto + Fujimoto 2000, ApJ 538, 837

(F) Studies of the Episodes of Extra Mixing

1) Charbonnel 1995 ApJ 453, L41
2) Charbonnel et al. 1998, AA 332, 204 — best physical discussion; focus on molecular weight barrier
3) Gratton et al. 2000, AA, 354, 169
4) Charbonnel + Balachandran 2000, AA 359, 563 — meat skewering of claims of Li-rich giants; good study of few confirmed cases

Which gets us to globular cluster chemistry in general

- a super-Li-rich star in M3
- more general look at "halo" clusters
- definition of the "second parameter" problem
- first composition clue: lots of C→N processing, increasing with luminosity in some clusters
- surprising oxygen deficiencies cluster↔cluster; star↔star

The extreme: M13

(1) no evidence for any variations in elements other than those affected by "proton-captures"
(2) (N, Na, Al) anticorrelate with (O, Mg)

(3) The O-Na (anti) correlation is general, but only in globular clusters

(4) CNO is conserved

(5) The nucleosynthesis is "obvious"

O⇔N is accompanied by Ne⇔Na and sometimes Mg⇔AL

(6) The Temperature requirements are awkward

So <u>if</u> these stars are self-poluted then some of the "2nd parameter problem" is solved:

- if [Fe/H] is first parameter then <u>age</u>, <u>He content</u>, <u>mass loss</u> all drive HB's <u>bluer</u>
- but the T is awkward, as is the discovery of C, N, Na variations near ms of 47 Tuc (Briley and co-workers)

A nod at mass loss:

turnoff masses for globular clusters:

$$\simeq 0.8\, M_\odot$$

HB mass limit:

$$\simeq 0.55\, M_\odot \; ?$$

$\Rightarrow$ somehow $\sim 0.3\, M_\odot$ disappears on RGB

do see "outer atmosphere" signatures

H_α, Na D, Mg II

at a) RGB tip ; b) AGB

But this is totally inferential right now

AGB nucleosynthesis in brief

- We observe: cool luminous M, MS, S, SC, C ★'s
- these objects often are enriched in the products of n-capture nucleosynthesis, definitely of the s-process kind:

$$_{Z}^{A}El + n \rightarrow {}_{Z}^{A+1}El \rightarrow {}_{Z+1}^{A+1}El + \beta^-$$

β decay timescales < n-capture rates

He shells are unstable; thermal pulsing of shells

$3\alpha \rightarrow C^{12}$ and $C^{12}(\alpha,\gamma)O^{16}$

which material, if it is mixed with H-rich stuff, goes to N^{14} via CNO cycling

then during the next pulse, we can have

$N^{14}(\alpha,\gamma)F^{18}(\beta^+\nu)O^{18}(\alpha,\gamma)Ne^{22}$

which (Finally) can create neutrons via

$Ne^{22}(\alpha,n)Mg^{25}$

But alternately, if one can avoid complete CN cycling, then $C^{13}(\alpha,n)O^{16}$ is equally efficient

- The Ne^{22} source is ineffective in low-mass AGB ⋆'s
- The C^{13} source gives larger # of n's per target nucleus ⇒ can give heavier n-capture elements, which is observed
- There must be mixing (convective) cross-talk between shells if this nucleosynthesis is to work at all

An example: Fluorine production in AGB ⋆'s

OBservations: Jorissen, Smith, Lambert 1992, AA, 261, 164

Interpretation: Lattanzio et al. 1997, in "Advances in Stellar Evolution"

Everything must work together....

Further discussion of heavy element enrichment in AGB ⋆'s:

Busso et al. 1992 ApJ 399, 218

Lambert et al. 1995 ApJ 450, 302

An "old" theoretical late stellar path

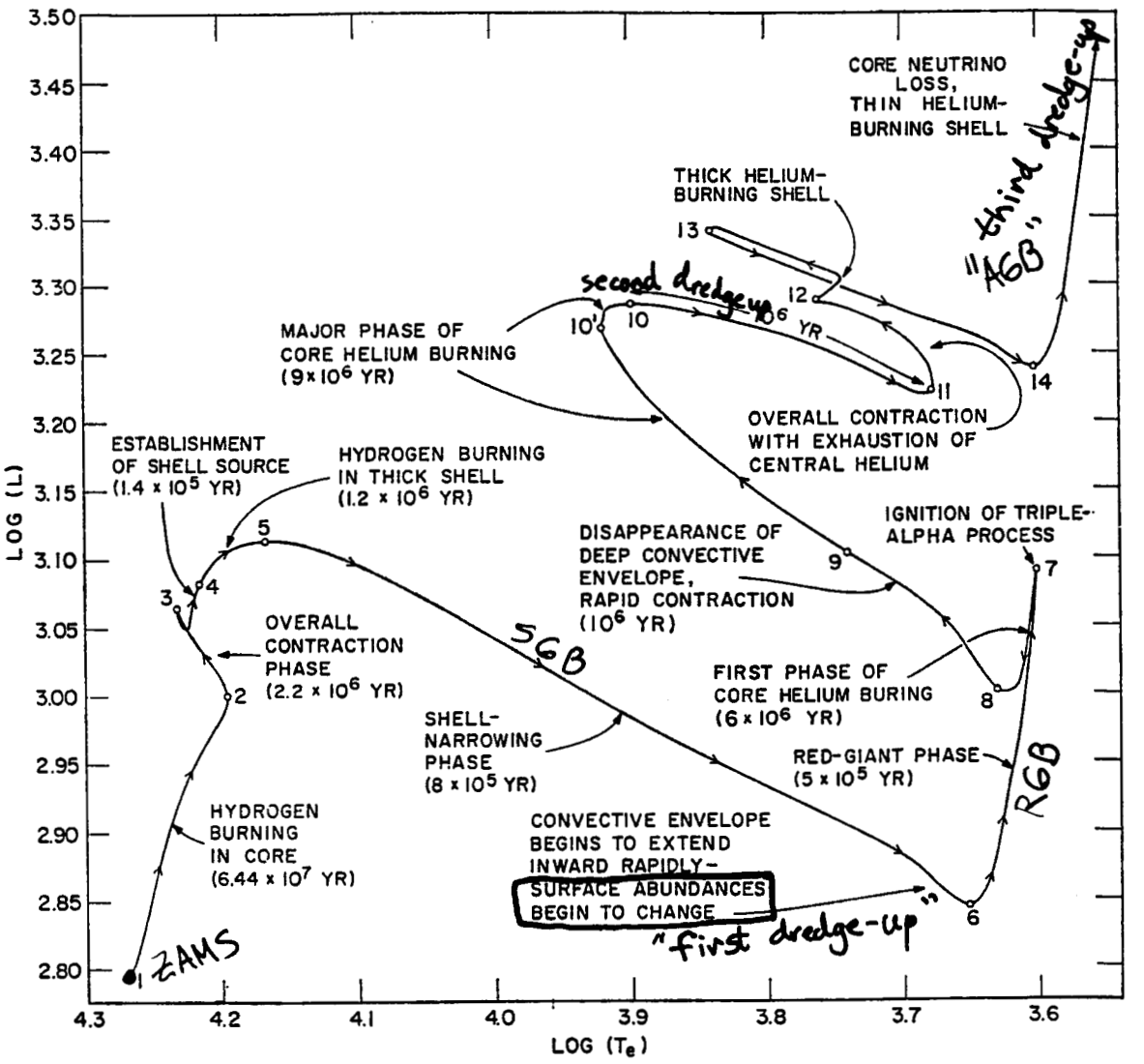

FIG. 1. The path of a metal-rich $5M_\odot$ star in the Hertzsprung-Russell diagram. Luminosity is in solar units, $L_\odot = 3.86 \times 10^{33}$ erg/sec, and surface temperature T_e is in deg K. Traversal times between labeled points are given in years.

Iben 1967 ARAA

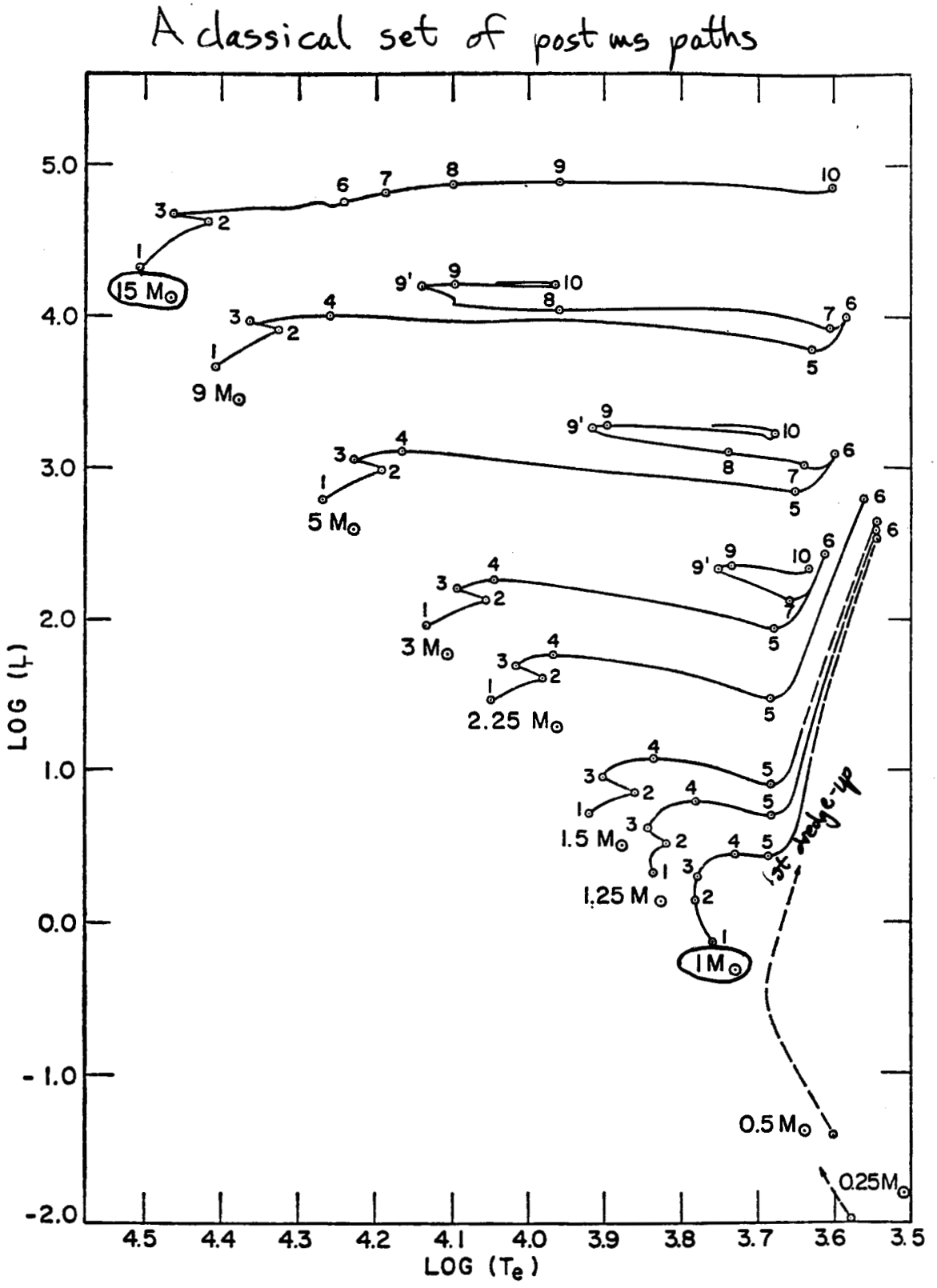

FIG. 3. Paths in the H-R diagram for metal-rich stars of mass $(M/M_\odot) = 15$, 9, 5, 3, 2.25, 1.5, 1.25, 1, 0.5, 0.25. Units of luminosity and surface temperature are the same as in Figure 1. Traversal times between labeled points are given in Tables III and IV. Dashed portions of evolutionary paths are estimates.

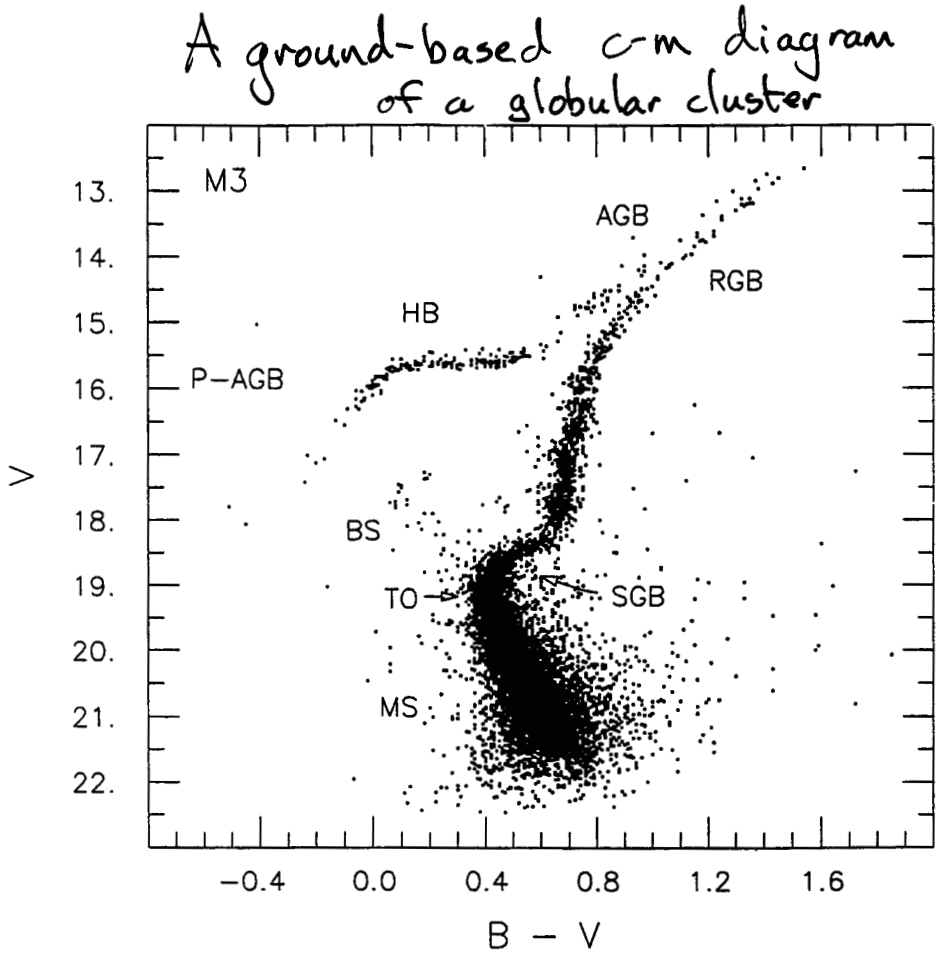

Figure 1 The CMD of the cluster M3 (Buonanno et al. 1986a, 1987). In this diagram, 10,637 stars are plotted, 9879 from a sample that is complete down to $V = 21.5$ and totals $\sim 30{,}000\ L_\odot$ of cluster light, while the remaining 758 stars are drawn from a sample that is complete down to $V = 18$ and totals $\sim 50{,}000\ L_\odot$ of cluster light. The stars brighter than $V = 18$ therefore belong to a sample totaling $\sim 80{,}000\ L_\odot$ of cluster light ($\sim 30\%$ of the total luminosity of M3). More information on this diagram can be found in Table 2. The following classification has been adopted for the various evolutionary stages: 1. main sequence (MS)—core hydrogen-burning phase; 2. blue stragglers (BS); 3. subgiant branch (SGB)—shell hydrogen-burning phase, from the MS turnoff (TO) to the Hayashi line; 4. red giant branch (RGB)—shell hydrogen-burning phase along the Hayashi line, until helium ignition in the core; 5. horizontal branch (HB)—core helium-burning phase; 6. asymptotic giant branch (AGB)—shell hydrogen- and helium-burning phase; 7. post-AGB (P-AGB)—final evolution from the AGB to the white dwarf (WD) stage.

Oxygen in Halo Field Giants from [O I] Lines

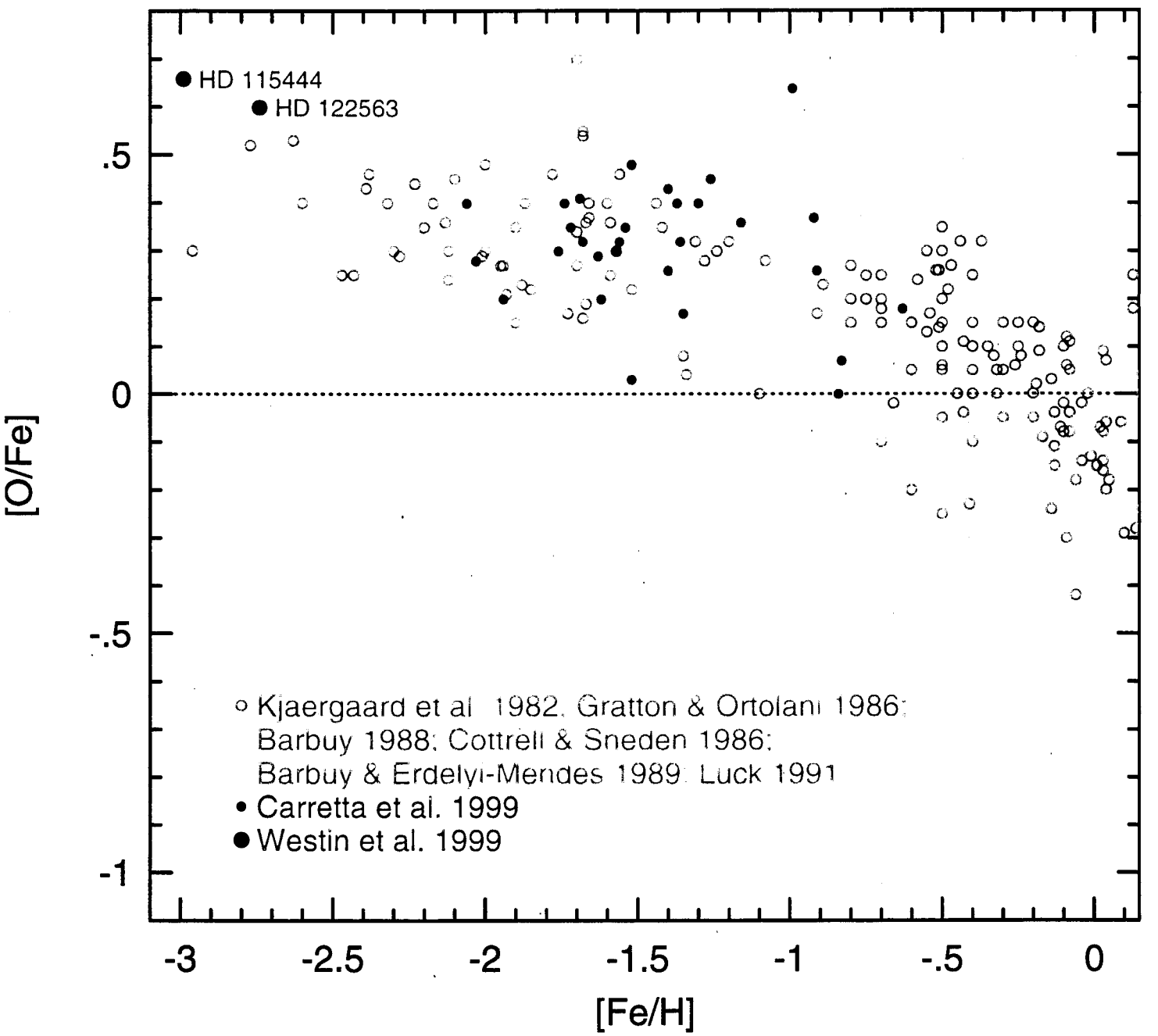

Results from OH_{uv} bands Boesgaard et al 1999

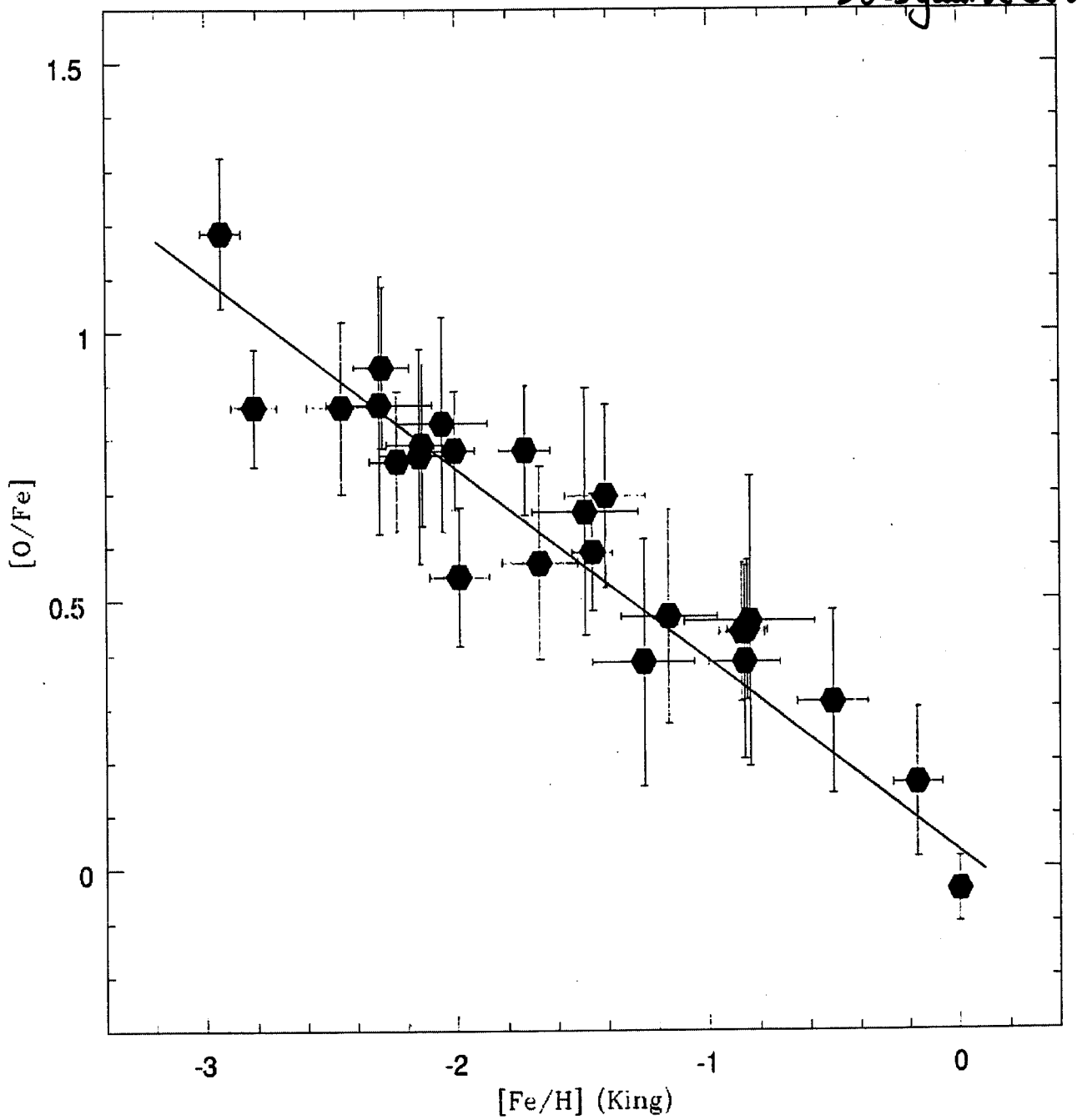

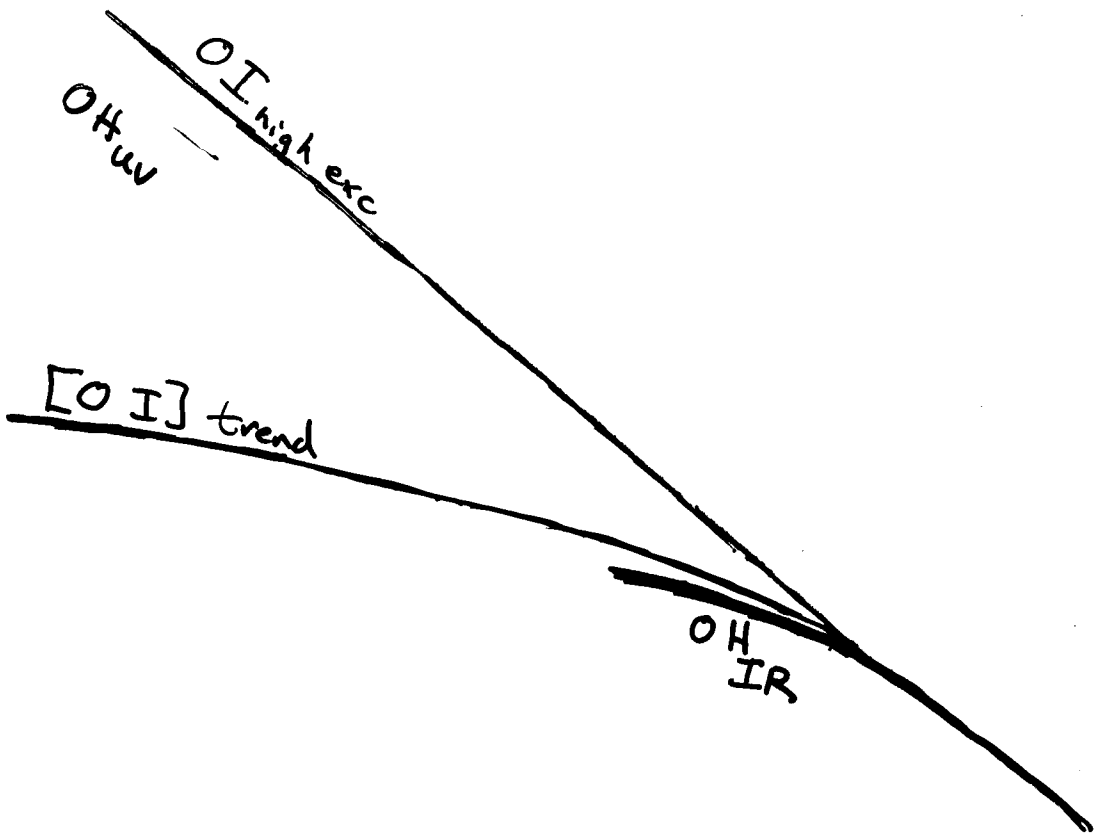
OI high exc
OH uv
[O I] trend
OH IR

Barnes & Evans 1976, MNRAS, 174, 489

"it is easy to derive the equation"

$$\log T_{eff} + 0.1BC = 4.2207 - 0.1V_0 - 0.5\log\phi$$

BC: bolometric correction; V_0: unreddened V; ϕ: angular diameter (milliarcsec)

$4.2207 - 0.1V_0 - 0.5\phi = F_V$

$\phi \equiv \theta$

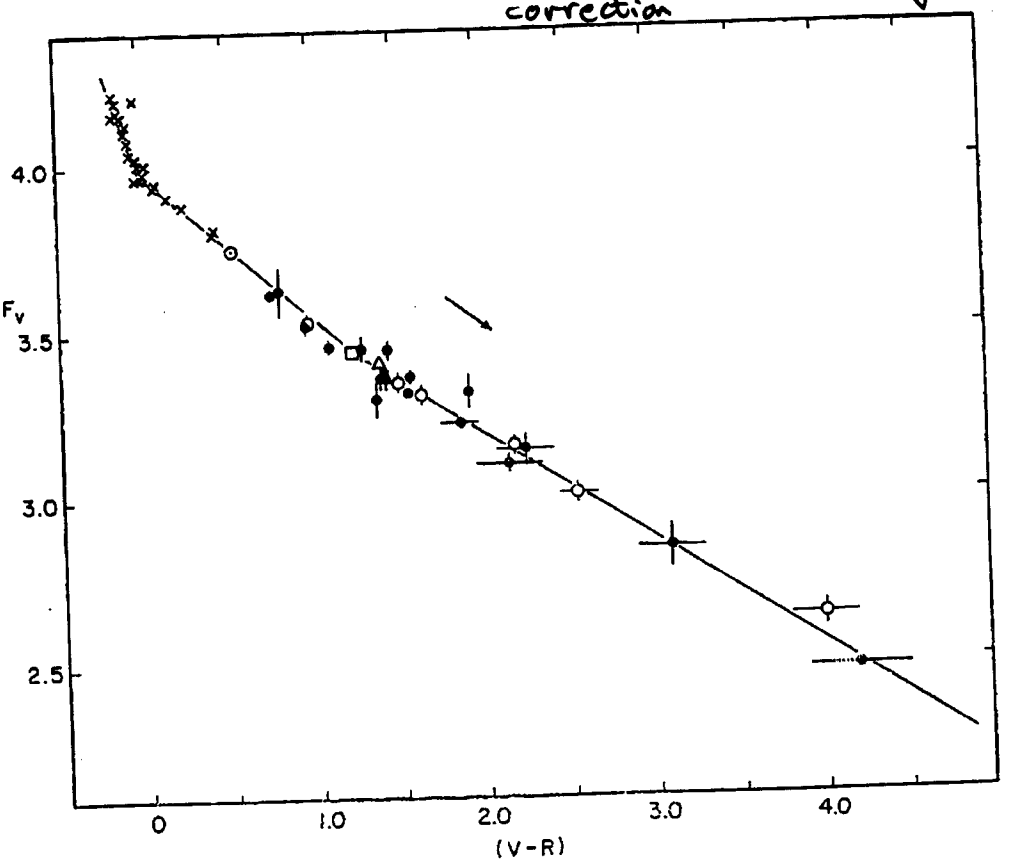

FIG. 2. *The surface brightness parameter F_V as a function of colour index (V–R). Symbols are the same as in Fig. 1.*

empirically, the best color correlation

Blackwell et al. 1979, MNRAS, 188, 847

$$\theta = 2\sqrt{\frac{F_{earth,\lambda}}{F_{surface,\lambda}}}$$

But T_{eff} affects the $\lambda \cong$ "IR" flux very little
(Rayleigh-Jeans tail of BB function)

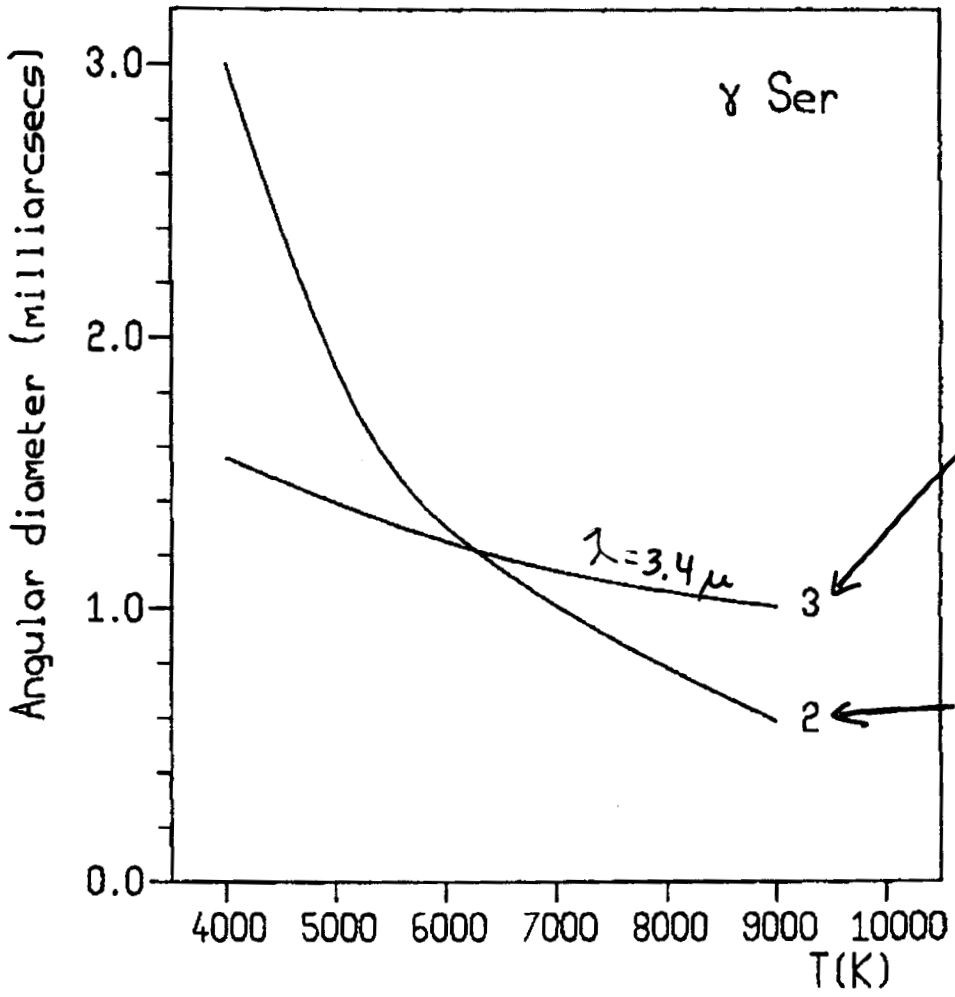

$$F_{earth,\lambda} = \frac{\theta^2}{4} F_{surface,\lambda} = \frac{\theta^2}{4} f(T_{eff}, g, \lambda)$$

$$\mathcal{F}_{Earth} = \int_0^\infty F_{earth,\lambda}\, d\lambda = \frac{\theta^2}{4}\sigma T_{eff}^4$$

1. Formal solution of equations (2) and (3) in text for γ Ser at $\lambda_0 = 3.4\ \mu$m. Curve 2 gives the n between θ and T_e for equation (2) and curve 3 gives this relation for equation (3).

In the purest form, an observed total flux and modeled/observed IR flux can yield θ and T_{eff}

Alonso et al. 1999, A&A Supp 139, 335

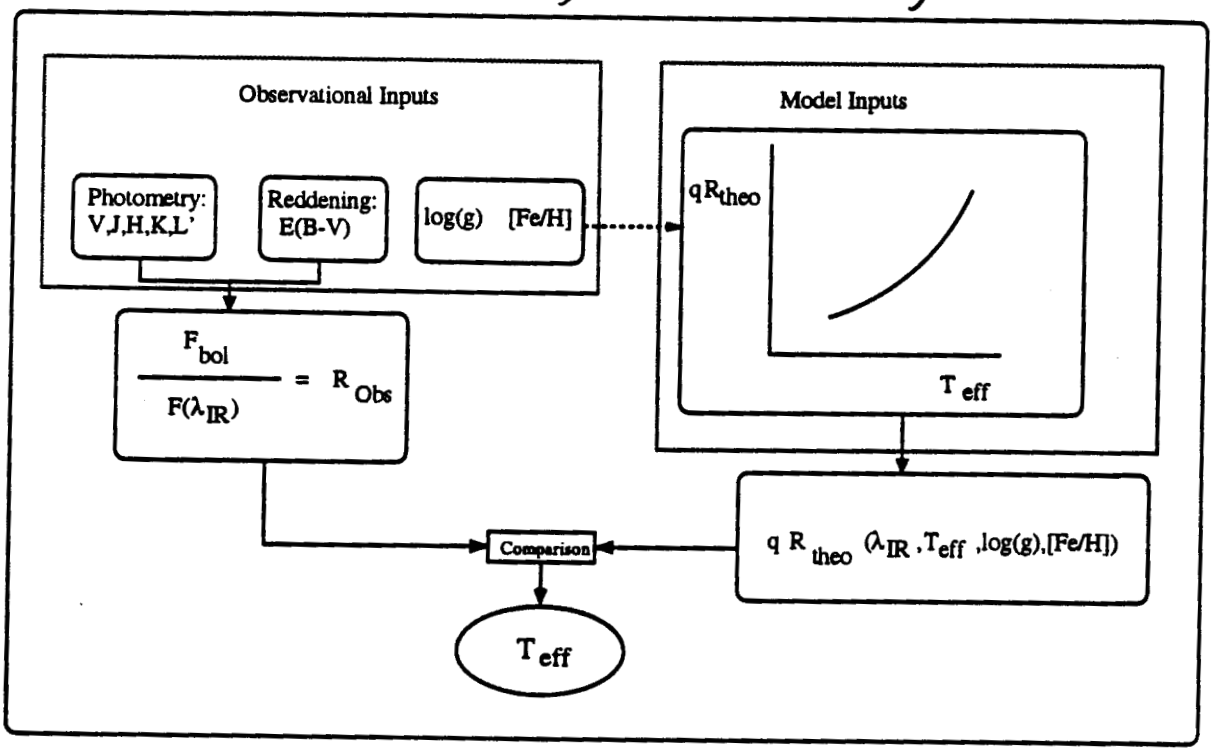

Fig. 1. Outline of the IRFM as implemented in the present work

q is fudge factor that relates real, model stars!

Once [Fe/H] and log(g) are known for a certain star, the observational quantities on the left-hand side of Eq. (3) determine the star's effective temperature by comparing with the theoretical values obtained from models on the right-hand side. An outline of the practical application of the IRFM is shown in Fig. 1.

As expected IRFM T_{eff}s have multi-valued correlations with B-V

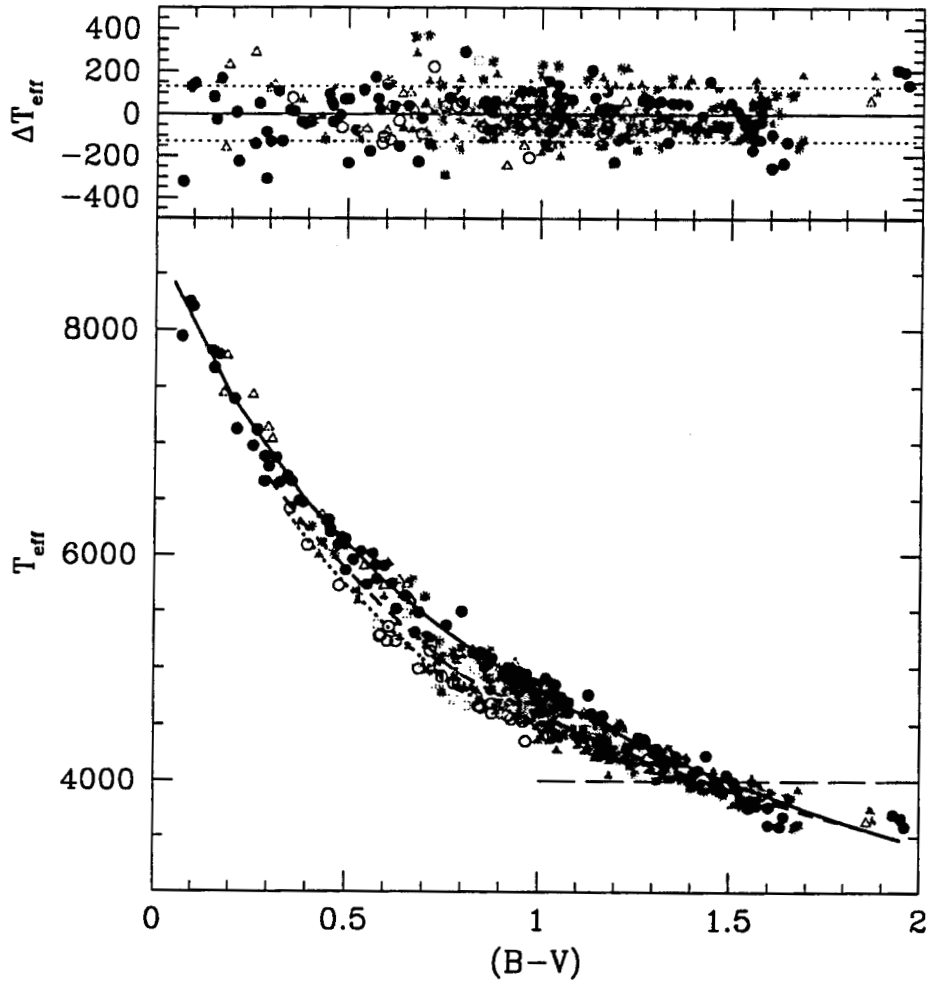

Fig. 2. $T_{\rm eff}$ against $(B-V)$. The lines display the fit corresponding to Eqs. (3) and (4) for [Fe/H] = 0 (solid line), [Fe/H] = −1 (dashed line), [Fe/H] = −2 (dotted line). Symbols stand for the same metallicity groups as in Fig. 1. The horizontal long-dashed line delineates the region $T_{\rm eff} \leq 4000$ K where temperatures derived by means of the IRFM have lower accuracy. The top panel of the figure shows the residuals of the fit

V-K again shown to be
best correlator with T_{eff} from IRFM

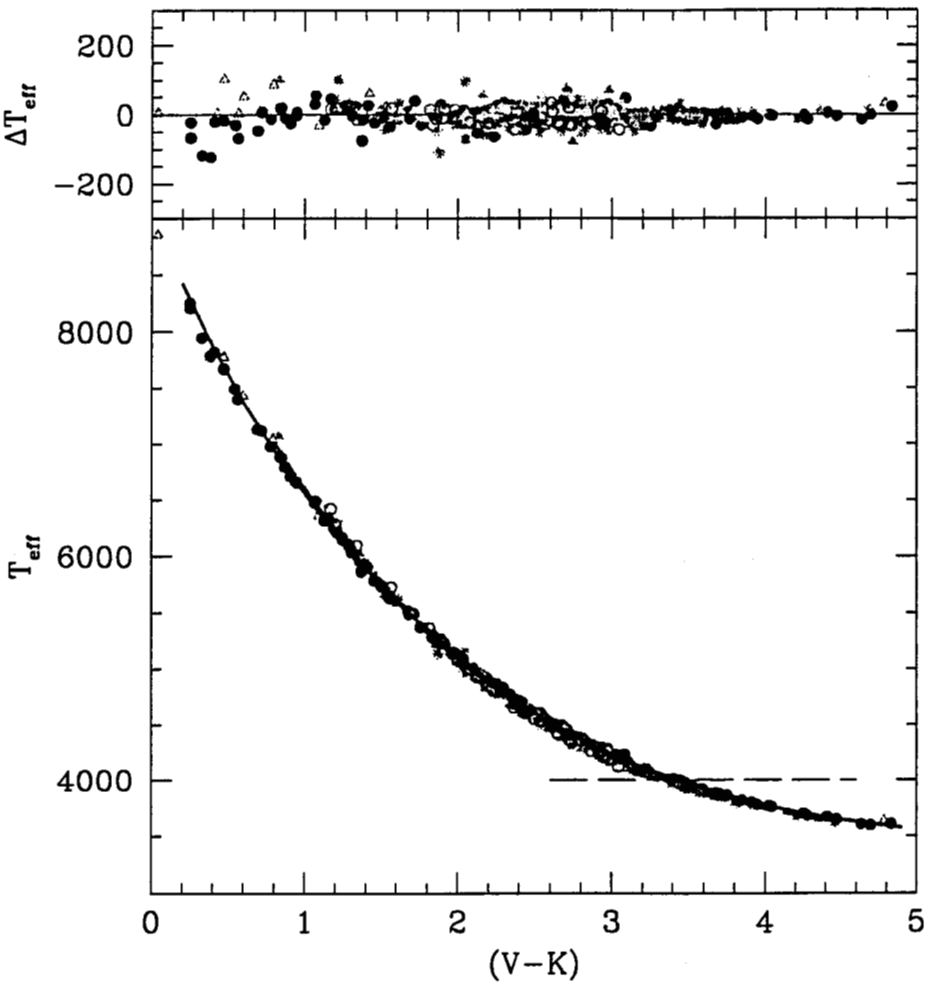

Fig. 8. $T_{\rm eff}$ vs. $(V-K)_{\rm TCS}$. The lines display the fit corresponding to Eqs. (8) and (9). Symbols and lines are the same as for Fig. 2. Recall that $(V-K)_{\rm J} = -0.05 + 1.007(V-K)_{\rm TCS}$

"Acceptable" correlations with measured Θ's

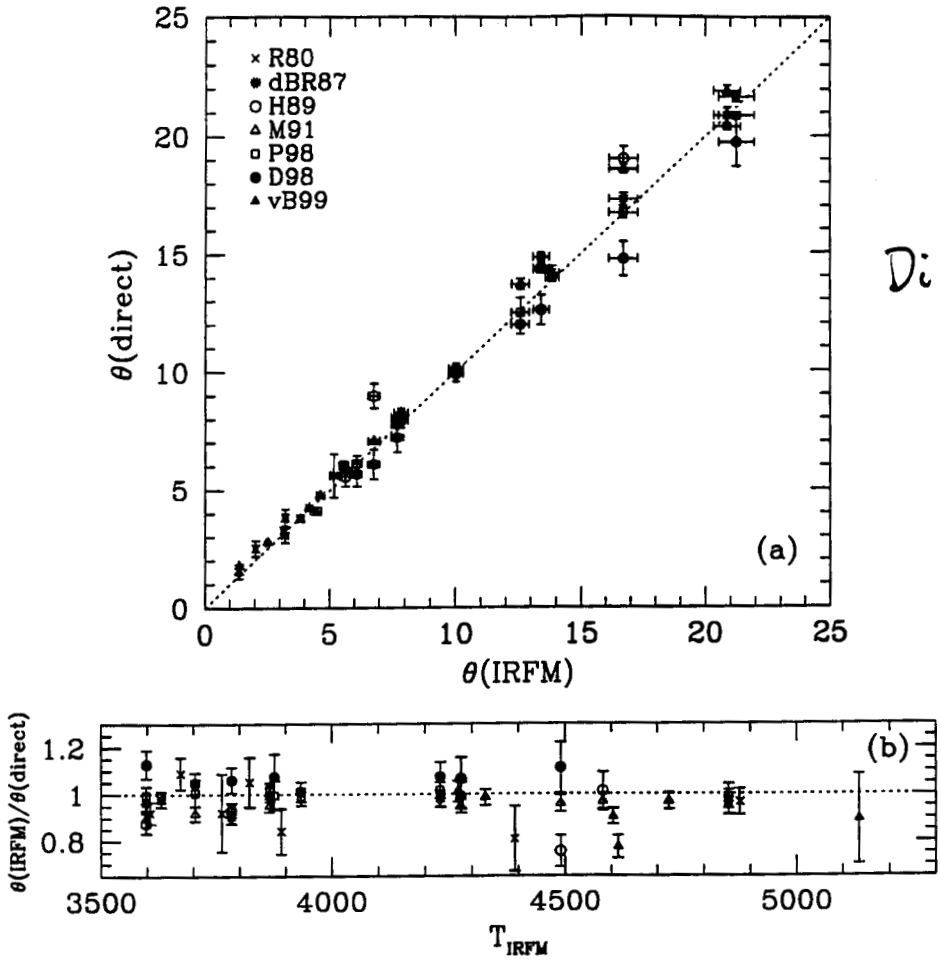

Di Benedetto 1998

Fig. 1. Comparison between angular radii derived by means of the IRFM and those directly measured by lunar occulation or Michelson interferometry. Symbols stand for the following references: R80 Ridgway et al. (1980); dBR87 Di Benedetto and Rabbia (1987); H89 Hutter et al. (1989); D98 Dick et al. (1998); P98 Perrin et al. (1998); vB99 van Belle et al. (1999).

Lithium dilution predictions

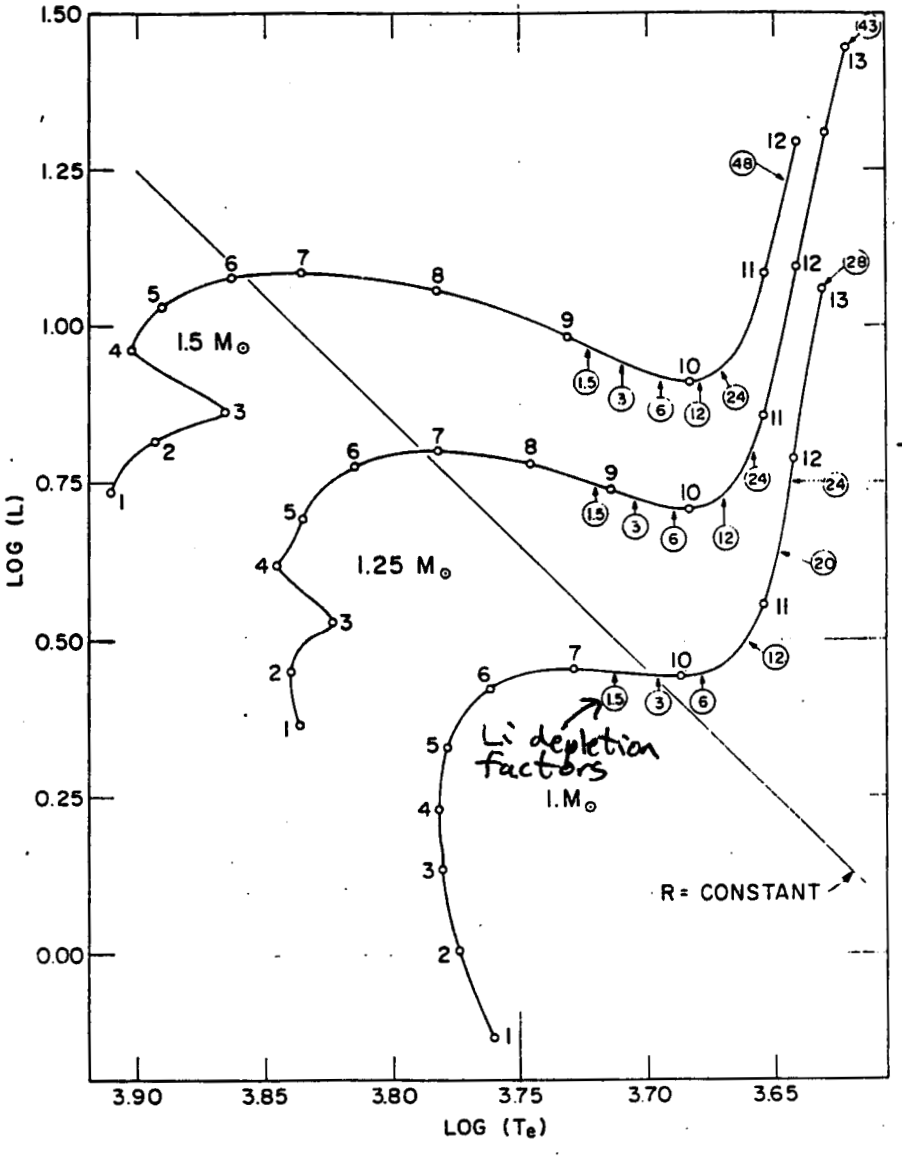

⇒ steady dilution as convective envelope deepens

3. 1.—Evolutionary paths for Population I stars of mass $M/M\odot = 1$, 1.25, and 1.5. Times to labeled points along each track are given in Table 1. Luminosity L is in solar units and surface rature T_e is in degrees Kelvin. Circled numbers represent the factors by which surface Li^7 abun- has been depleted relative to its main sequence value. The straight line is one of constant radius R.

Iben 1967 ARAA

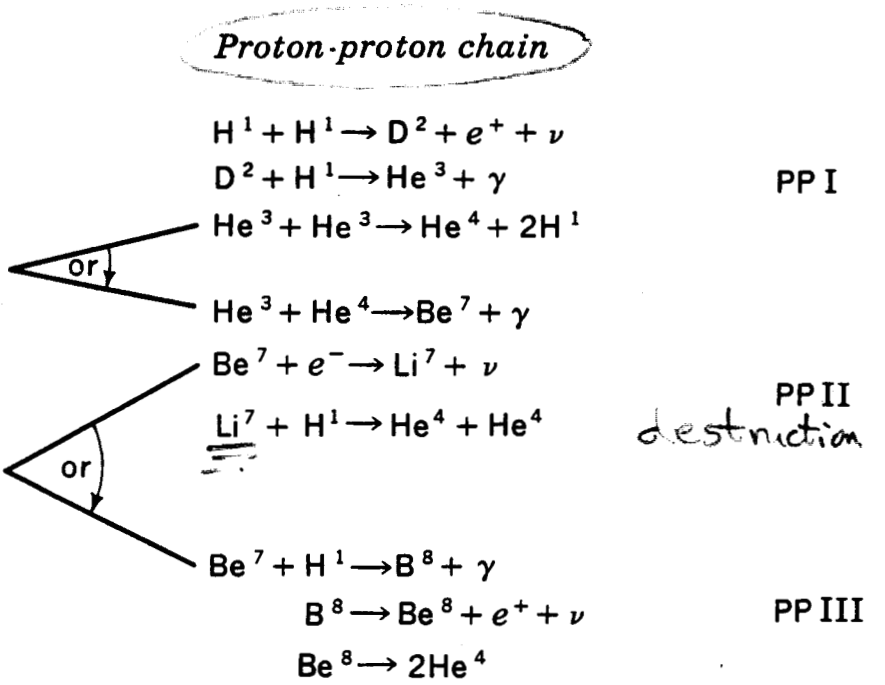

Fig. 5-7 The alternative PP chains. When He^3 is destroyed by the capture of an alpha particle, the chain is completed either through PPII or PPIII, depending upon the fate of the Be^7 nucleus.

Table 5-1 Reactions of the PP chains

Reaction	*Q value, Mev*	*Average ν loss, Mev*	S_0, *kev barns*	$\frac{dS}{dE}$, *barns*	*B*	τ_{12}, *years*†
$H^1(p,\beta^+\nu)D^2$	1.442	0.263	3.78×10^{-22}	4.2×10^{-24}	33.81	7.9×10^9
$D^2(p,\gamma)He^3$	5.493		2.5×10^{-4}	7.9×10^{-6}	37.21	4.4×10^{-8}
$He^3(He^3,2p)He^4$	12.859		5.0×10^3		122.77	2.4×10^5
$He^3(\alpha,\gamma)Be^7$	1.586		4.7×10^{-1}	-2.8×10^{-4}	122.28	9.7×10^5
$Be^7(e^-,\nu)Li^7$	0.861	0.80				3.9×10^{-1}
$Li^7(p,\alpha)He^4$	17.347		1.2×10^2		84.73	1.8×10^{-5}
$Be^7(p,\gamma)B^8$	0.135		4.0×10^{-2}		102.65	6.6×10^1
$B^8(\beta^+\nu)Be^{8*}(\alpha)He^4$	18.074	7.2				3×10^{-8}

† Computed for $X = Y = 0.5$, $\rho = 100$, $T_6 = 15$ (sun).

from Clayton's text

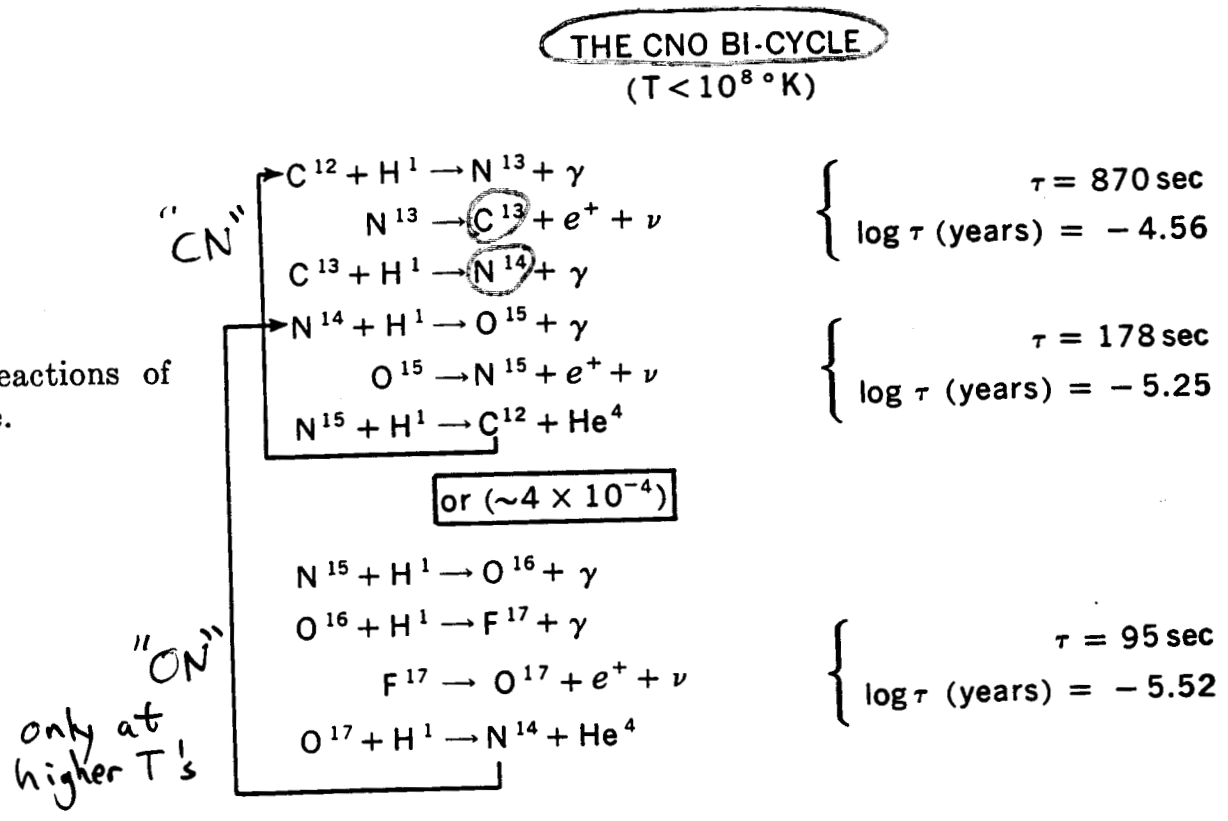

Fig. 5-12 The reactions of the CNO bi-cycle.

Table 5-2 The CNO reactions

Reaction	*Q value, Mev*	*Average ν loss, Mev*	$S(E=0)$, *kev barns*	$\frac{dS}{dE}$, *barns*	B
$C^{12}(p,\gamma)N^{13}$	1.944		1.40	4.26×10^{-3}	136.93
$N^{13}(\beta^+\nu)C^{13}$	2.221	0.710			
$C^{13}(p,\gamma)N^{14}$	7.550		5.50	1.34×10^{-2}	137.20
$N^{14}(p,\gamma)O^{15}$	7.293		2.75		152.31
$O^{15}(\beta^+,\nu)N^{15}$	2.761	1.00			
$N^{15}(p,\alpha)C^{12}$	4.965		5.34×10^{4}	8.22×10^{2}	152.54
$N^{15}(p,\gamma)O^{16}$	12.126		2.74×10^{1}	1.86×10^{-1}	152.54
$O^{16}(p,\gamma)F^{17}$	0.601		1.03×10^{1}	-2.81×10^{-2}	166.96
$F^{17}(\beta^+\nu)O^{17}$	2.762	0.94			
$O^{17}(p,\alpha)N^{14}$	1.193		Resonant reaction		167.15

From Clayton's text

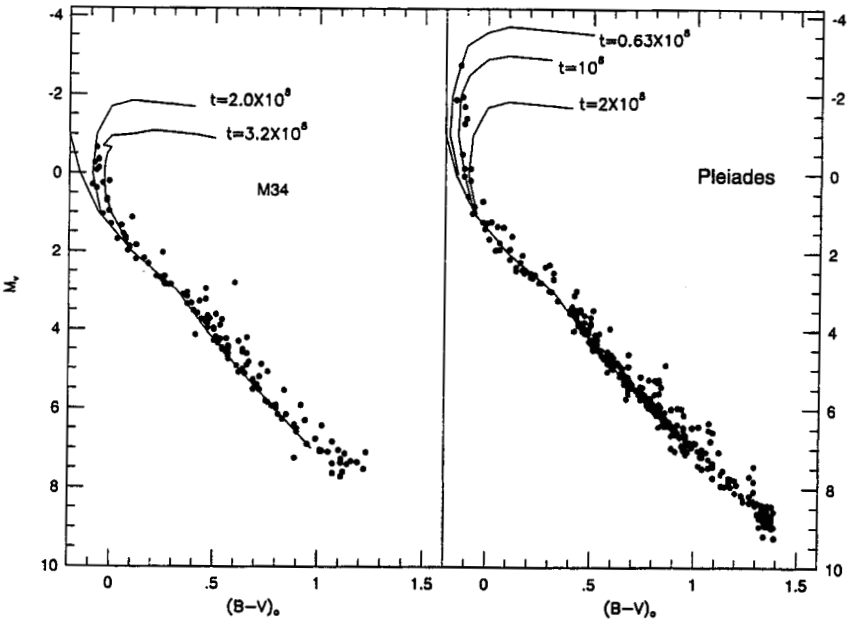

FIG. 2. Color-magnitudes for M34 and the Pleiades. The reddening assumed for M34 is $E_{(B-V)}=0.07$, that for the Pleiades 0.04. The apparent distance modulus assumed for M34 is 8.60, and that for the Pleiades is 5.65. The isochrones are from Meynet *et al.* (1993).

Jones, Fischer, Soderblom
1999 AJ 117, 330

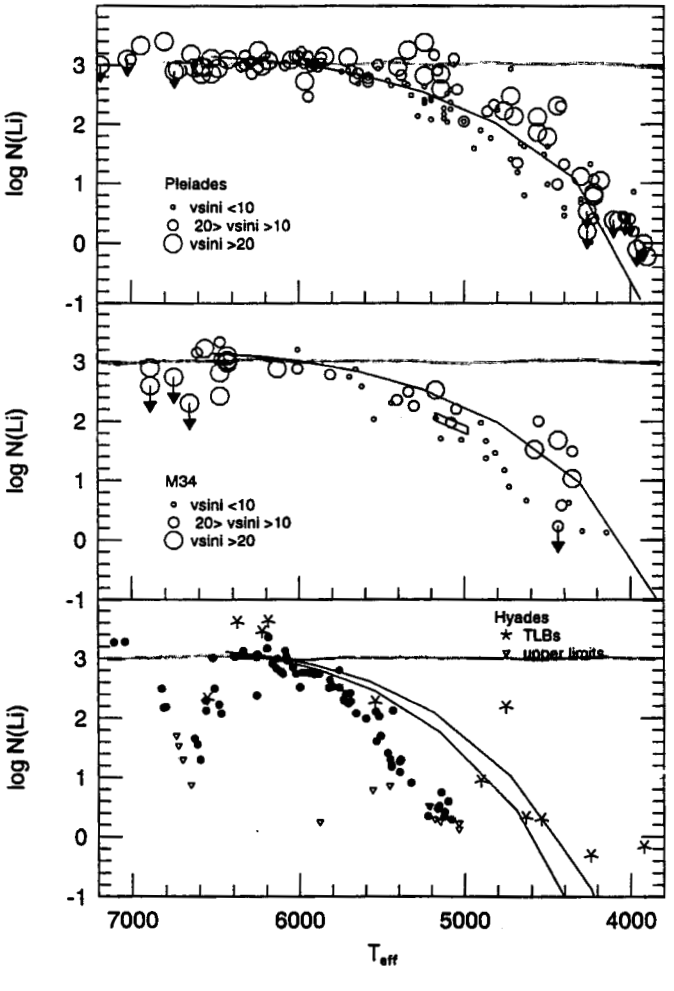

FIG. 3. Plots of Li abundance vs $T_{\rm eff}$ for the Pleiades, M34 and the Hyades. The sources for the data are given in the text. The solid lines are predicted Li depletions for the standard models of Pinsonneault *et al.* (1996) assuming an initial Li abundance of 3.2. For the Pleiades and M34 the models are for solar abundance and ages of 100 Myr and 300 Myr, respectively. For the Hyades the predictions are for an age of 700 Myr and [Fe/H] of +0.10 (top) and +0.15 bottom. The figure for M34 contains a typical error parallogram for an equivalent width error of 10% and a temperature error of ± 100 K.

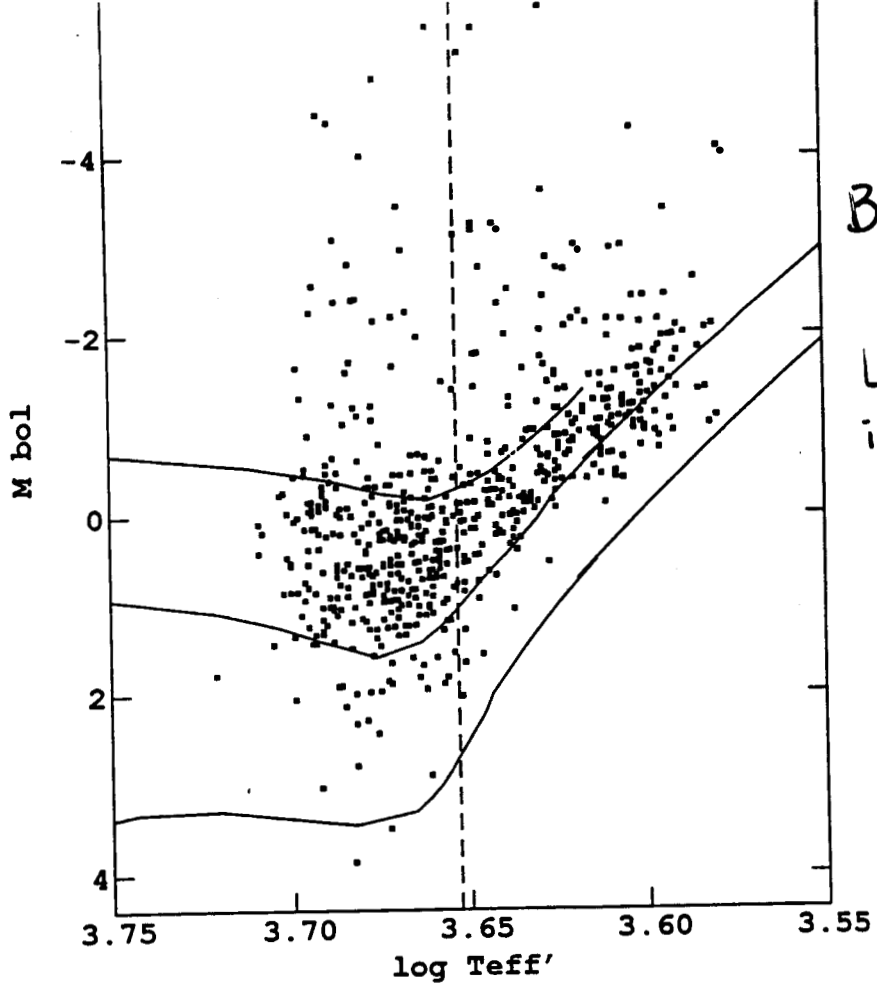

Brown et al. 1989 ApJ 336, 293
Li survey in giants

FIG. 20.—An H-R diagram for all program stars. The abscissa values are log $T_{\rm eff}$ values corrected to a common metallicity as described in the text.

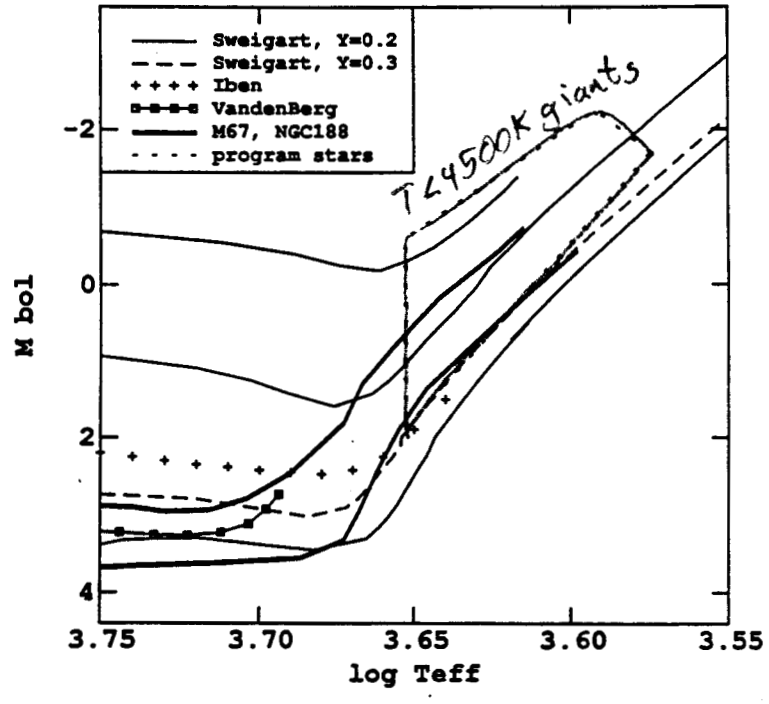

FIG. 21.—Theoretical and empirical curves in the H-R diagram for giant stars. A box indicating the positions of the program stars with $T_{\rm eff} < 4500$ K is shown.

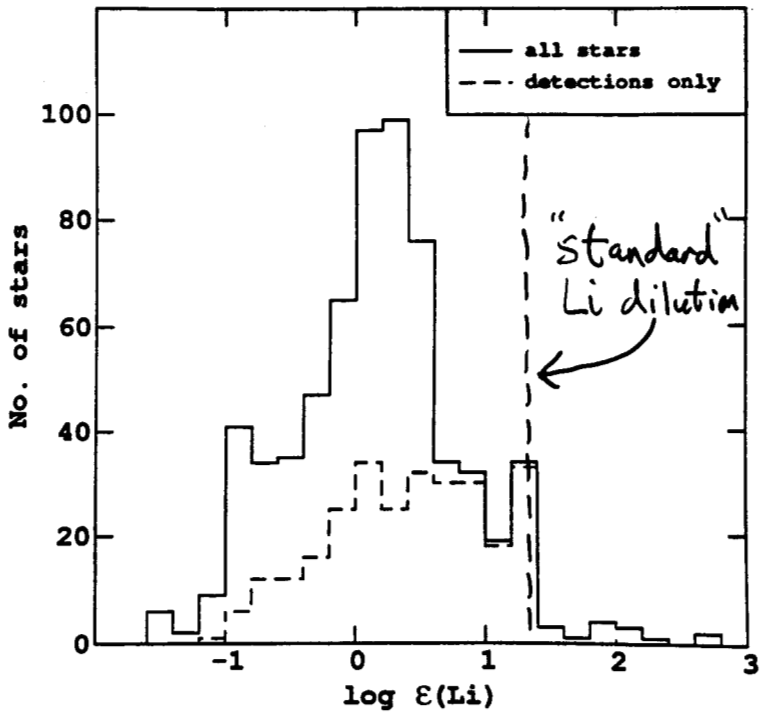

FIG. 13.—Histogram of Li abundances for the program stars. The bin size for the abundance groups is 0.2 dex. The nondetections dominate the statistics below log ε(Li) $\approx +0.5$.

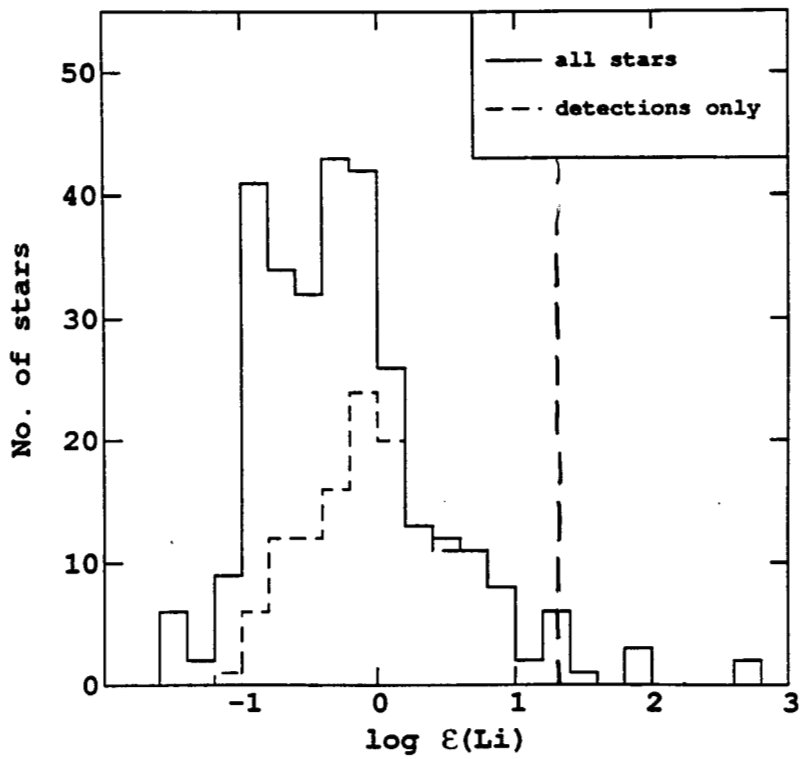

having only stars with $T_{eff} < 4500$ K:
a) avoids He-burn clump
b) makes Li detect easier

FIG. 18.—Histogram of Li abundances for the program stars with $T_{\rm eff} < 4500$ K. The abundance bin size is 0.2 dex. Here the nondetections do not dominate the statistics until log ε(Li) ≈ -0.4.

Variations in Lithium in Unevolved ★s of different Metallicities

Rebolo, Molaro, Beckman 1988, AA, 192, 192

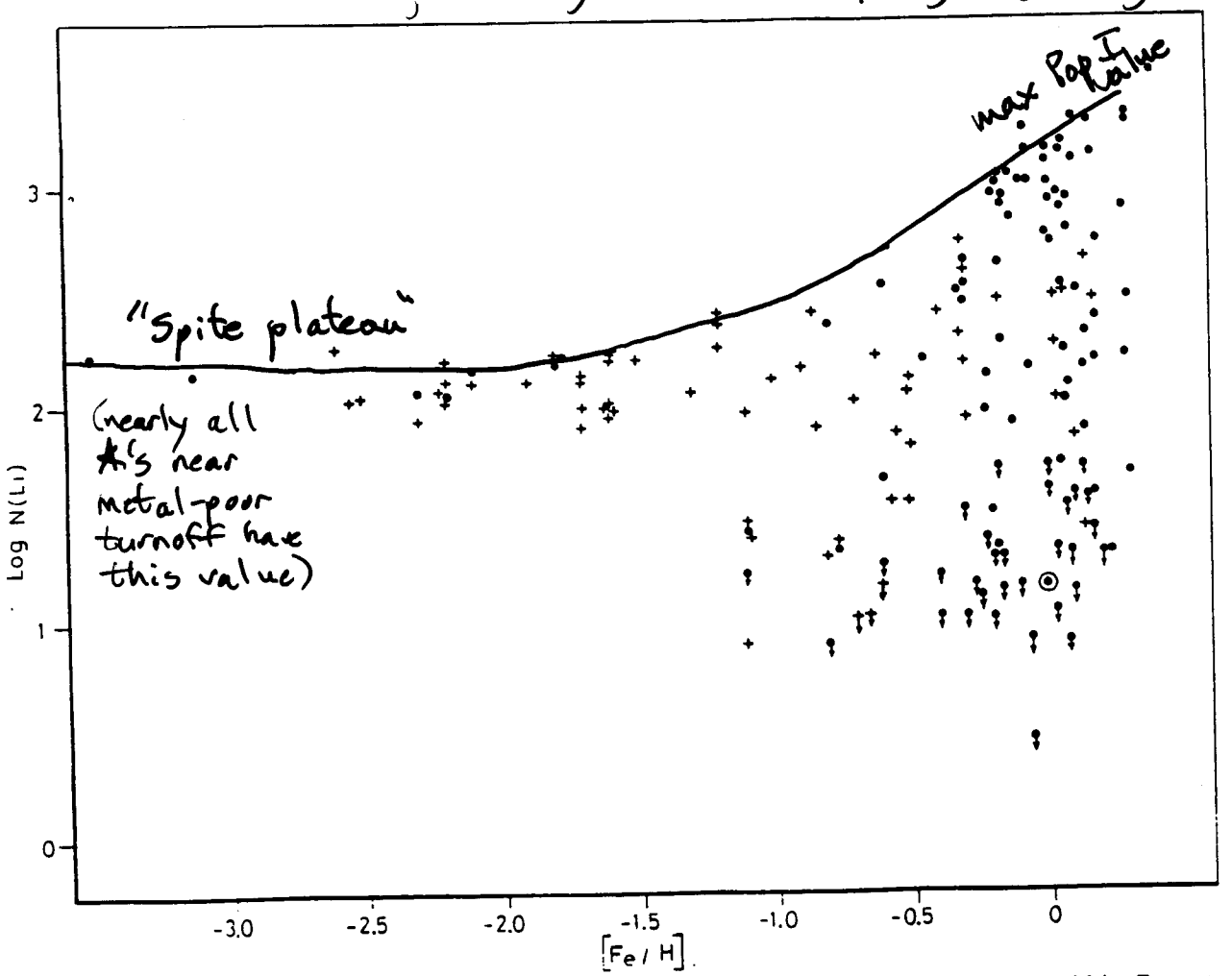

Fig. 3. Lithium abundance against metallicity for stars with $T_{\rm eff} > 5500$ K. Typical error bars for $\log N(\mathrm{Li})$ and [Fe/H] are 0.1 – 0.2 dex. Temperature ranges: • $T_{\rm eff} > 6000$ K: + 6000 K $< T_{\rm eff} <$ 5500 K. Sources of data: Spite and Spite (1982, 1986); Spite et al. (1984); Boesgaard and Trippico (1986a, b); Rebolo et al. (1987b). This work

Field stars now can be assigned evolutionary states

Gratton et al. 2000, AA, 354, 169

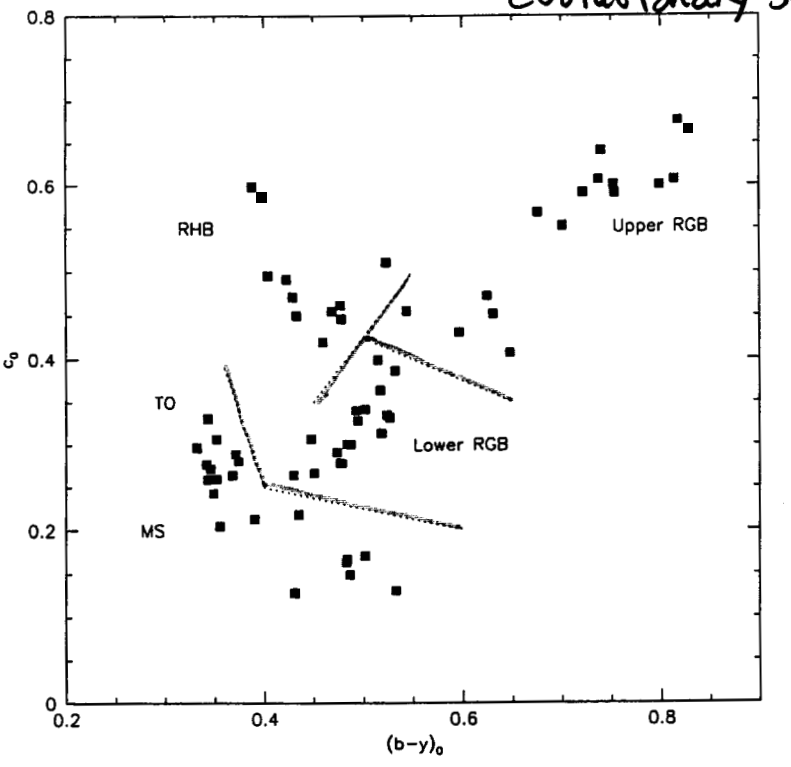

Fig. 1. $(b-y)_0 - c_0$ diagram for the programme stars. Different evolutionary phases as defined in this paper are marked. Lower-RGB and upper-RGB stars are stars climbing-up the RGB below and above the RGB bump respectively

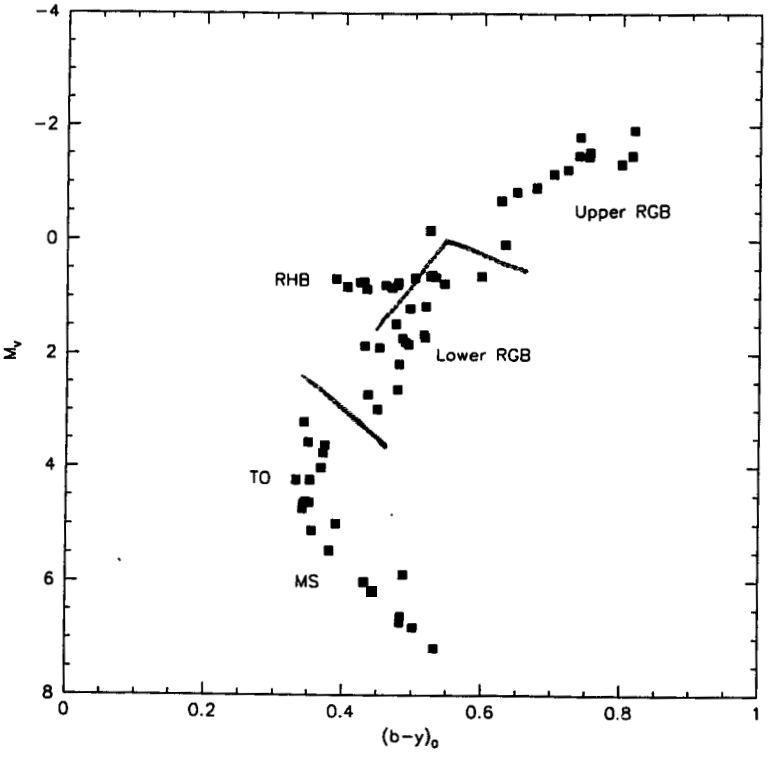

Fig. 2. Colour-magnitude diagram for the programme stars. Different evolutionary phases as defined in this paper are marked. lower-RGB and upper-RGB stars are stars climbing-up the RGB below and above the RGB bump respectively

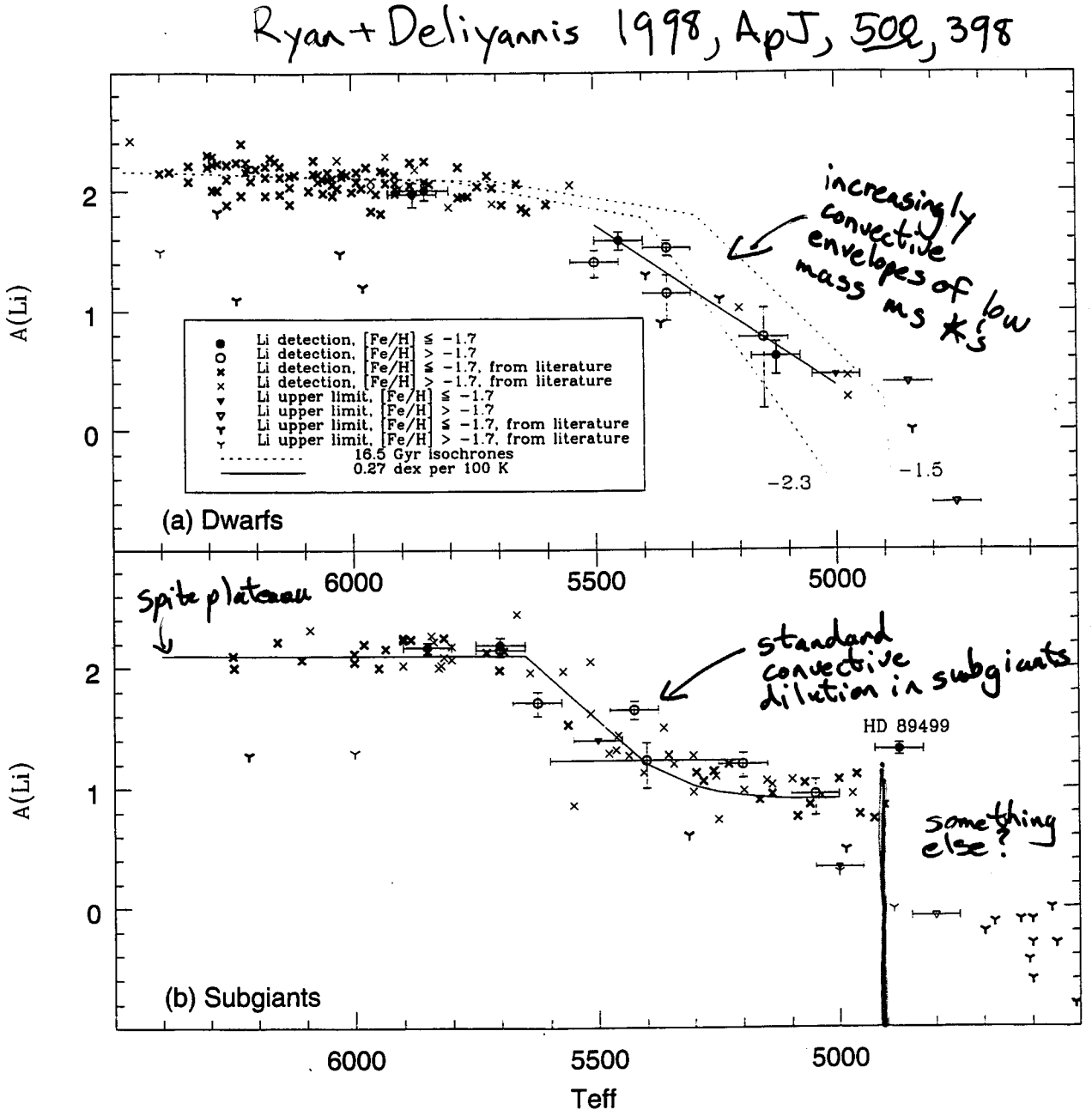

FIG. 4.—Lithium abundances as a function of effective temperature for our sample (*circles*; upper limits, *triangles*) and literature data (*crosses*; upper limits, *Y symbols*) referenced in text. Our measurements are divided into [Fe/H] ≤ -1.7 (*filled symbols*) and [Fe/H] > -1.7 (*open symbols*). Error bars are for random 3 σ errors in A(Li) and 50 K for $T_{\rm eff}$. Systematic errors up to 100 K in the temperatures, corresponding to 0.1 dex in A(Li), could be present (see text). (*a*) Dwarfs: Isochrones based on Deliyannis & Demarque (1991) "standard" Yale models at 16.5 Gyr for [Fe/H] $= -2.3$ (*lower dashed curve*) and -1.5 (*upper dashed curve*) are shown. An approximate linear fit to the data is also shown to lead the eye. (*b*) Subgiants: Dilution curve from Deliyannis et al. (1990) for a 0.775 $M_\odot$, $Z = 10^{-4}$, $\alpha = 1.5$ star is shown.

Lambert+Ries 1981

(Pop I solar metallicity giants)

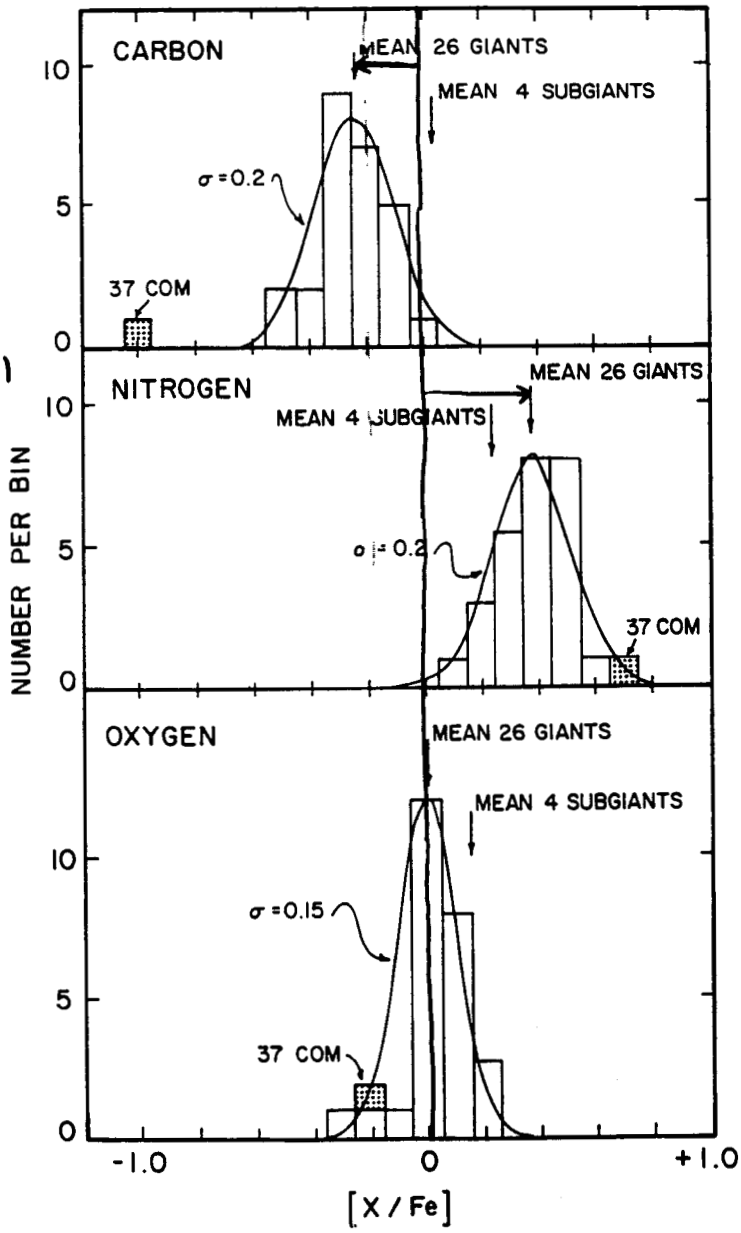

FIG. 1.—The frequency distribution for the CNO abundances in the giants. For C and N, the histograms refer to $[X/Fe] = \log(X/Fe) - \log(X/Fe)_\odot$ where X=C or N. See text for a comment on the O histogram. The smooth lines refer to Gaussian functions $n(X) = n(O) \exp(-x^2/\sigma^2)$.

the abundance sums are "constant"

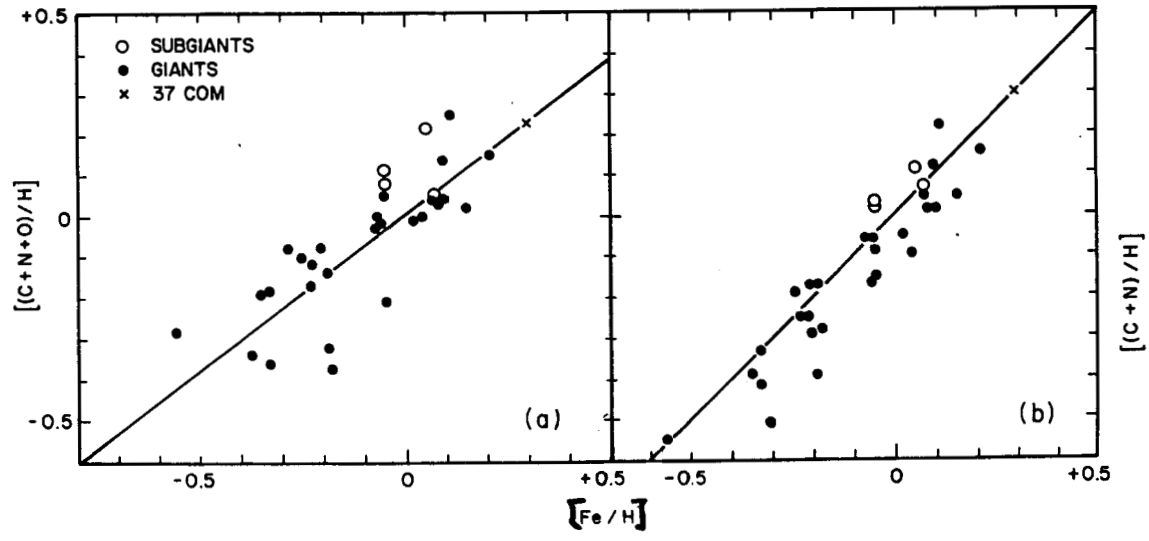

Sneden 1991
IAU Symp
145

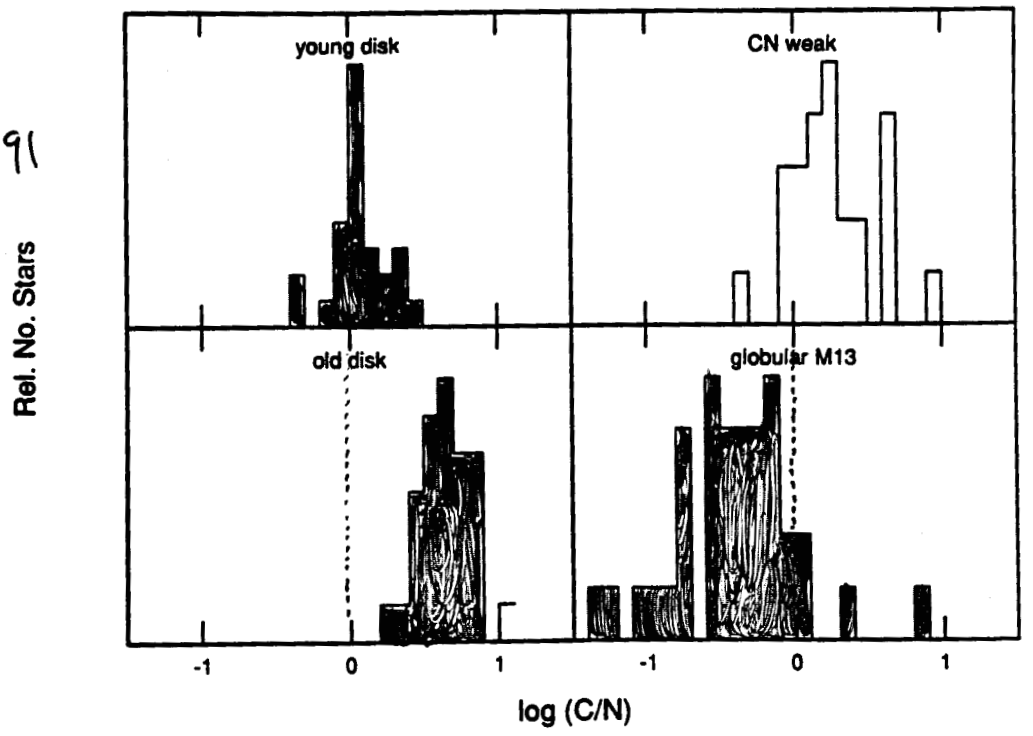

Figure 2. Distributions of C/N ratios among ordinary giants of different stellar populations. The cluster M13 has been chosen for illustration, and is not meant to represent completely the variety of possible C/N ratios that have been observed in globular clusters.

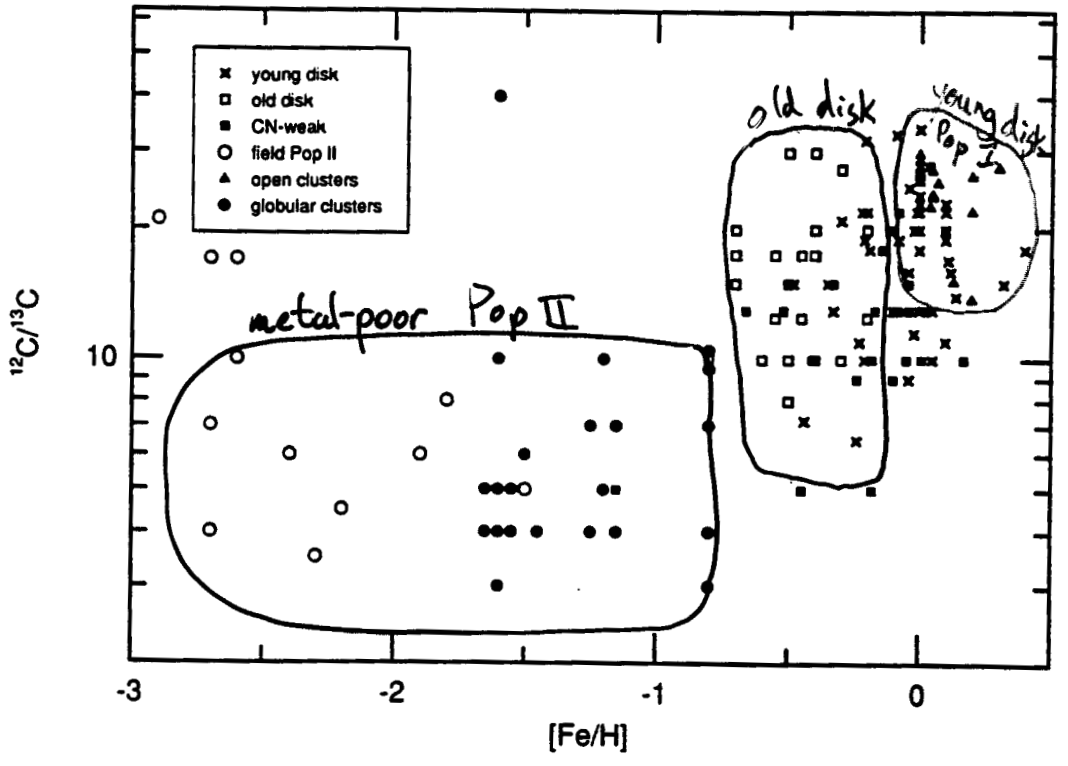

Figure 1. Carbon isotope ratios for giants as functions of their metallicities. For this figure an attempt has been made to include only ordinary giants, excluding subgiants, supergiants, and stars with very anomalous abundances.

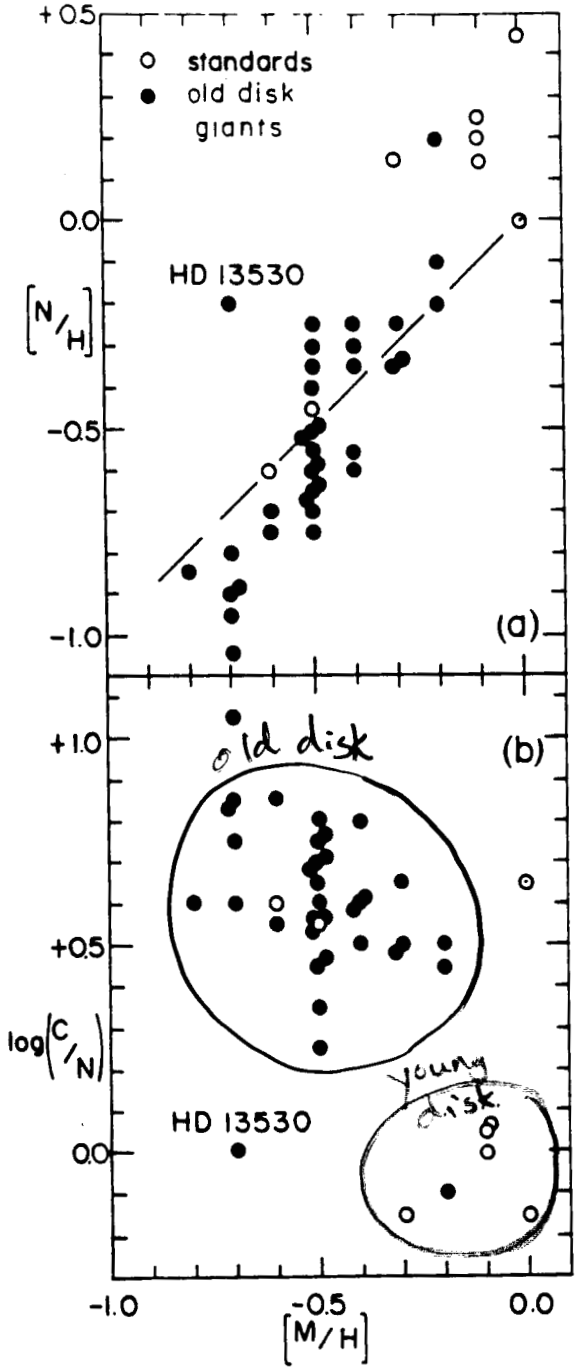

Cottrell + Sneden 1985, A&A

Fig. 14a and b. Derived **a** [N/H] versus overall metallicity [M/H] and **b** log (C/N) ratio versus [M/H] for all standard and old disk giant stars. The mean position of dwarf star abundances from Clegg, Lambert and Tomkin (1981) are shown by a dashed line in **a**

Old Disk Giants: $^{12}C/^{13}C$ a severe function of Luminosity

Shetrone et al. 1993 PASP 105, 301

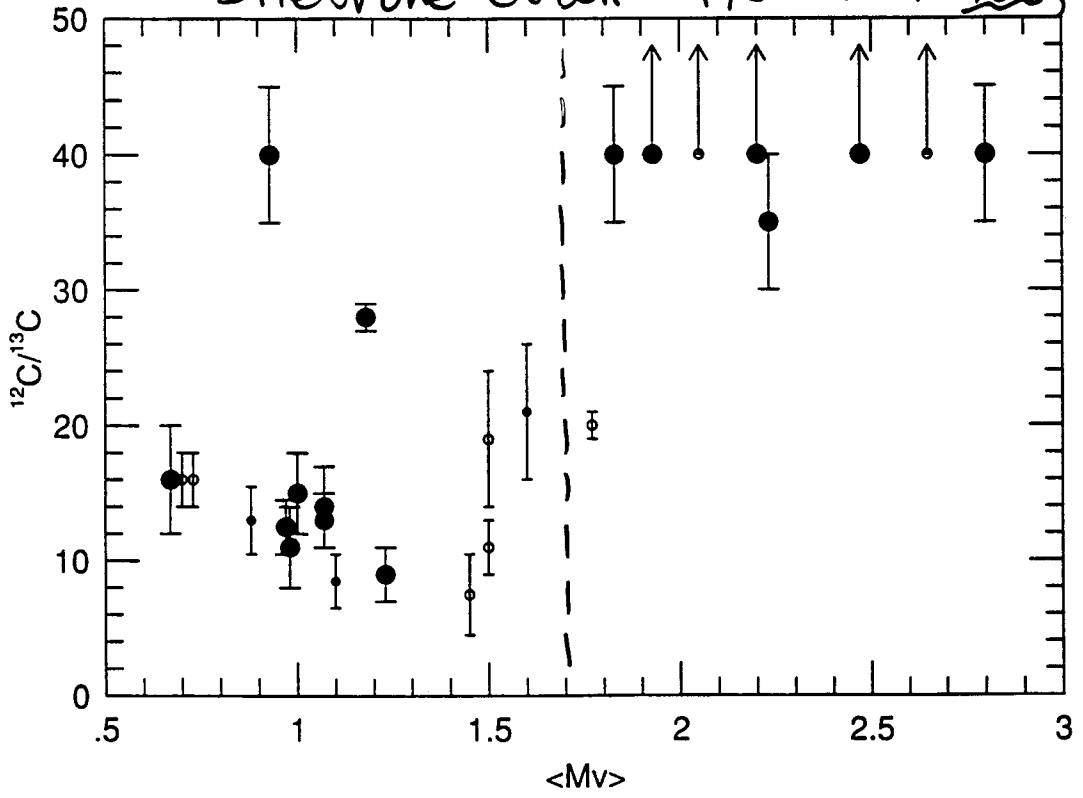

FIG. 6—Derived $^{12}C/^{13}C$ ratios vs. M_V (see Table 6) for the old disk stars. The possible non-old disk giants identified in the preceding figure have been omitted here. Large points represent the greatest certainty in M_V while open points represent the smallest certainty. Points which would have fallen on top of each other have been shifted slightly in M_V.

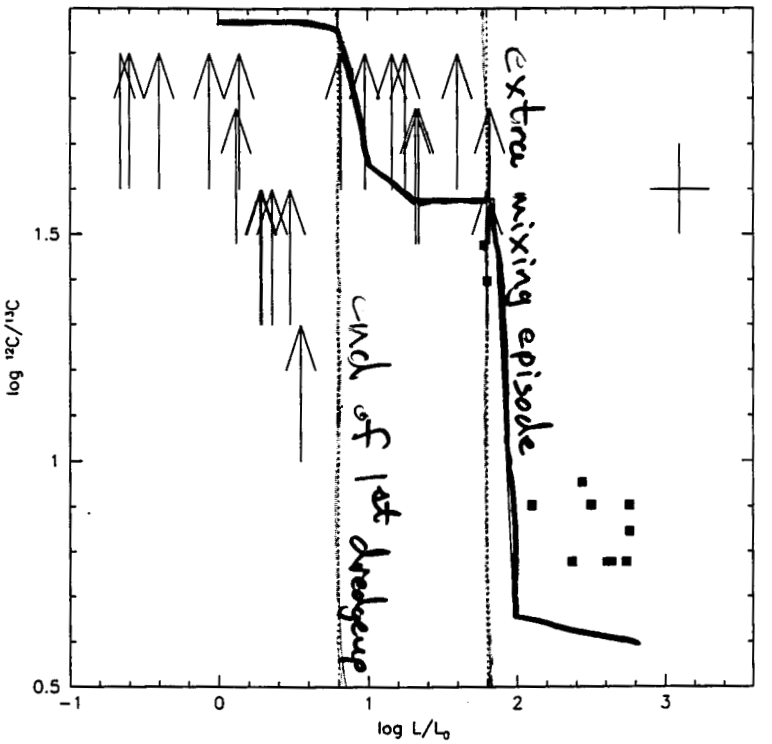

Gratton et al. (2000)

Fig. 12. Run of the isotopic ratio $^{12}C/^{13}C$ with luminosity for stars with -2 <[Fe/H]< -1. Filled symbols are actual measures; arrows symbols are lower limits. Superimposed is the evolutionary sequence for a 0.8 $M_\odot$ star with $Z = 10^{-3}$ experiencing a rotationally-induced deep mixing (Charbonnel 1995)

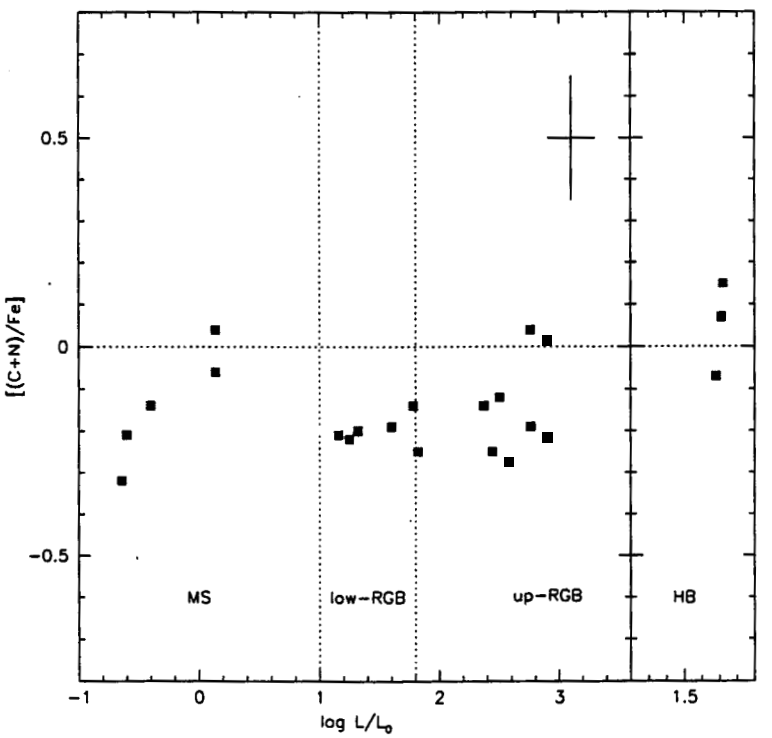

But, C+N stays ~constant

Fig. 13. Run of the ratio of the sum of C and N abundances with luminosity for stars with -2 <[Fe/H]< -1. Expected error bar is also shown

Gratton et al. 2000, A&A, 354, 169

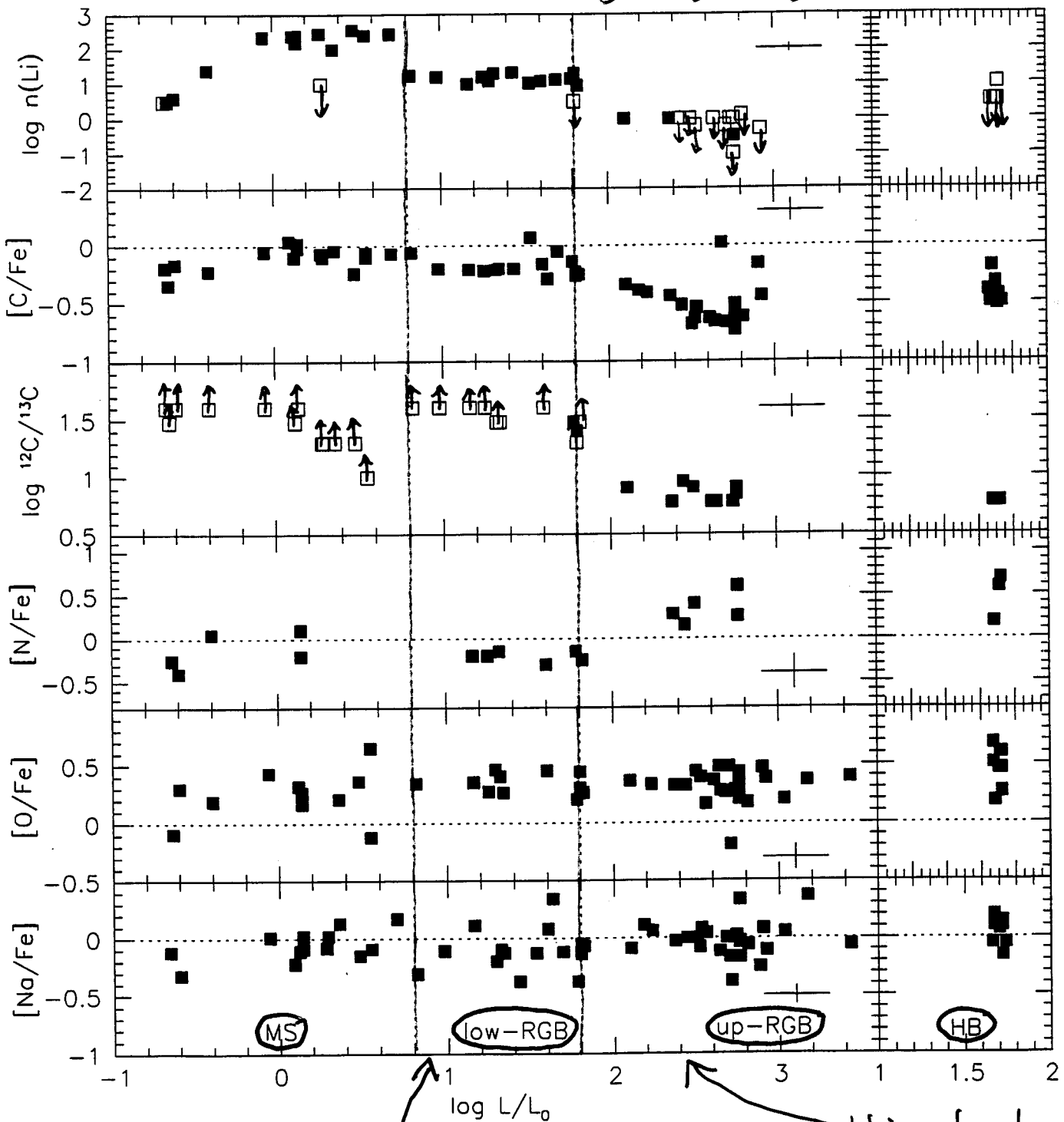

first dredge-up should be complete at this point!

this clearly marks an extra mixing episode on the RGB

A Link to Globular Clusters?

◂M04 . . Index . . more . . M06▸

Messier 5

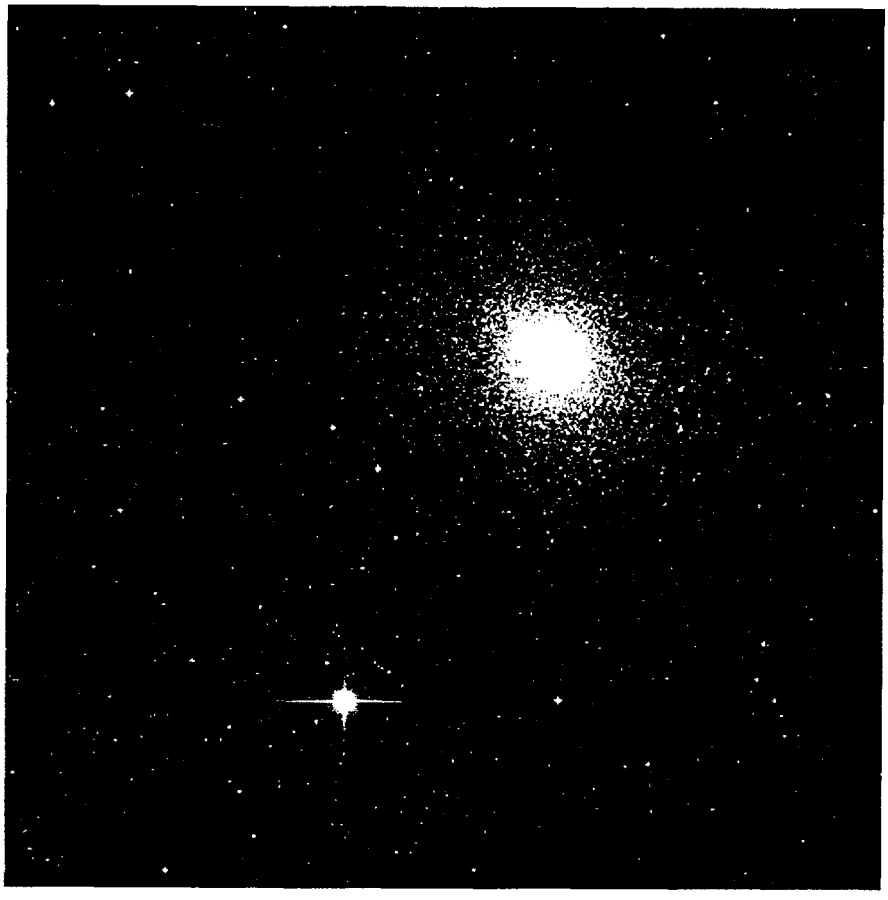

M	NGC	Con	RA	Dec	Mag	Size (min)	Typ	Distance	Common Name
5	5904	Ser	15 18.6	02 05	7.0	17.4	GCl	30	

Bill Arnett; last updated: 1995 August 25

A Recent c-m diagram for M5

Sandquist et al. 1997

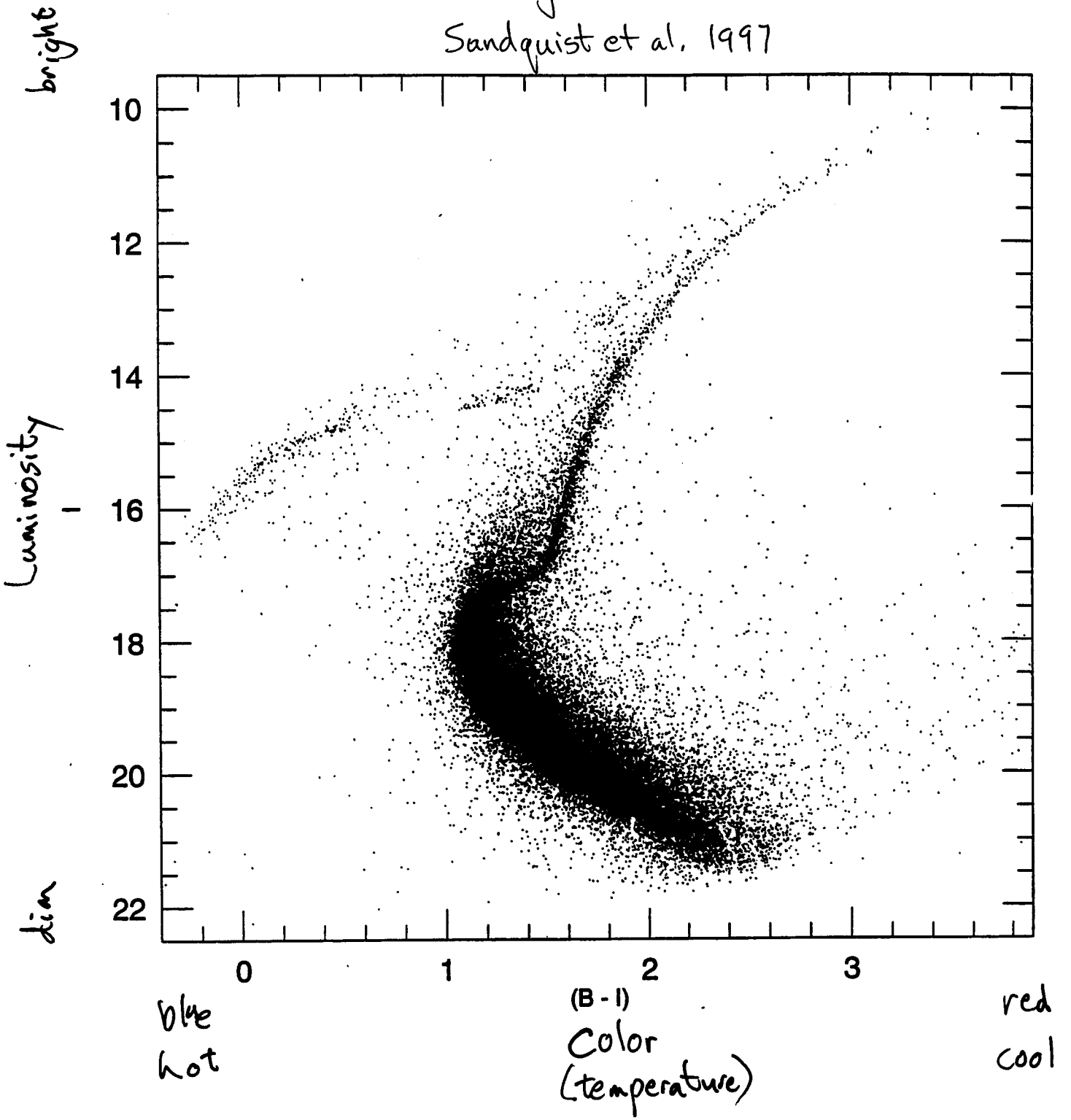

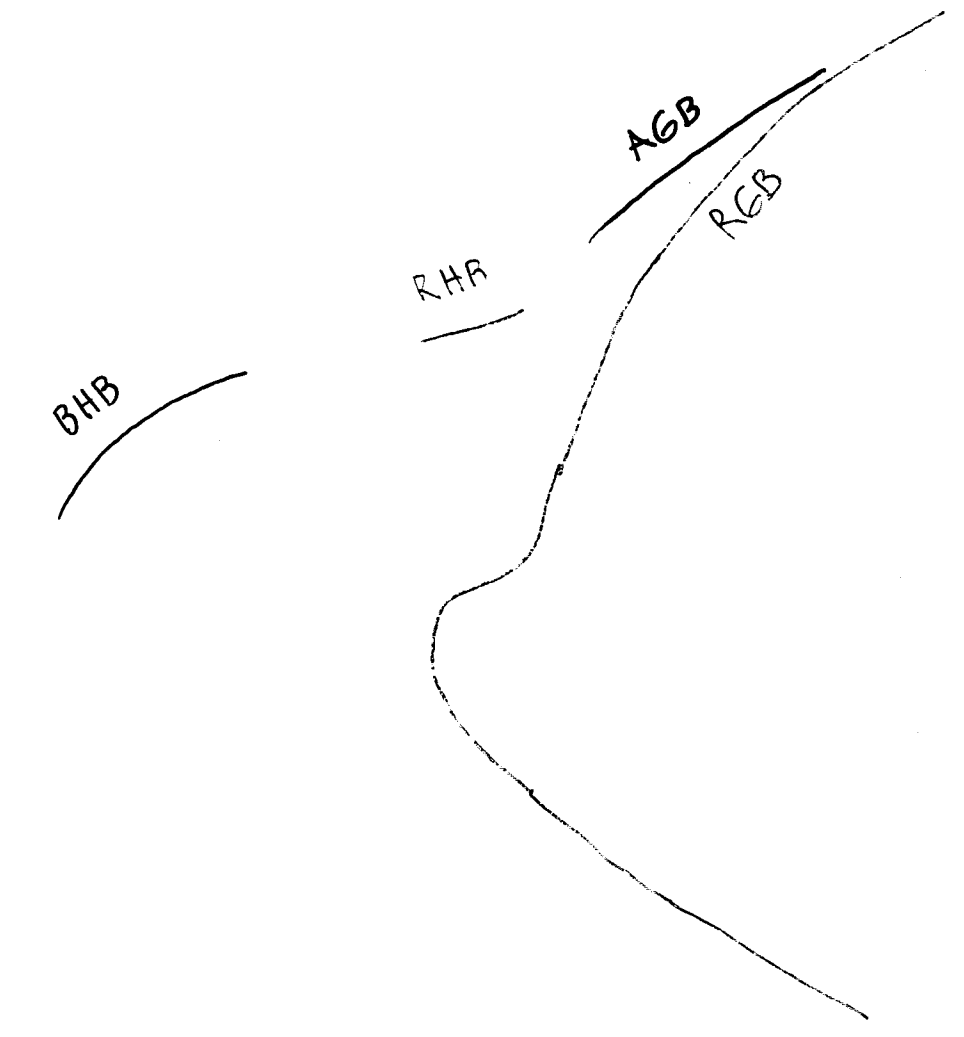
AGB
RGB
RHR
BHB

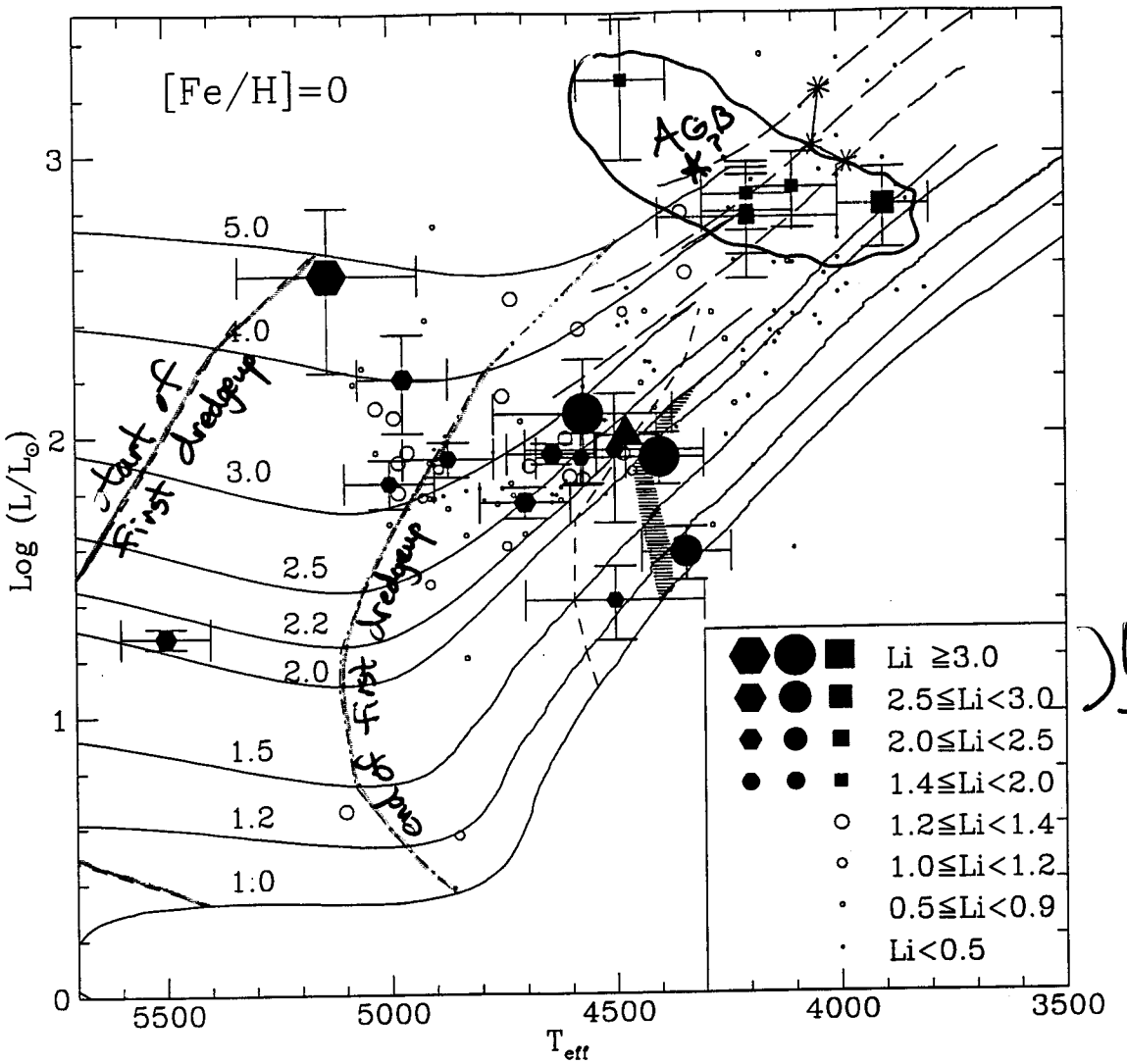

probably only these are true Li-rich giants

Fig. 1. The HR diagram for the Li-rich giants. Evolutionary tracks with [Fe/H]=0 are labelled by their masses. Two dashed lines delimit the first dredge-up; the warmer line corresponds to the start of Li dilution and the cooler line marks the deepest penetration of the convective zone. The dashed-dotted line indicates the start of the decrease in the carbon isotopic ratio due to dilution. The shaded region surrounds the location of the RGB bump. A solid line connects the points (asterisks) where a molecular weight barrier starts to appear due to the second dredge-up on the early-AGB. The filled symbols represent the so-called lithium rich stars which are grouped according to their evolutionary state as discussed in the text: hexagons indicate Li-normal stars undergoing first dredge-up dilution; circles and triangle (for HD 233517 whose luminosity was derived from P_{rot} and $v\sin i$) show stars at the RGB bump; and squares indicate the early-AGB stars. The open circles are stars with Hipparcos parallaxes and $-0.1 \leq [Fe/H] \leq +0.1$ from the Brown et al. (1989) survey. In all cases, the size of the symbol indicates the Li abundance of the star as shown in the legend. The error bars on luminosity are estimated from uncertainties in the Hipparcos parallax. Temperature uncertainties are taken from the literature (see Table 1).

$(^3He(\alpha,\gamma)^7Be(\beta^-\nu)^7Li)$

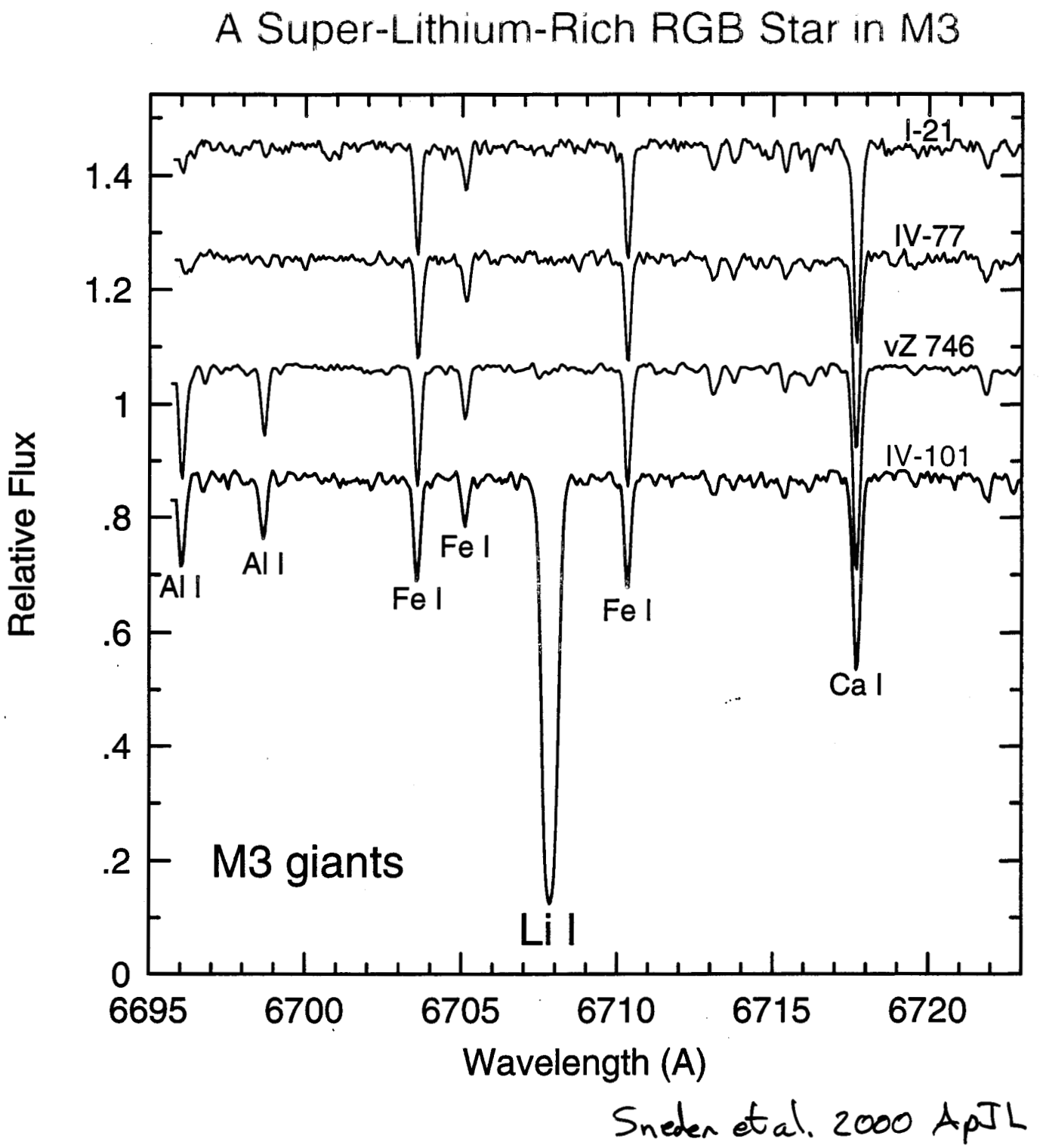
A Super-Lithium-Rich RGB Star in M3
I-21
IV-77
vZ 746
IV-101
Al I
Al I
Fe I
Fe I
Fe I
Ca I
Li I
M3 giants
Relative Flux
Wavelength (A)
0
.2
.4
.6
.8
1
1.2
1.4
6695
6700
6705
6710
6715
6720
Sneden et al. 2000 ApJL

No Unusual BV Photometry for the Li-Rich Star

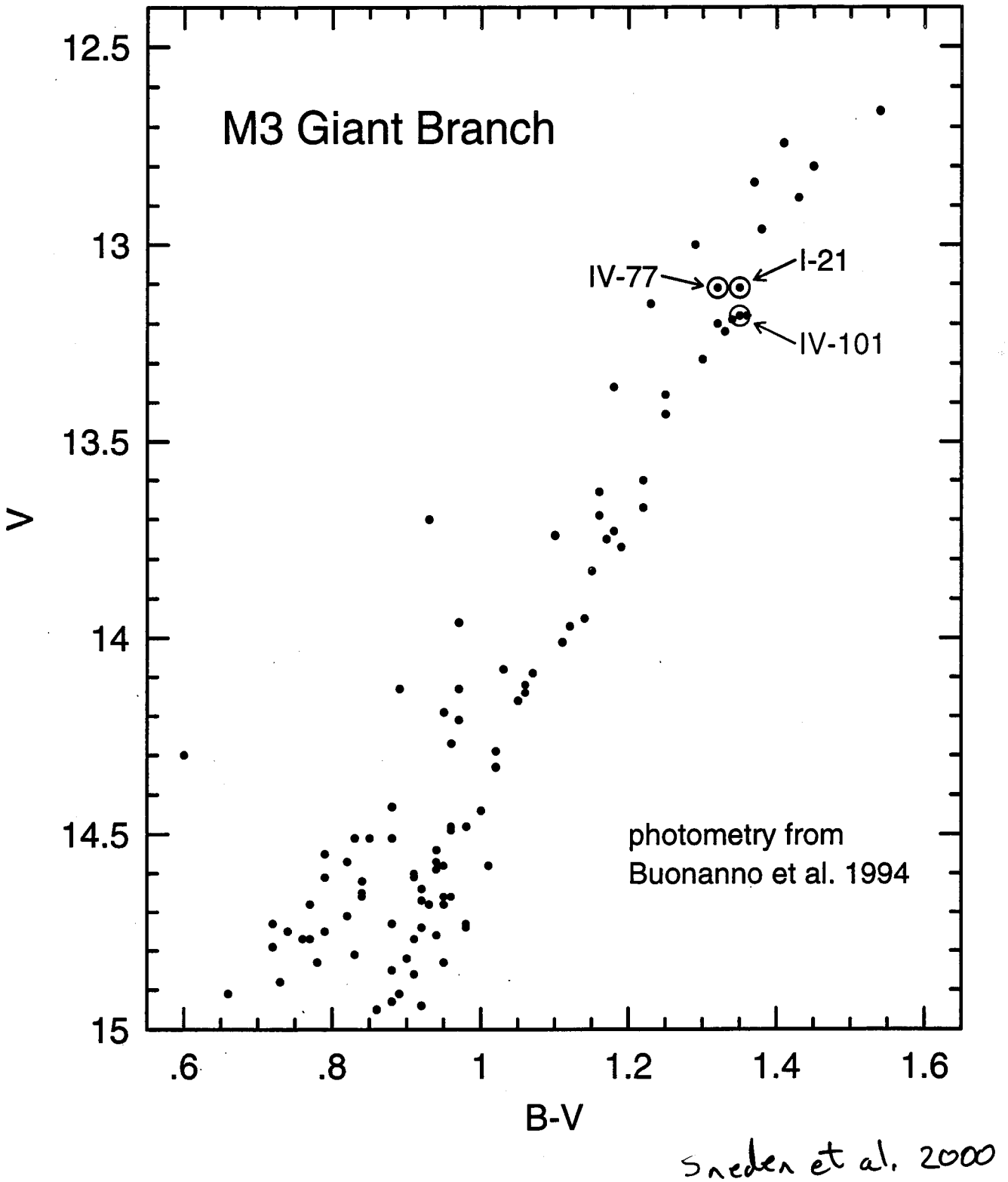

Sneden et al. 2000

Oxygen in Halo Field Giants from [O I] Line

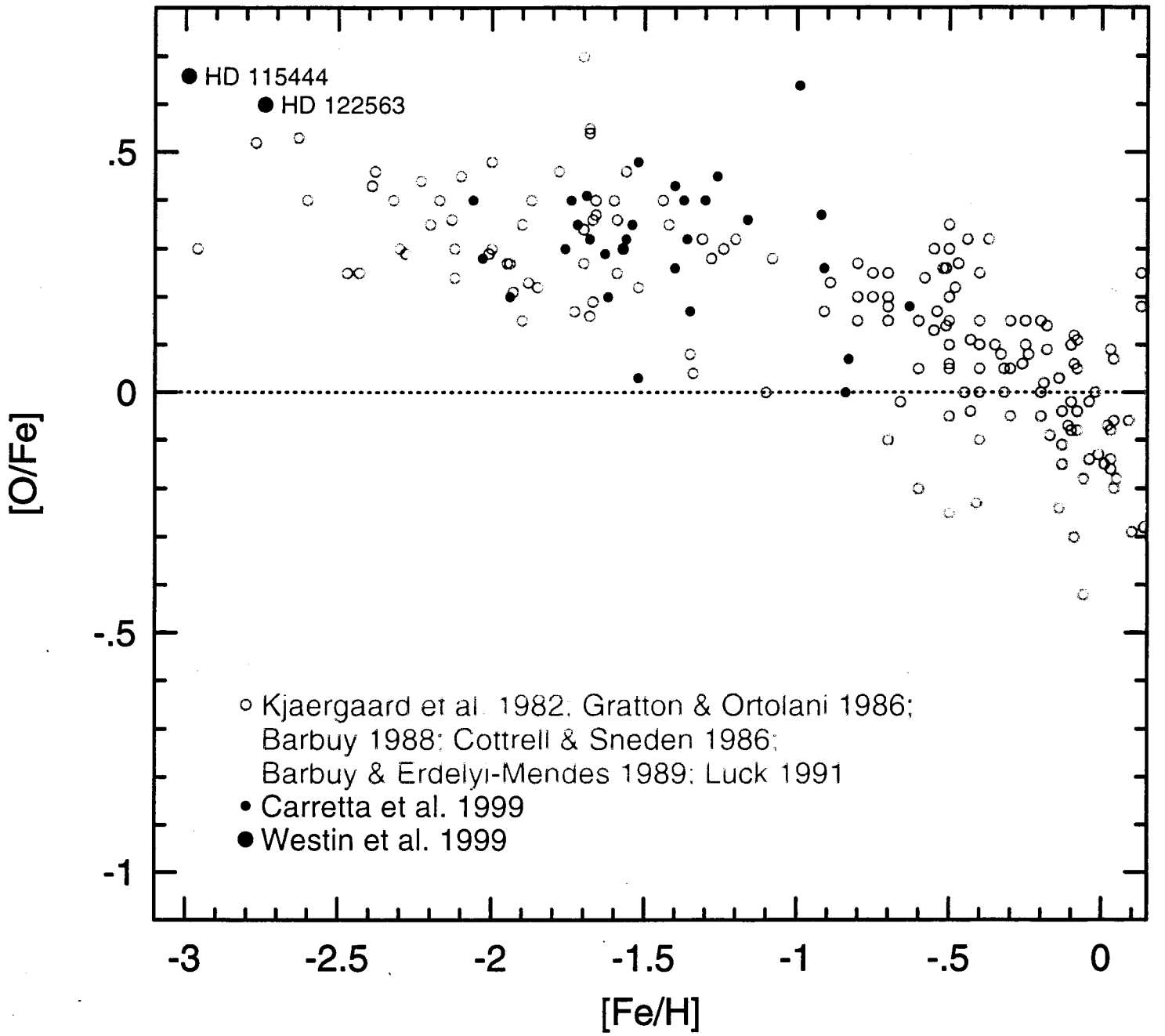

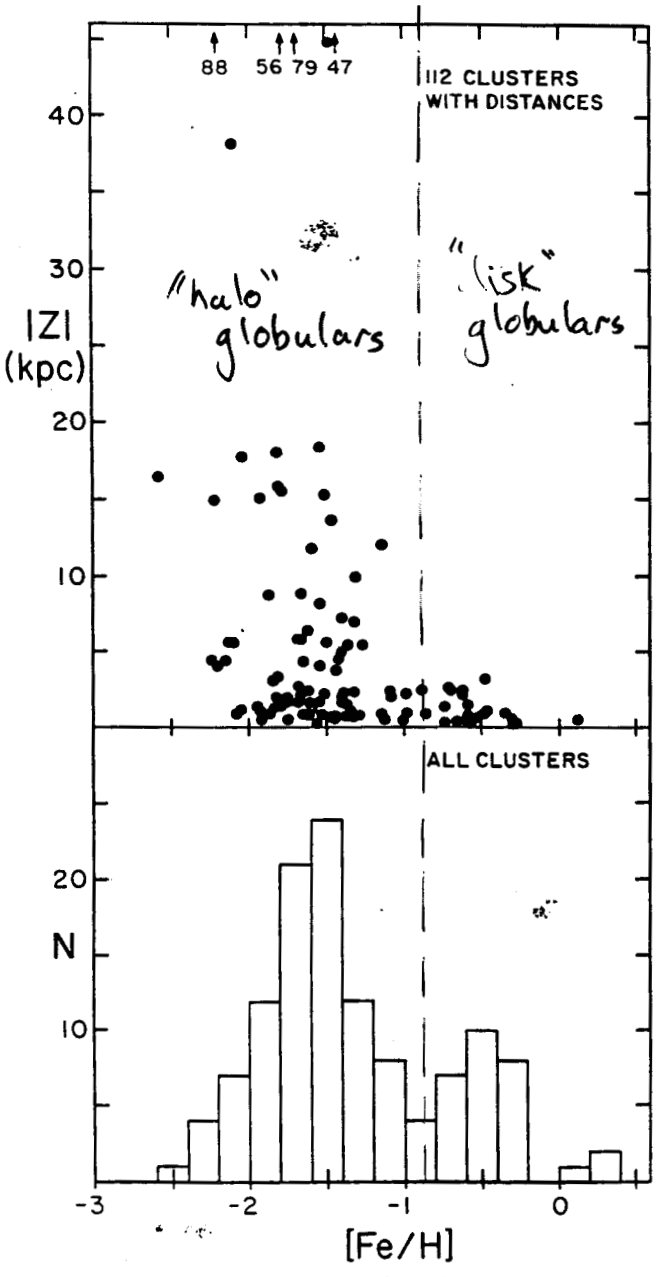

FIG. 1.—In the upper diagram, $|Z|$ is plotted against [Fe/H] for the 112 globular clusters of known distance. Notice that there are no clusters in the zone $20 \lesssim |Z| \lesssim 37$ kpc and that the $|Z|$ distribution changes suddenly at [Fe/H] ≈ -1. The lower diagram is a histogram of the values of [Fe/H] for all 121 clusters in Table 1. Notice that the valley in the distribution over [Fe/H] occurs at the same value as the sudden change in the $|Z|$ distribution.

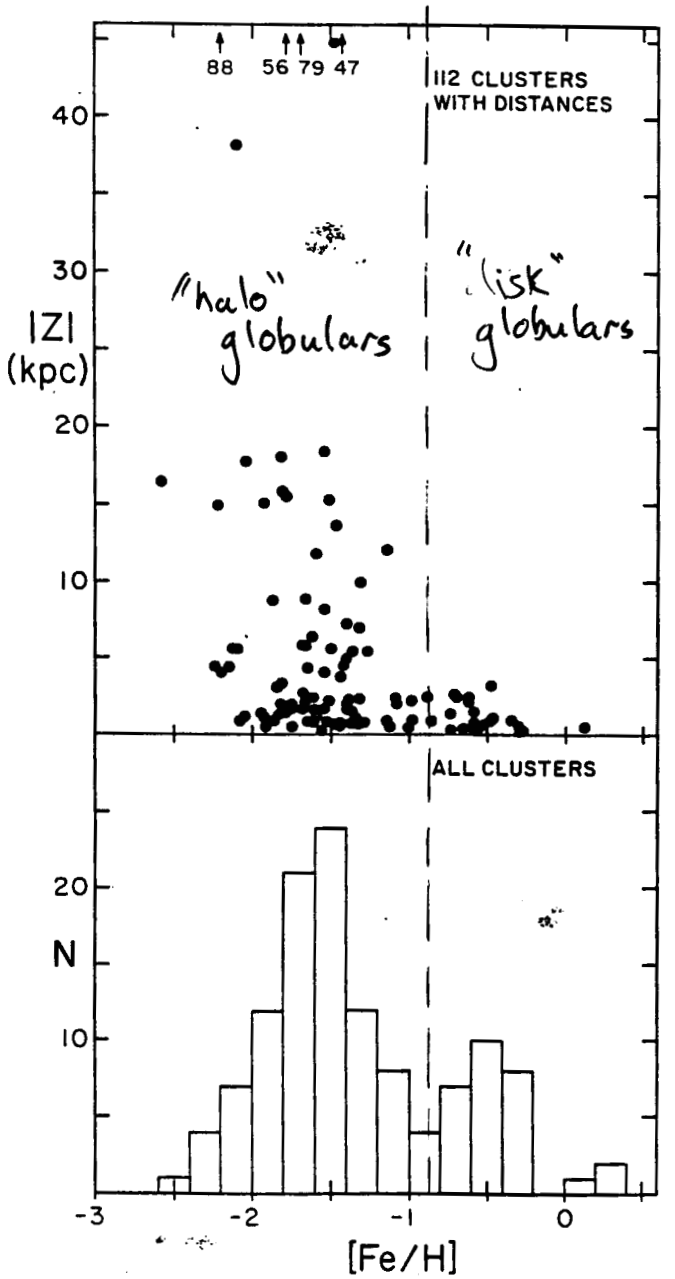

FIG. 1.—In the upper diagram, $|Z|$ is plotted against [Fe/H] for the 112 globular clusters of known distance. Notice that there are no clusters in the zone $20 \lesssim |Z| \lesssim 37$ kpc and that the $|Z|$ distribution changes suddenly at [Fe/H] ≈ -1. The lower diagram is a histogram of the values of [Fe/H] for all 121 clusters in Table 1. Notice that the valley in the distribution over [Fe/H] occurs at the same value as the sudden change in the $|Z|$ distribution.

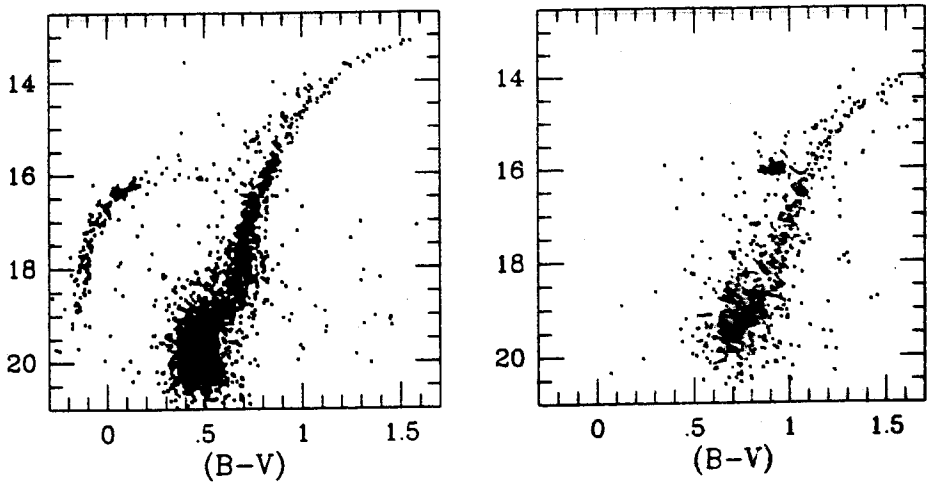

Fig. 2.2. The color–magnitude diagrams of NGC 1904 (left) and NGC 6637 (right) illustrating differences in horizontal branch morphology and the location of the main-sequence turn-off. (From data supplied by R. Buonanno and A. Sarajedini.)

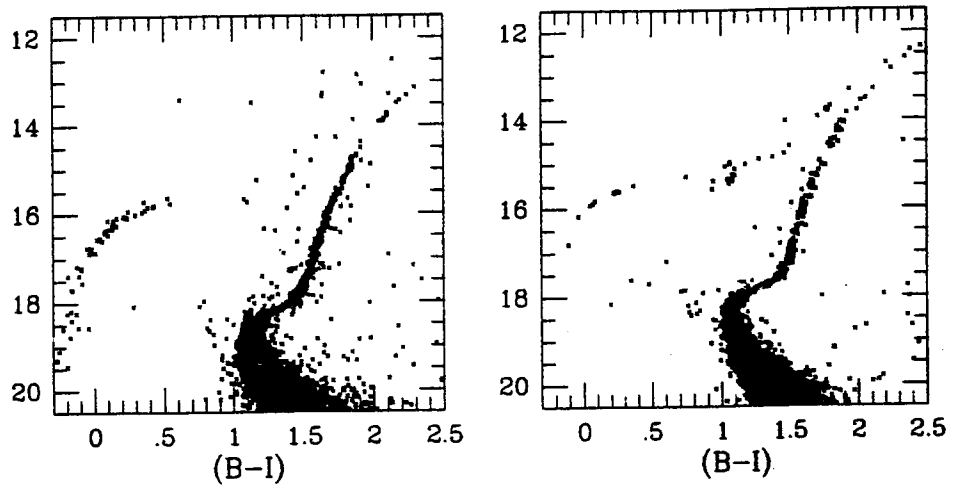

Fig. 2.3. The color–magnitude diagrams of M2 (left) and M3 (right). (From data supplied by P. Stetson.)

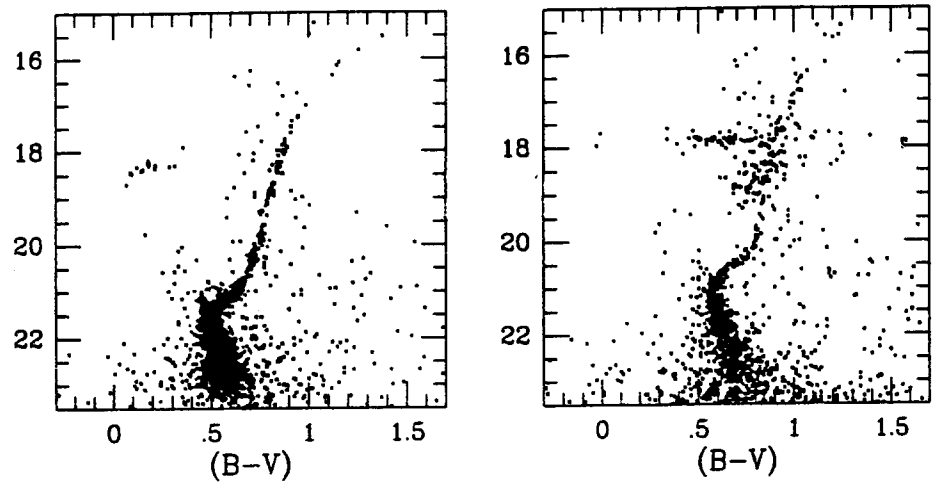

Fig. 2.4. The color–magnitude diagrams of Arp 2 (left) and Ruprecht 106 (right). (From data supplied by R. Buonanno.)

The "2nd Parameter" Problem

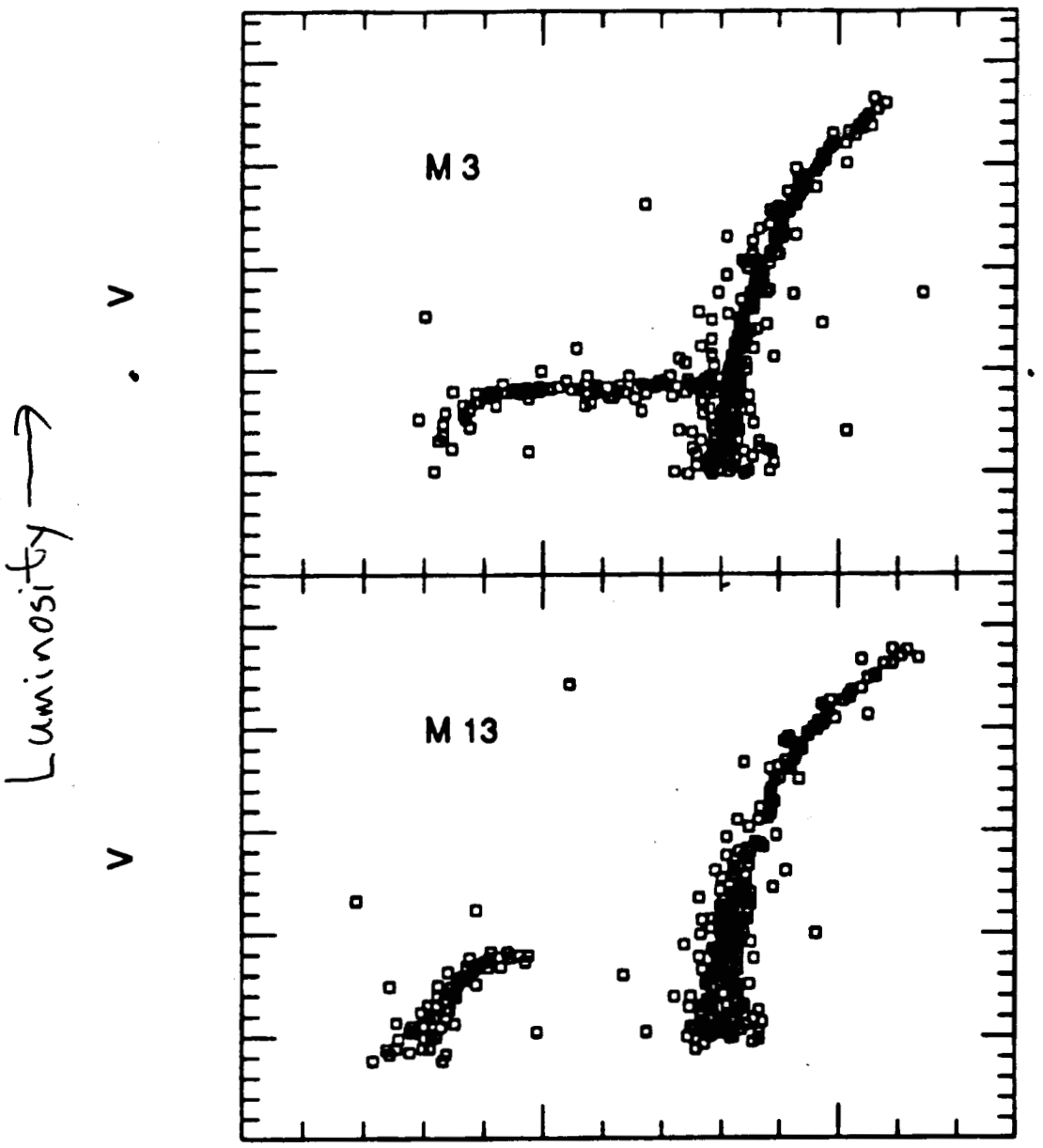

Both M3 and M13 have same metallicity [Fe/H] ≃ -1.

FIG. 3—A comparison of color–magnitude diagrams for M3 and M13, illustrating the second parameter effect. The two clusters differ in [Fe/H] by only 0.02 dex (Kraft et al. 1993). Diagrams courtesy of M. Bolte.

↑ unpublished as yet

Model Globular Cluster HB's

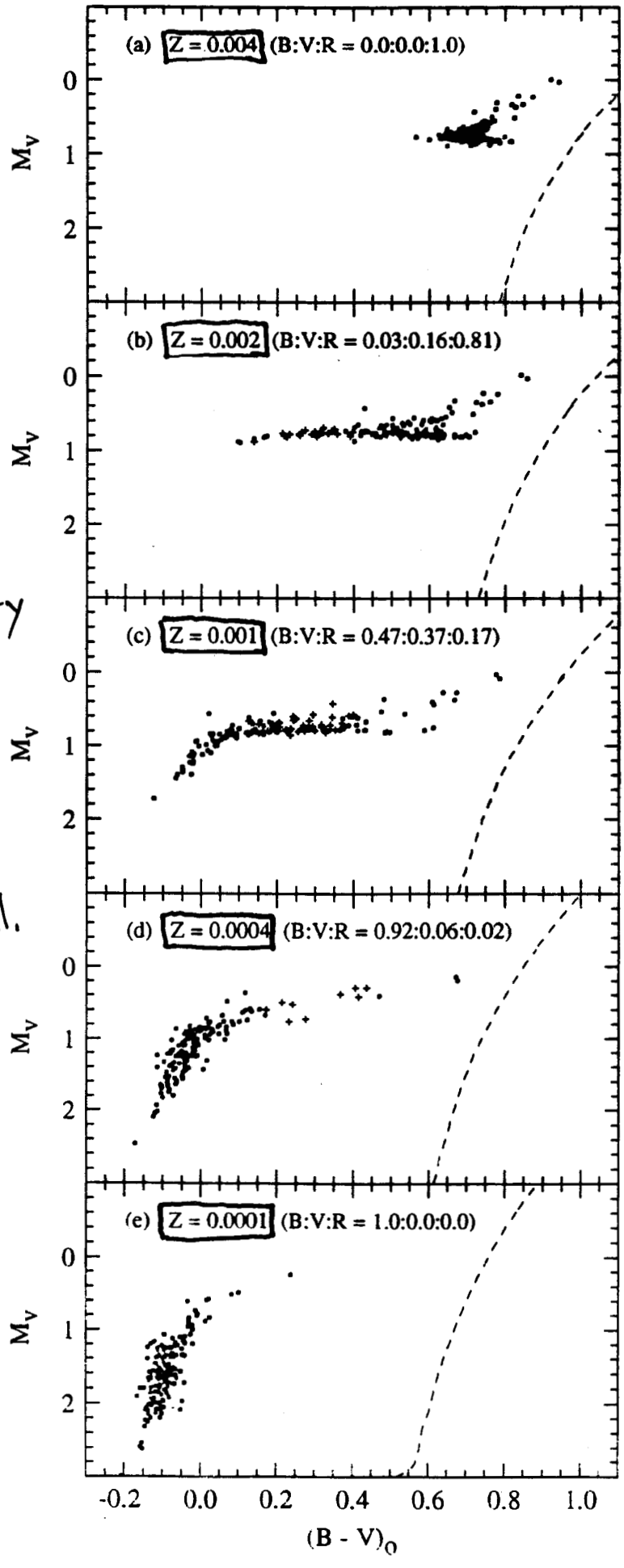

The first parameter: metallicity

Lee et al. (1994)

Model Globular Cluster HB's

A second parameter: Age

Lee et al. (1994)

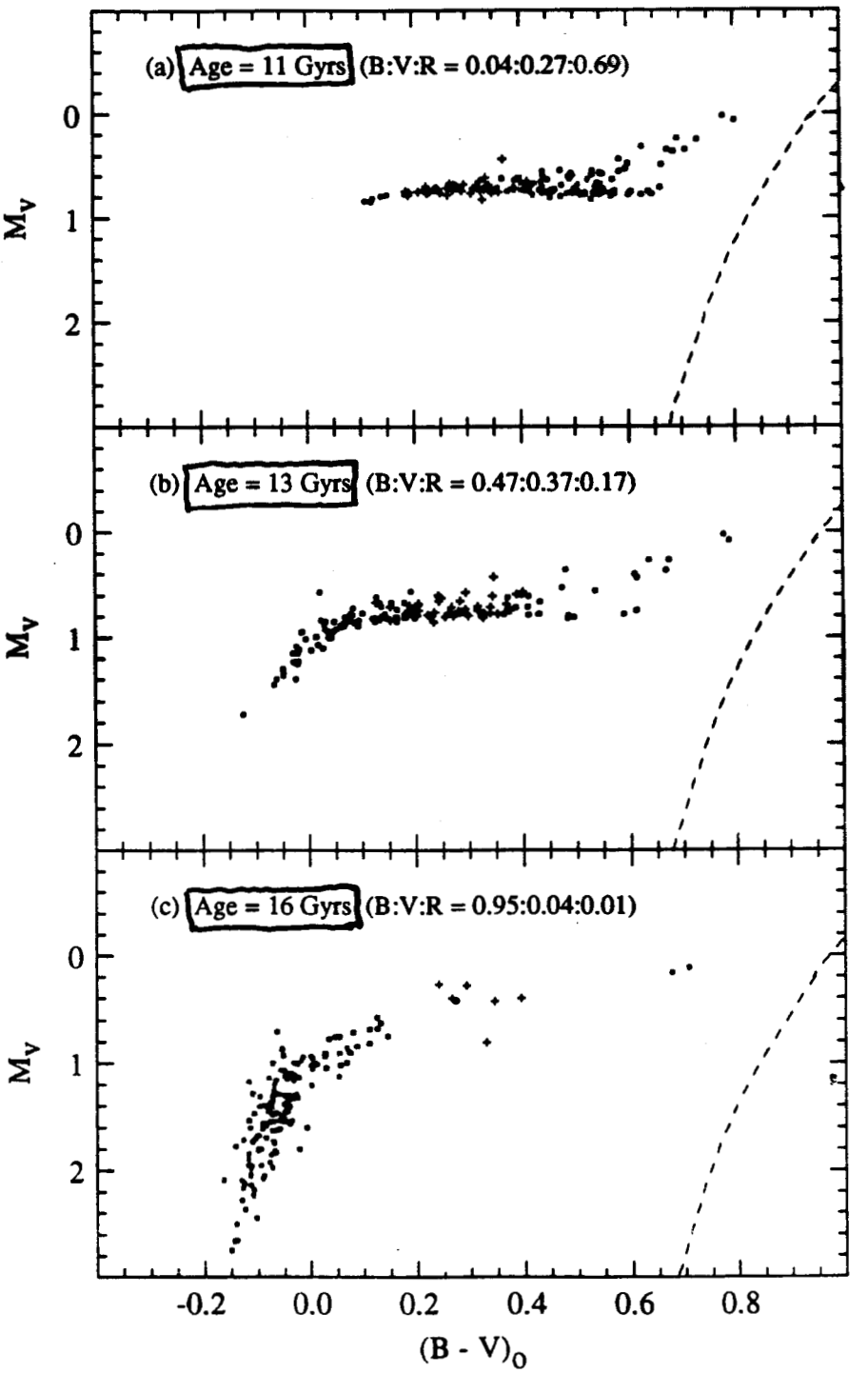

FIG. 2.—(*a–c*) The effect of cluster age on the morphology of the HB. Y_{HB} ($\sim$0.22), Z (0.001), and ΔM (0.223 $M_\odot$) are fixed.

Carbon Abundance Trends with Luminosity

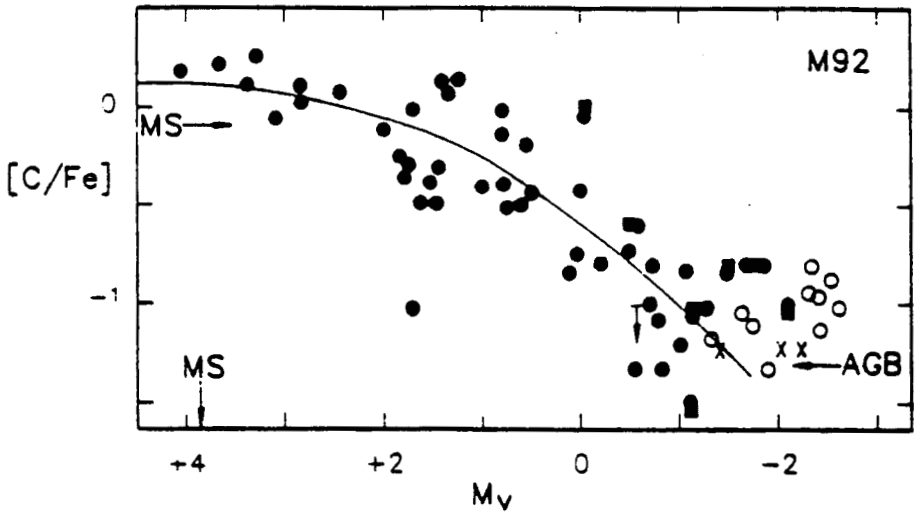

Kraft 1994, PASP 106, 553 and references therein

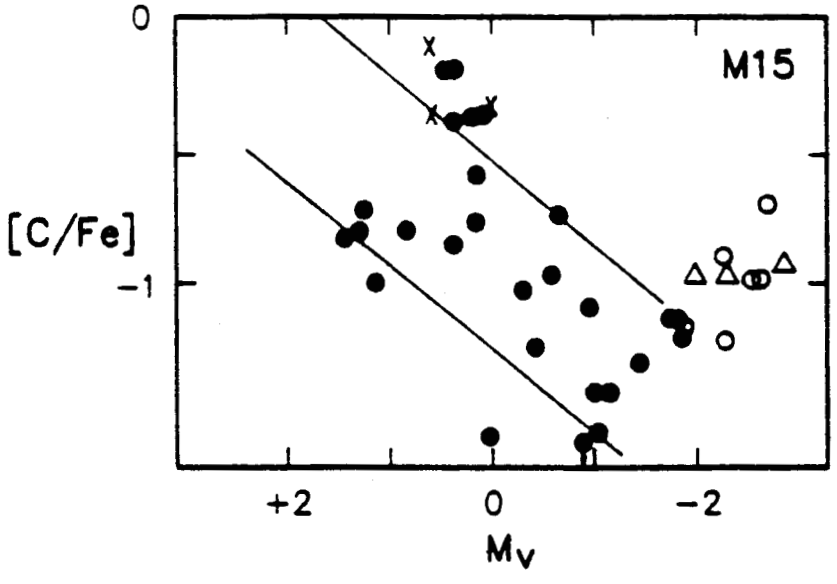

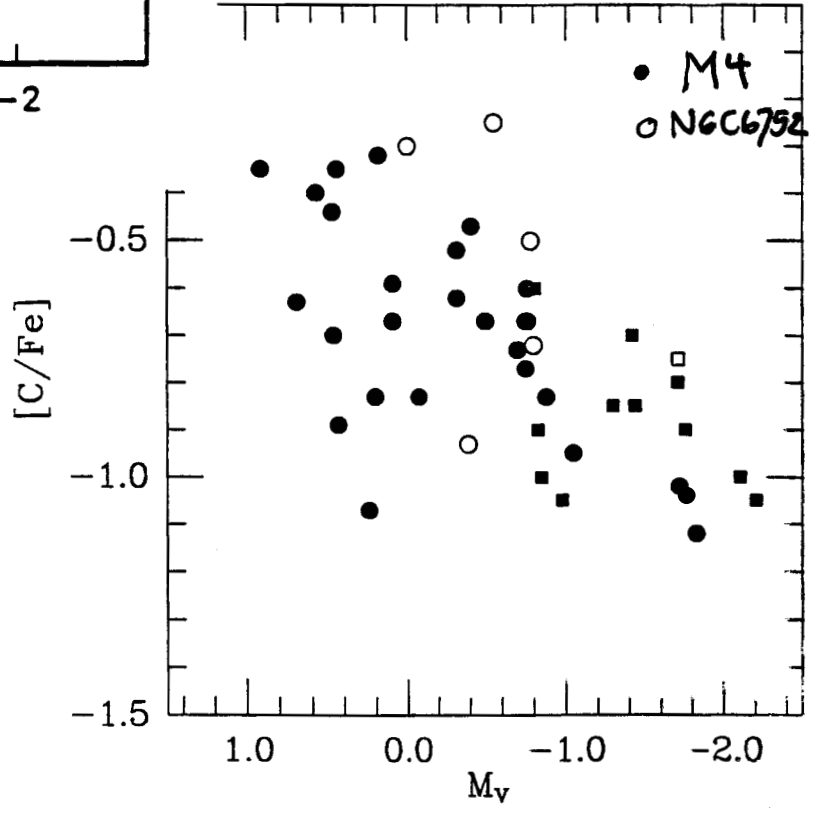

C & N in Field and Cluster Giants

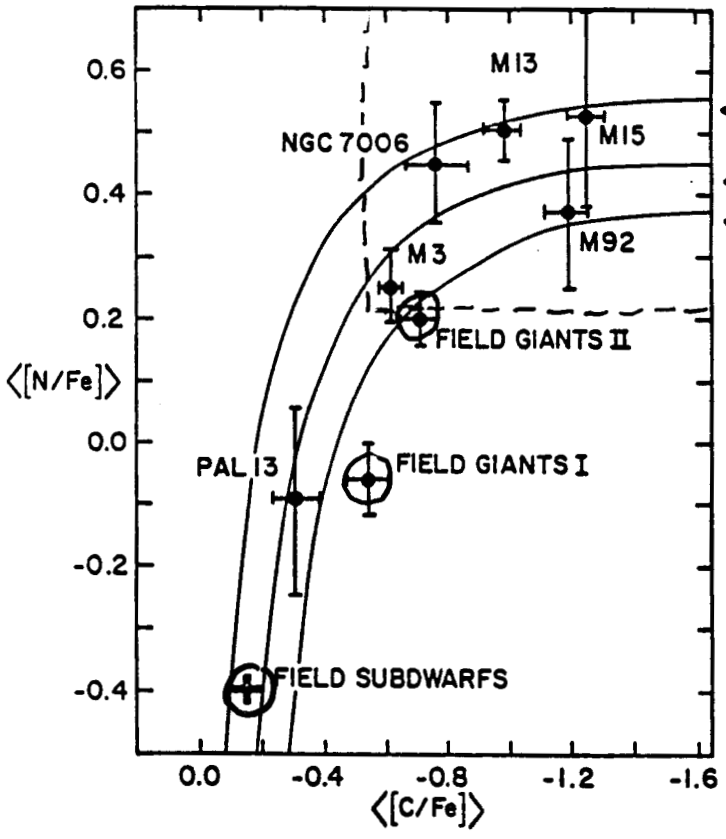

lines of constant C+N

Larger + Kraft 1984, PASP, 93, 339

CN bimodality

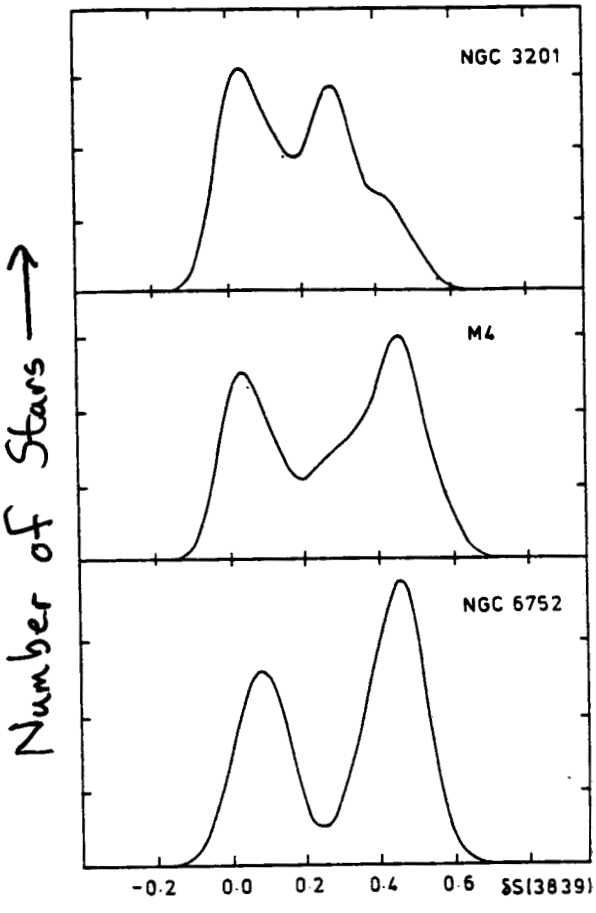

CN Bandstrength →

Smith + Norris 1982, ApJ, 254, 149

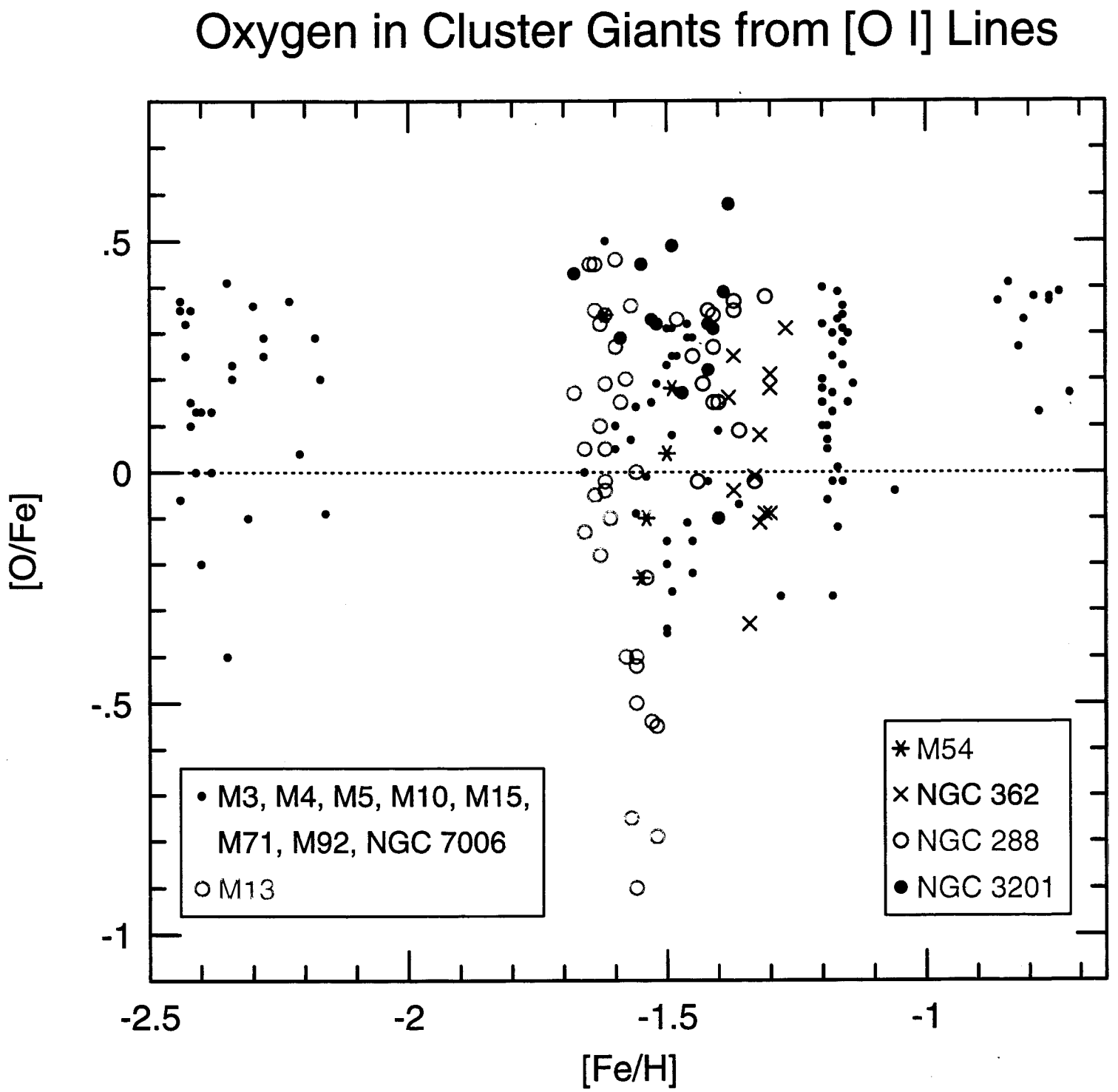
Oxygen in Cluster Giants from [O I] Lines
.5
0
-.5
-1
-2.5
-2
-1.5
-1
[O/Fe]
[Fe/H]
• M3, M4, M5, M10, M15,
M71, M92, NGC 7006
○ M13
✱ M54
× NGC 362
○ NGC 288
● NGC 3201

(Halo Field Giants)

Globular Star Cluster M13

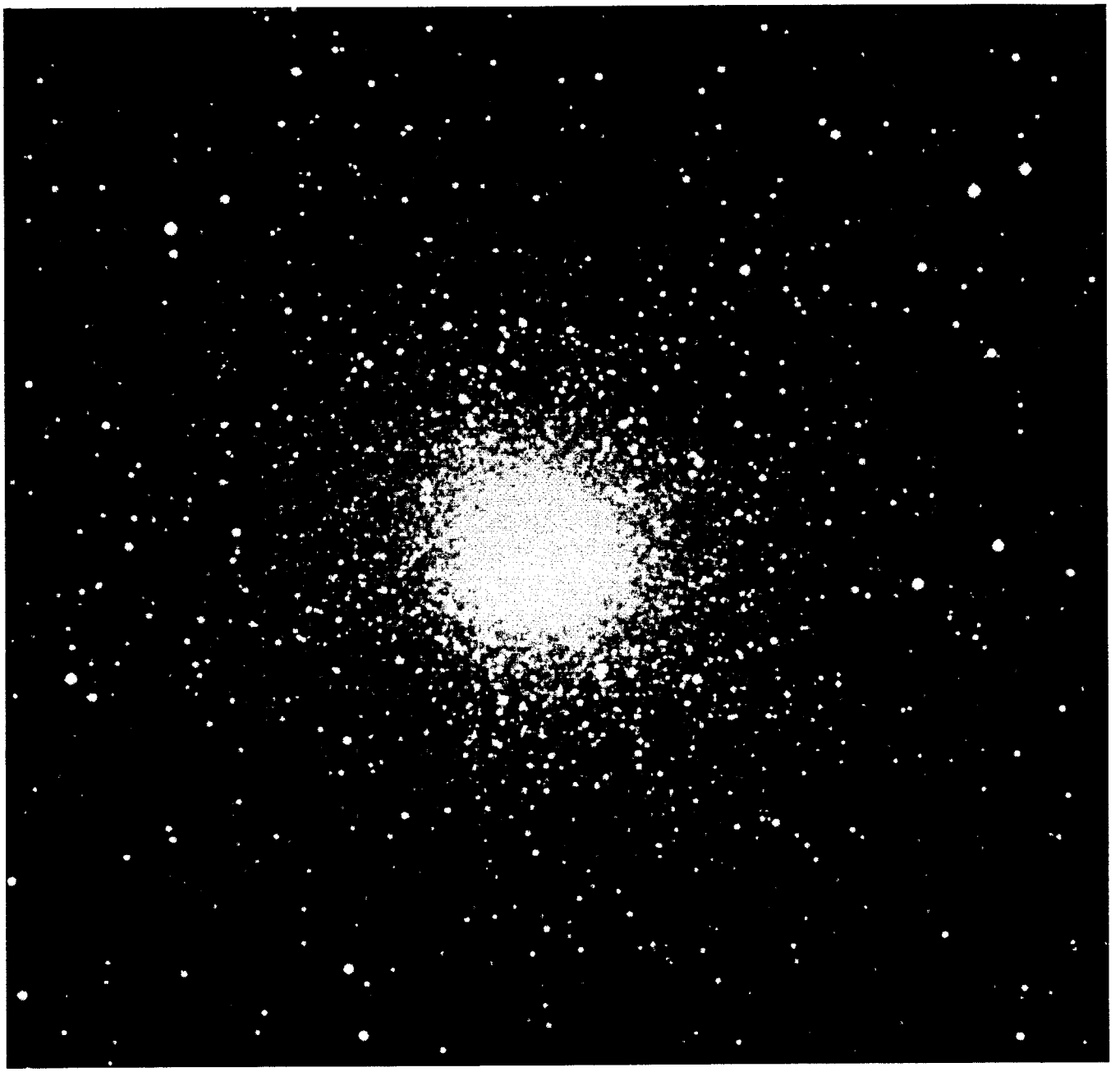

M 13
high resolution survey

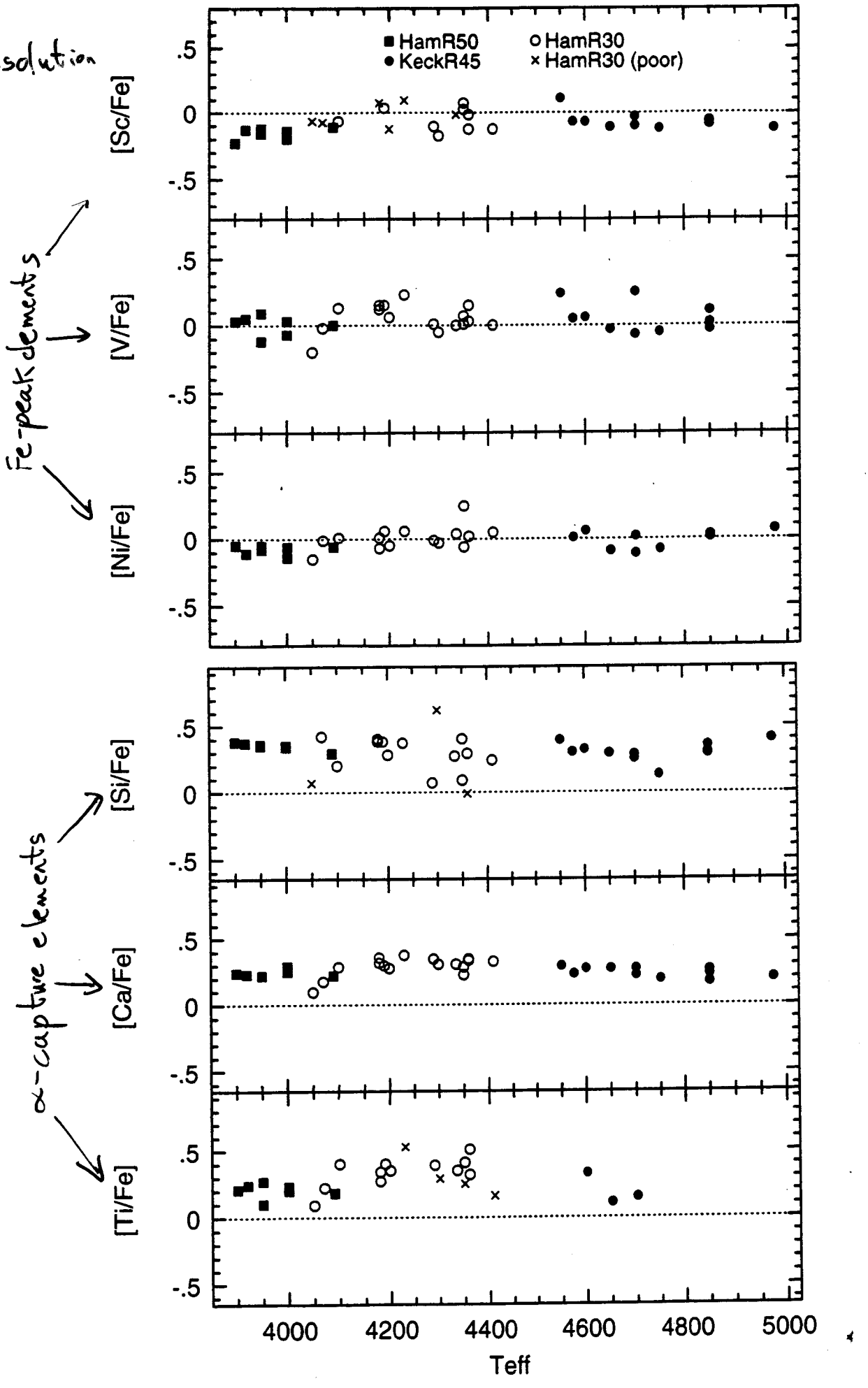

M13 proton-capture elements

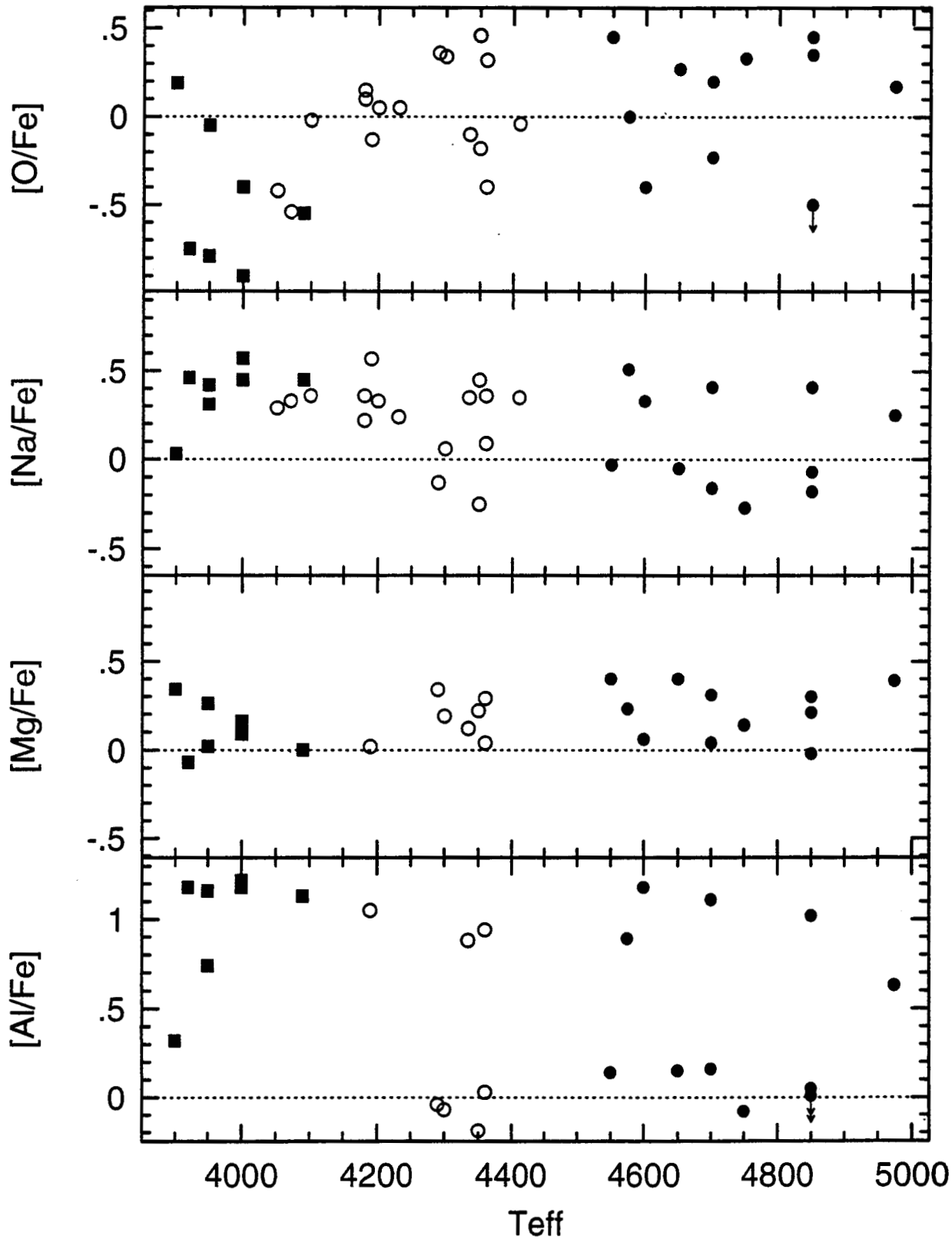

M13 proton-capture abundance correlations

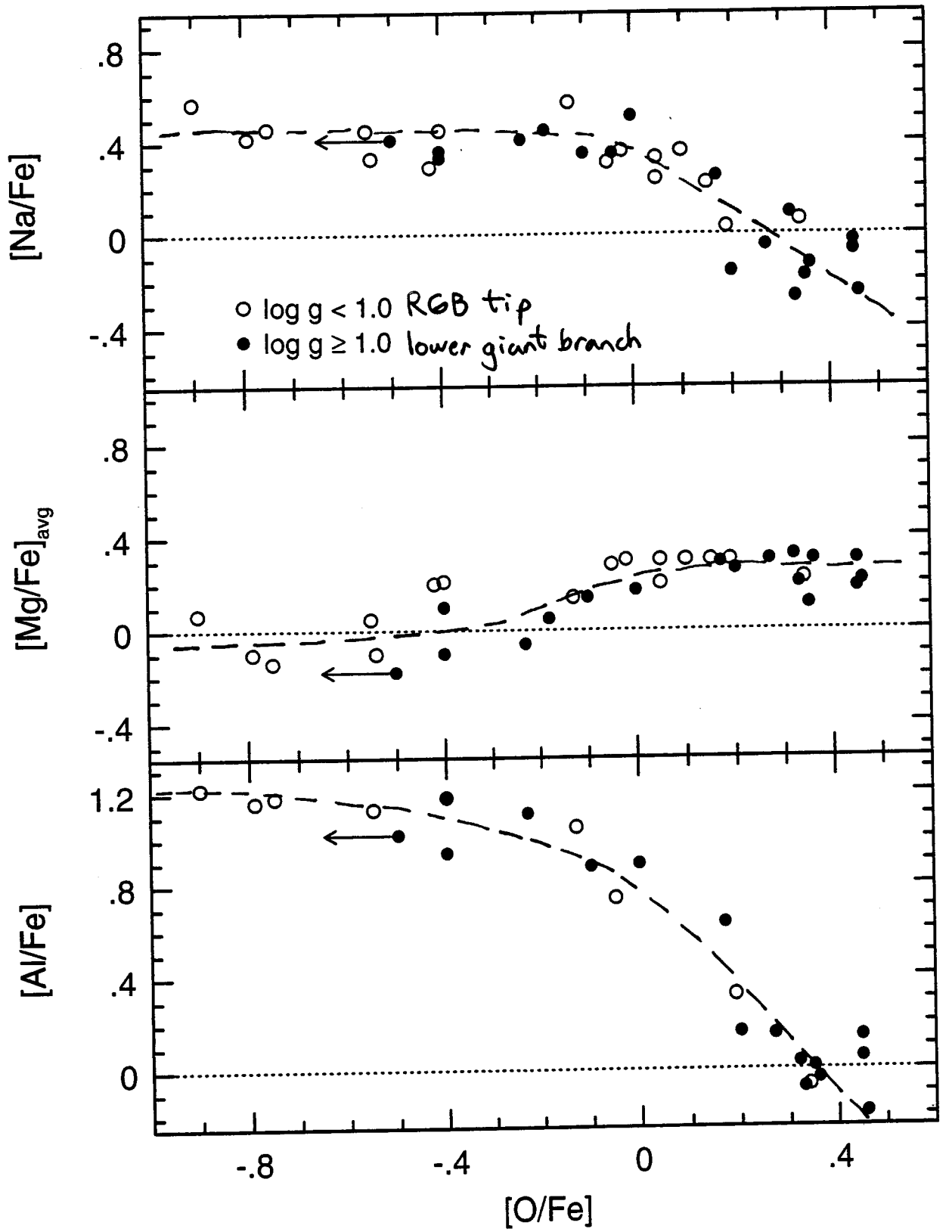

M13: a simple spectrum comparison

These stars have same (V, B-V) or (log g, Teff)

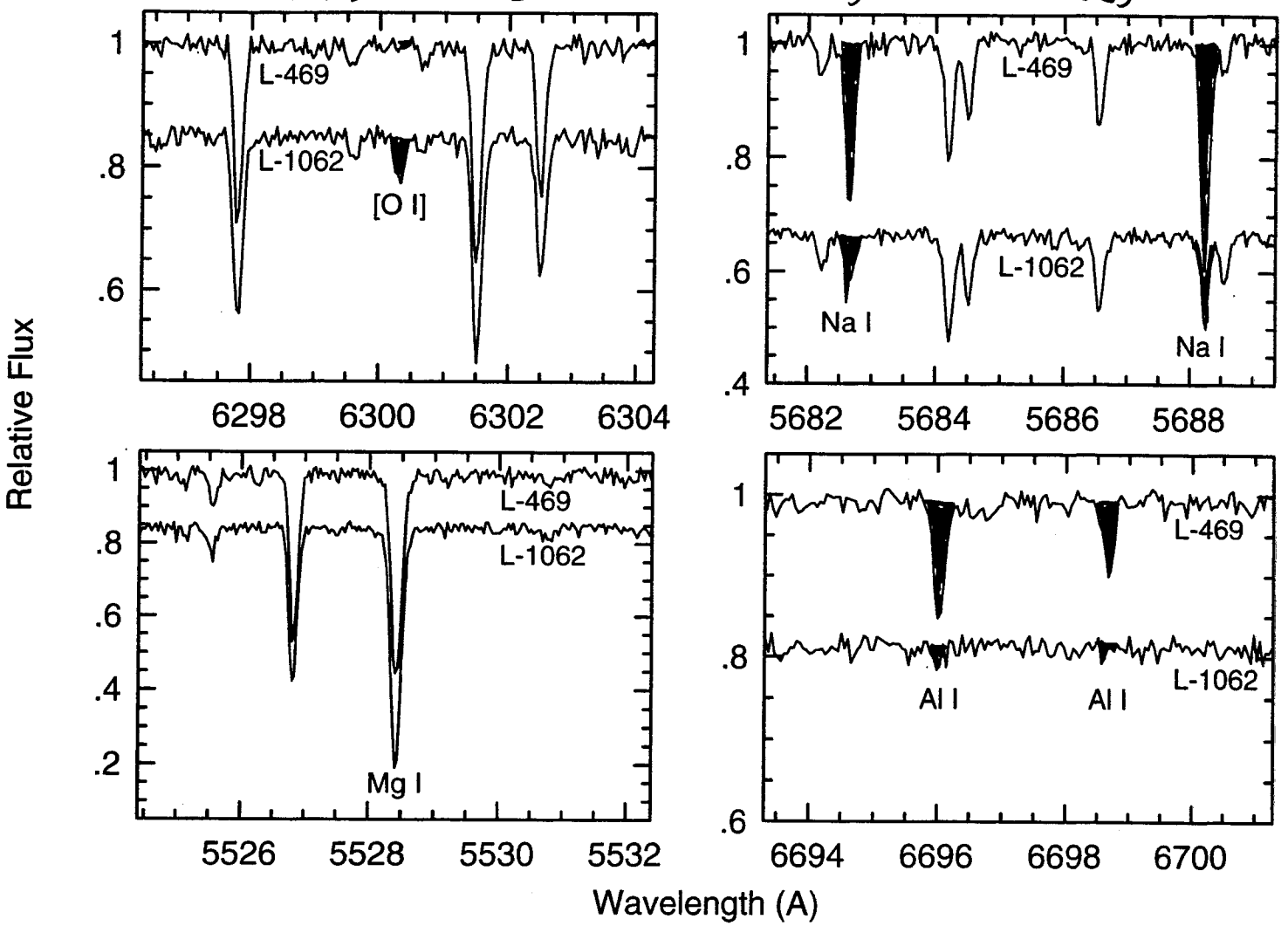

L469: O↓ Mg↓ Na↑ Al↑

L1062: O↑ Mg↑ Na↓ Al↓

Sodium & Magnesium in M13

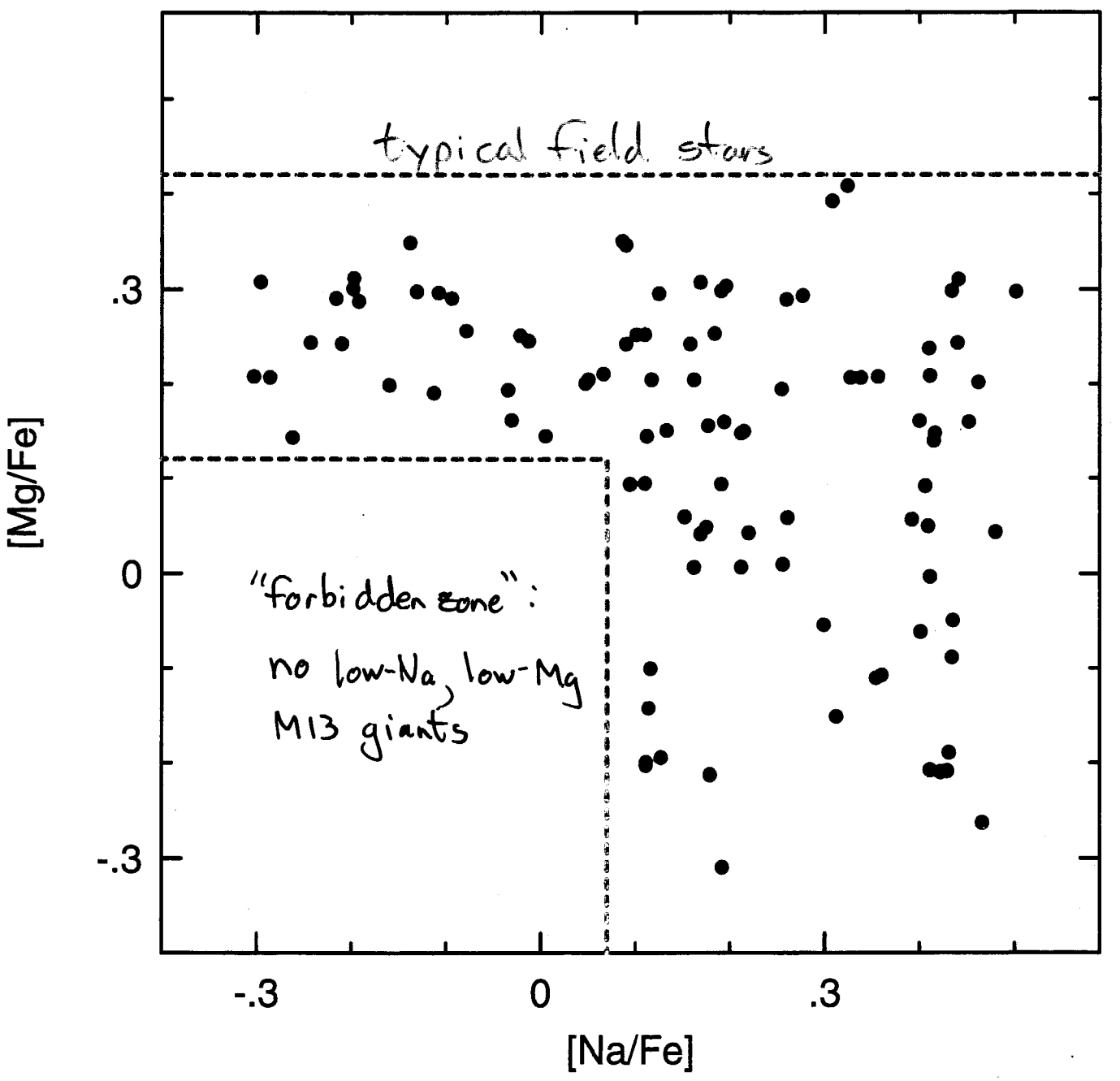

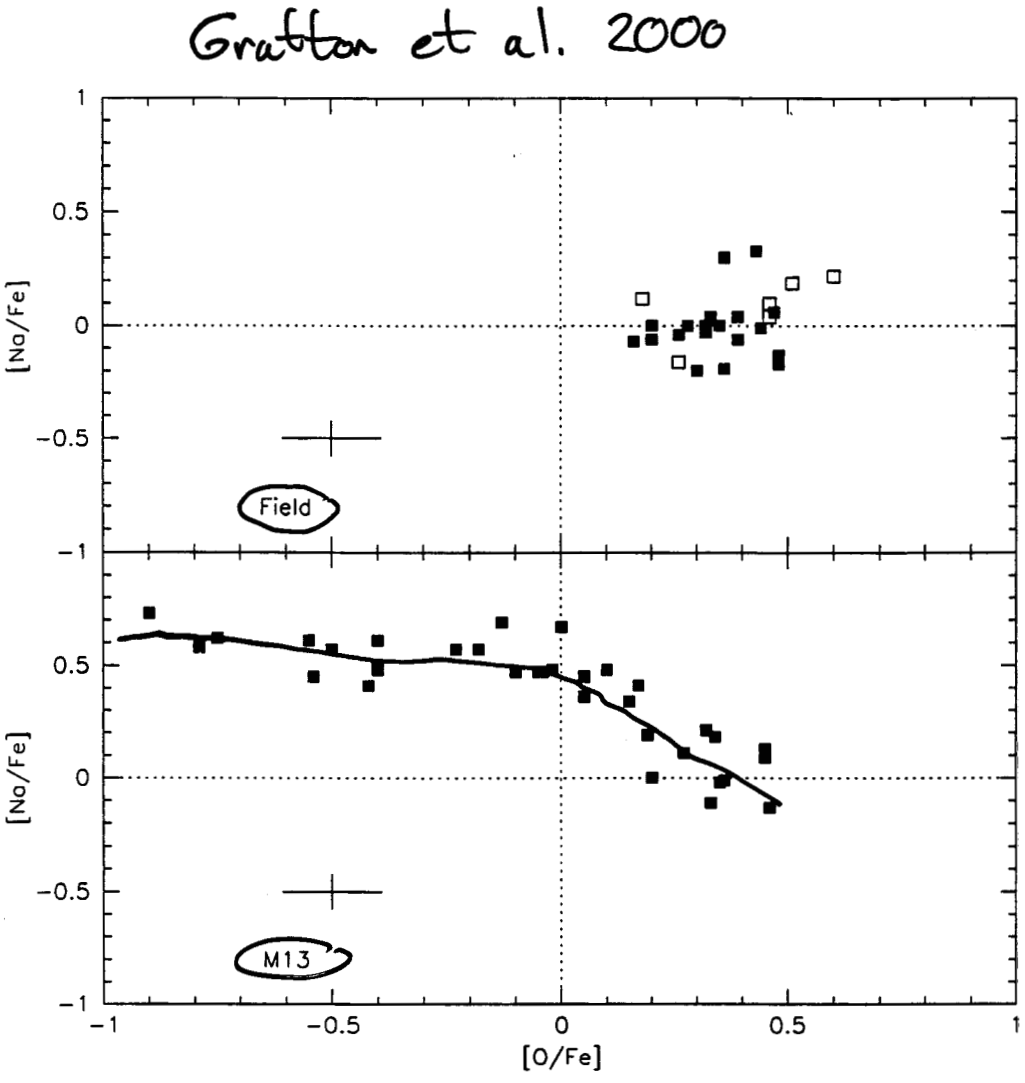

Fig. 14. The Na-O anticorrelation for field stars and for stars in M13. Filled symbols are stars first ascending the RGB (only upper-RGB stars are shown); open symbols are RHB stars. Error bars are shown at bottom left

Summary of the O-Na Anticorrelation

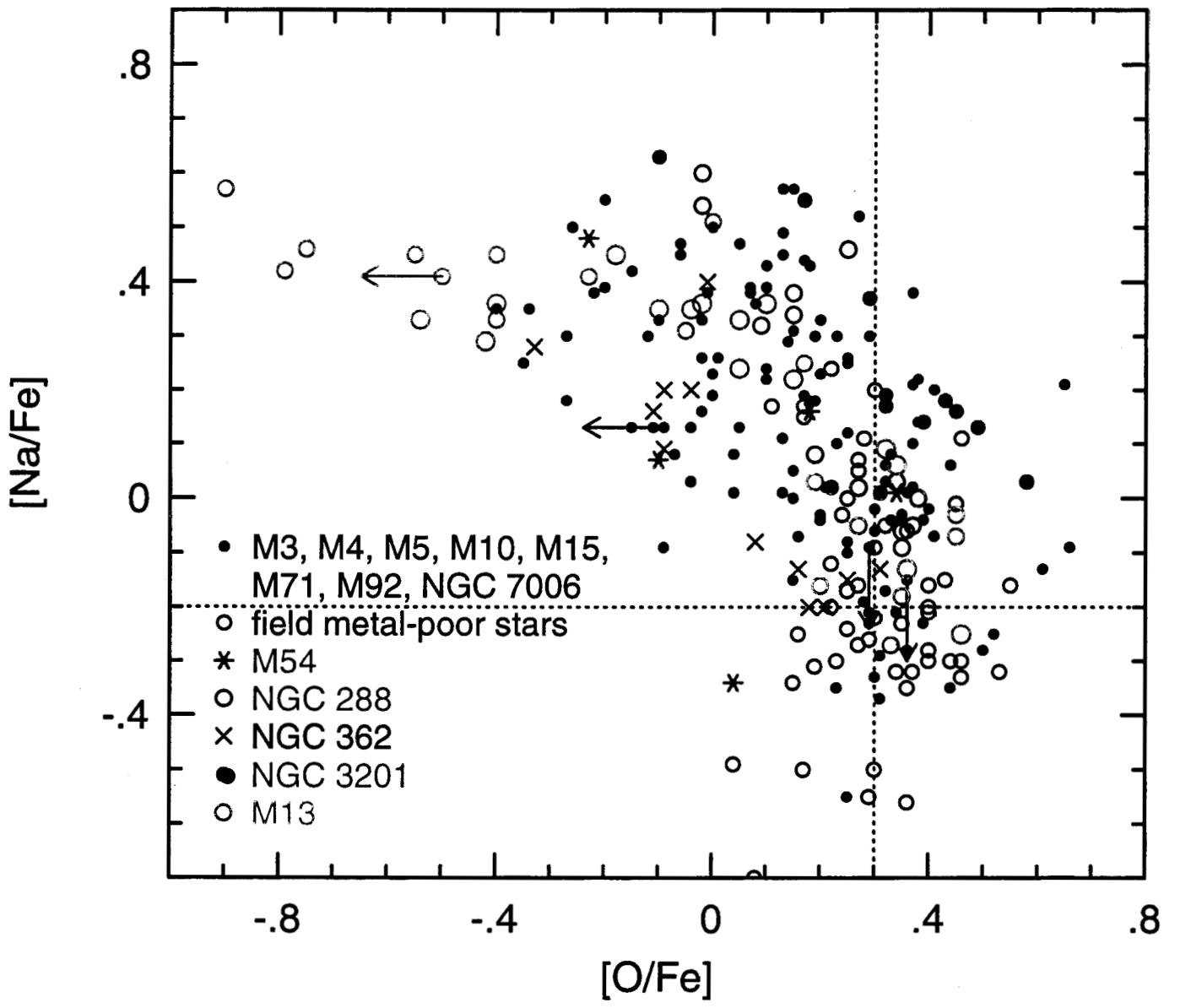

Late Stellar Evolution:
A Spectroscopists View

⇒ Schematic evolutionary paths

⇒ Qualitative agreement with cluster c-m diagram
(still small problems with
$(L, T_{eff}) \rightarrow (M_V, B-V)$
or equivalent photometric
system)

Why do I care about this workshop??

most simply: T_{eff}

Here is a simple example: what is the real oxygen abundance of metal-poor ★'s?

a) depends on whether one observes:

[O I], O I, OH_{UV}, OH_{IR}

[O I]: ↑ zero-volt forbidden lines

O I: ↑ very high-excitation lines

b) it matters!

1: early galactic nucleosynthesis

2: globular cluster ages
(O is a critical opacity source)

Is C+N+O Conserved in Cluster Giants?

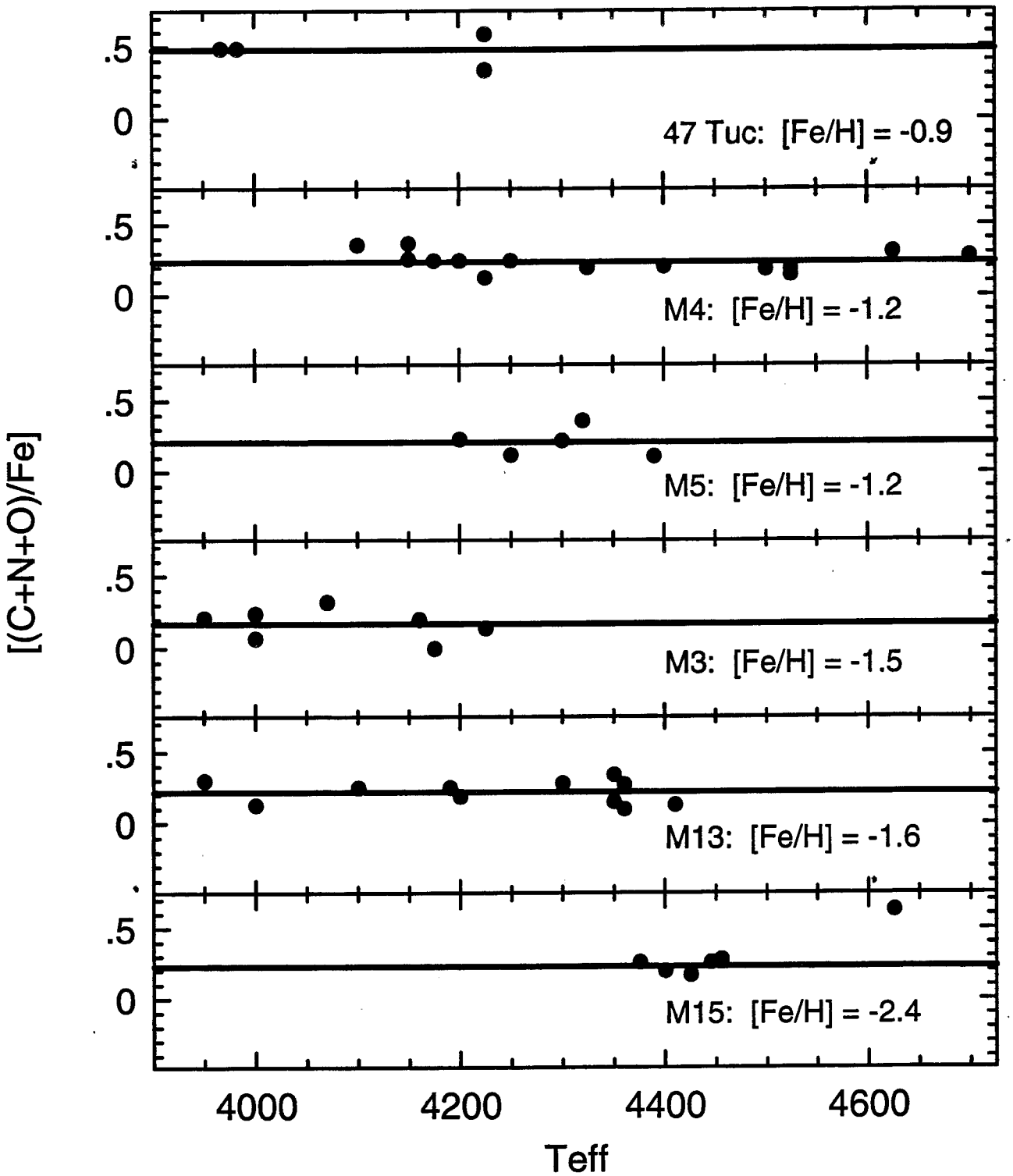

Advanced Proton-Capture Chains

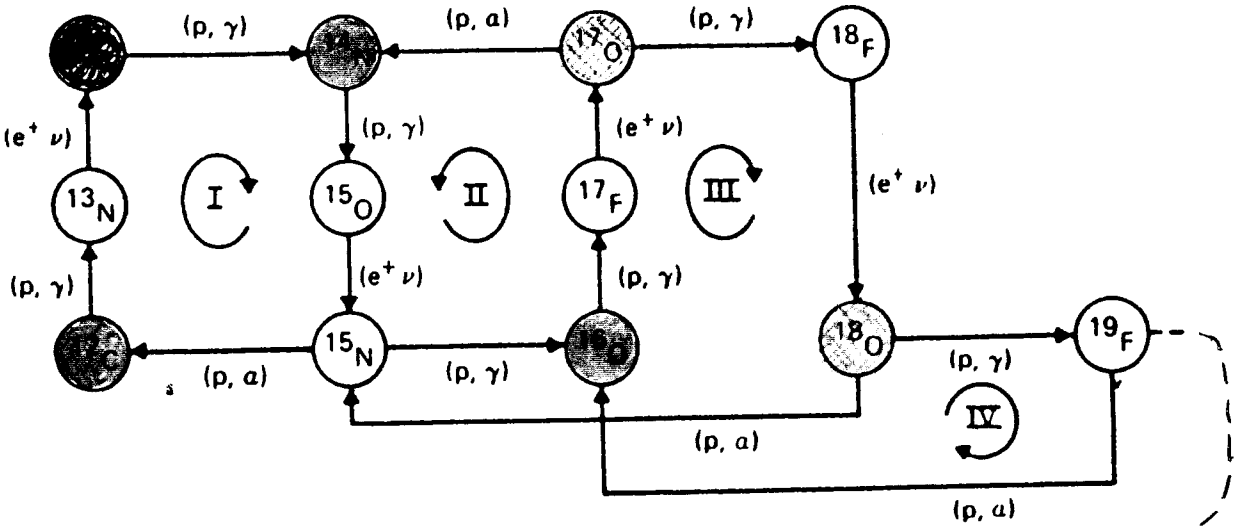

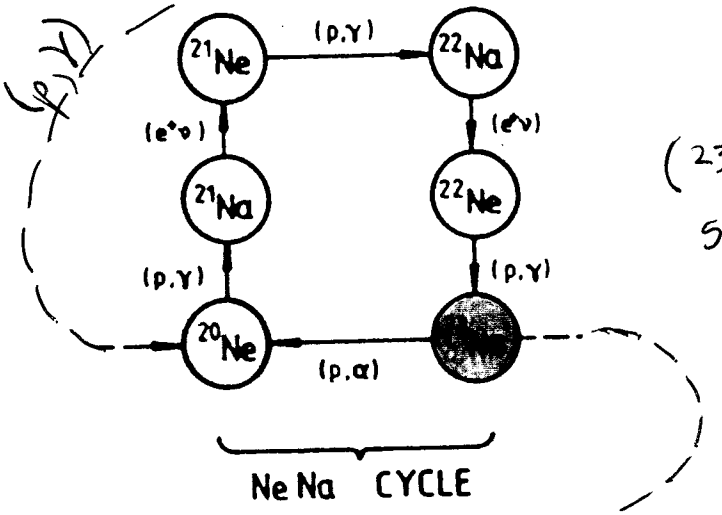

(23Na is the only observable species of this cycle)

NeNa CYCLE

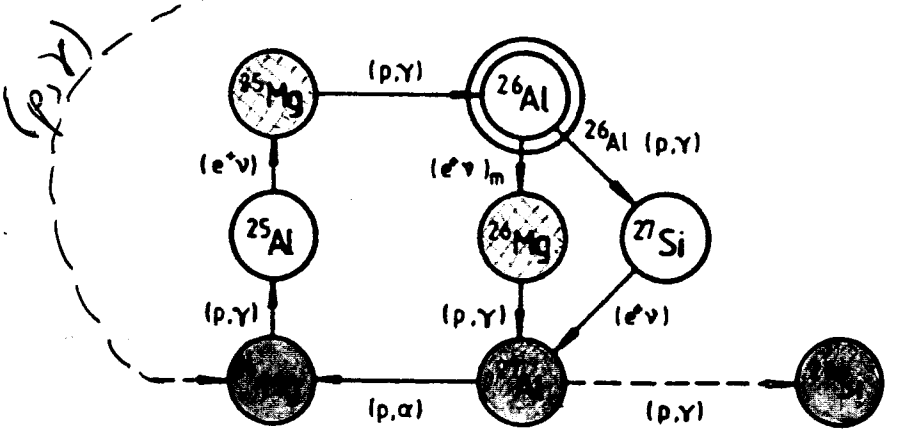

MgAl CYCLE

LEAKAGE OF CATALYTIC MATERIAL

Rolfs + Rodney text

Rolfs + Rodney text

THE CNO BI-CYCLE

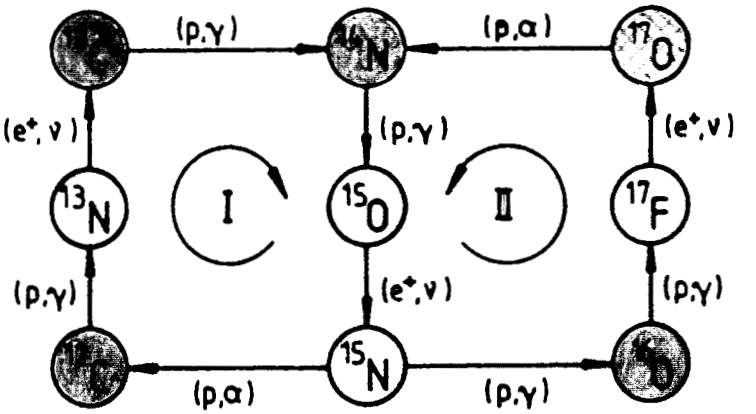

● = observable in most cool stars

◐ = "sometimes" observable in bright cool stars

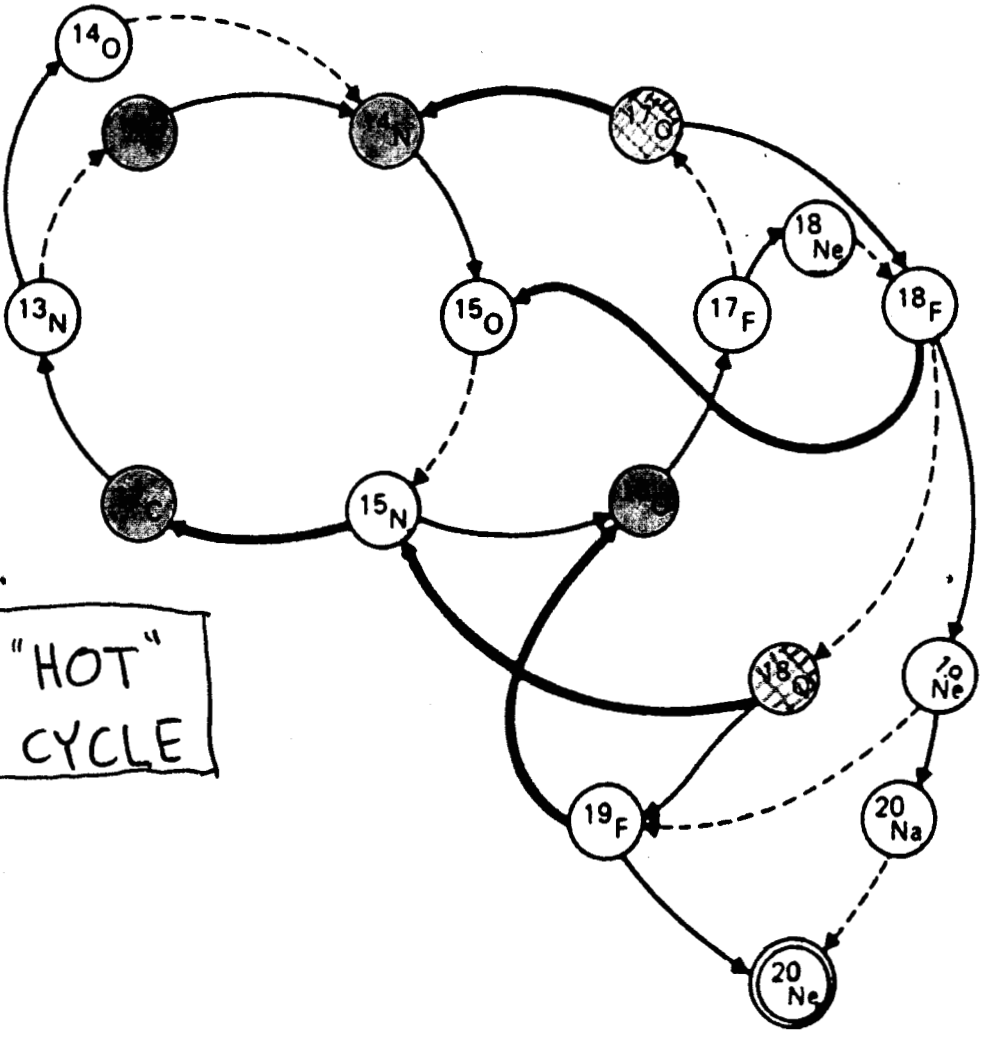

THE "HOT" CNO CYCLE

"NeNa-CYCLE"

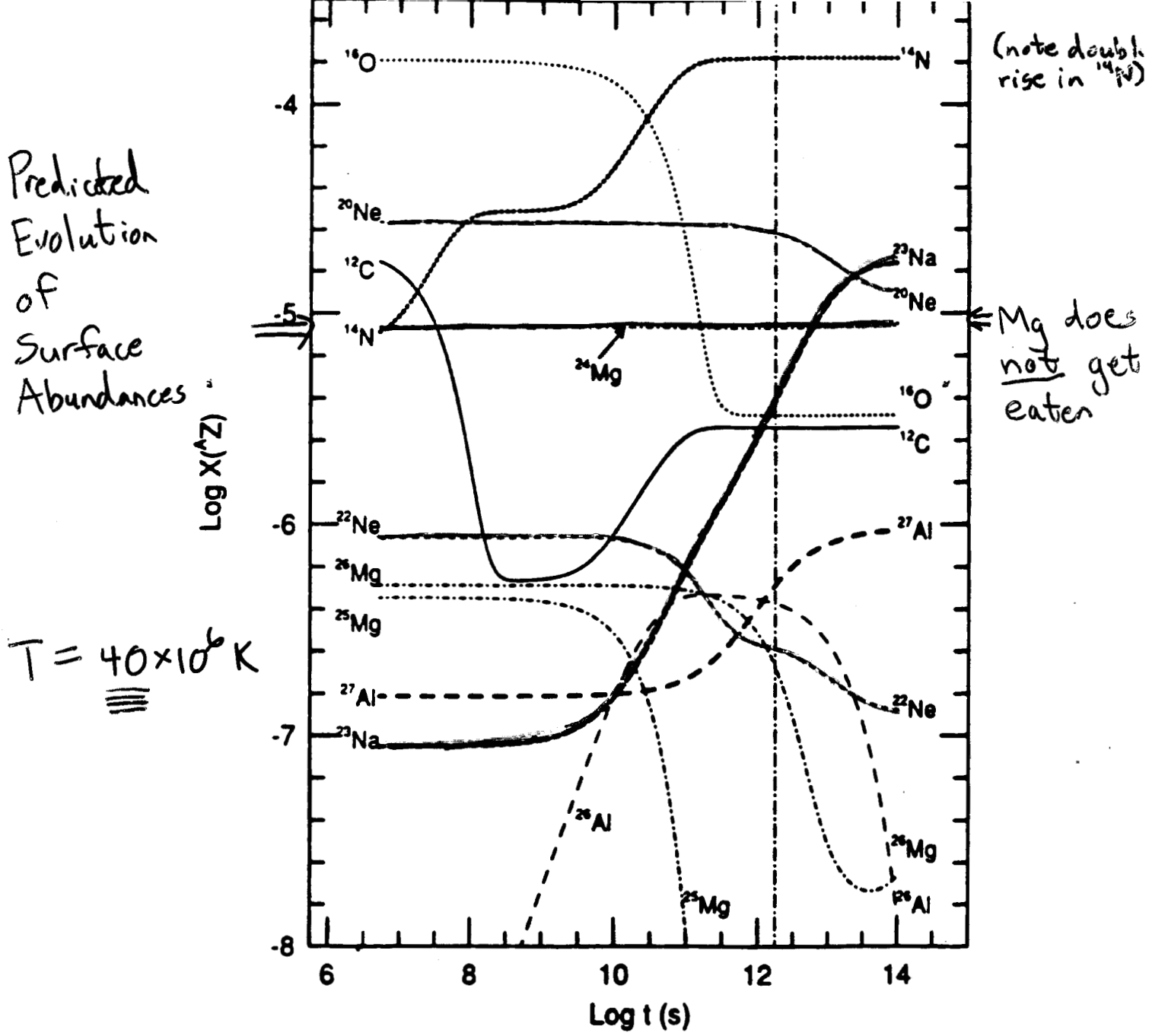

FIG. 9—(After Langer et al. 1993, copyright Astronomical Society of the Pacific. Reproduced with permission.) Mass fractions for ten isotopes in material that has been mixed to a temperature $T_9 = 0.40$ and density of 44.7 g cm^{-3}; the abscissa is the log of time since the mixing occurred. The mass fractions are 1/150 times their solar values for most isotopes. The four alpha isotopes, ^{16}O, ^{20}Ne, ^{24}Mg, and ^{28}Si, are assumed to be enhanced by a factor of 2.5 initially. The abundances of ^{23}Na and ^{27}Al are assumed to be 2.5 times less than their scaled solar values. At log $t = 12.25$ (60,000 yr), the abundance of hydrogen has dropped by 5% in the mixed material. Note that the outcome for ^{23}Na, after log $t = 12.25$, would be the same as shown here even if the initial abundance of ^{22}Ne had been set to zero. Note also the partial recovery of ^{12}C as time advances.

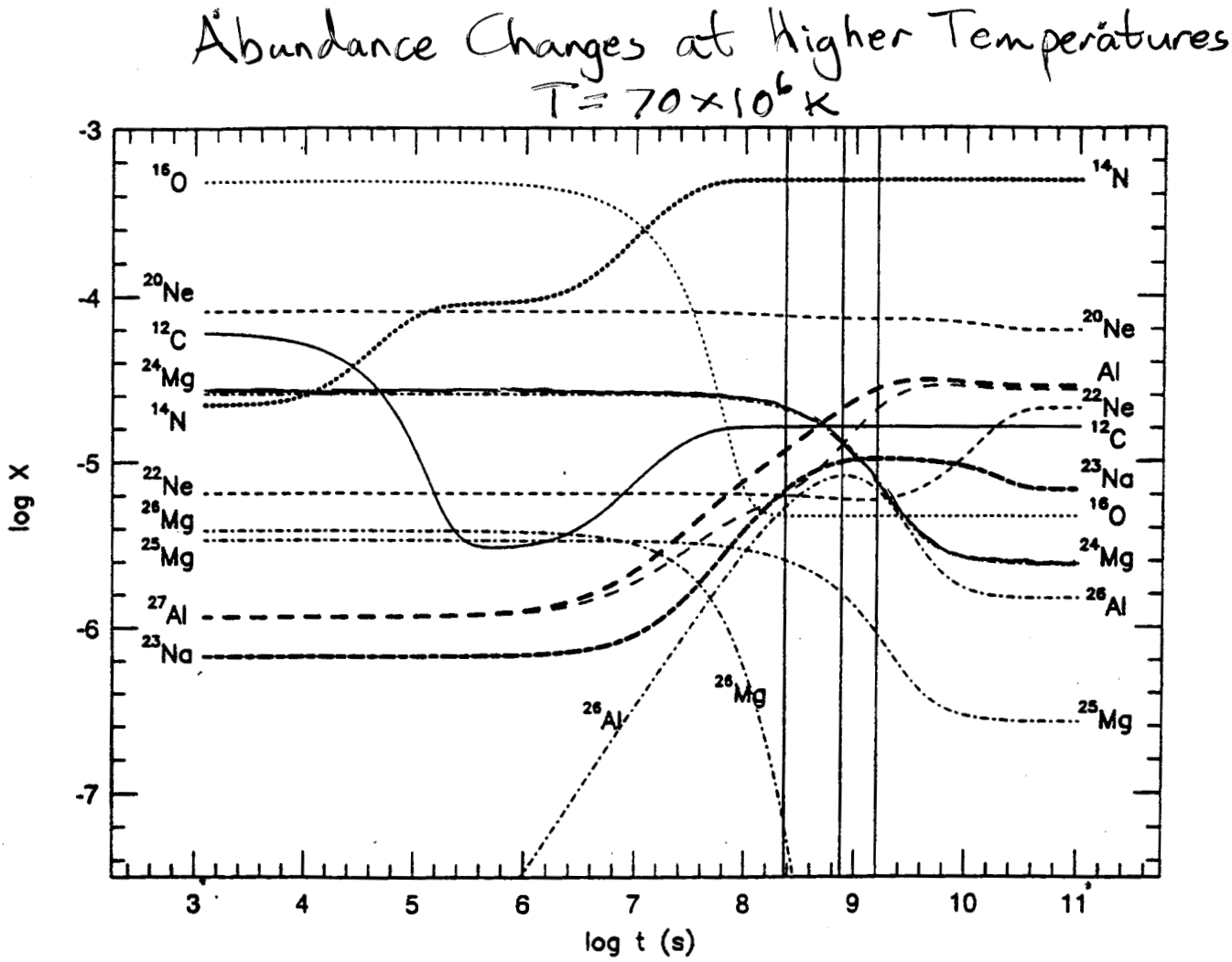

FIG. 2—Changes in the isotopic abundances in material with a density of 44.7 gms/cc raised to a temperature of 7×10^7 K. Log t(s) is the log of the time (in seconds) that the material has spent at 70 MK. The initial abundances are reduced from their solar values to values appropriate to moderately metal-poor globular cluster stars ($Z=0.0004$) with the following exceptions: the abundances of the alpha elements oxygen, neon, magnesium, and silicon are 0.4 dex above their scaled solar values. The solid vertical lines mark hydrogen depletions of 3, 10, and 20 percent.

Hα Emission in Field Metal-Poor Giants

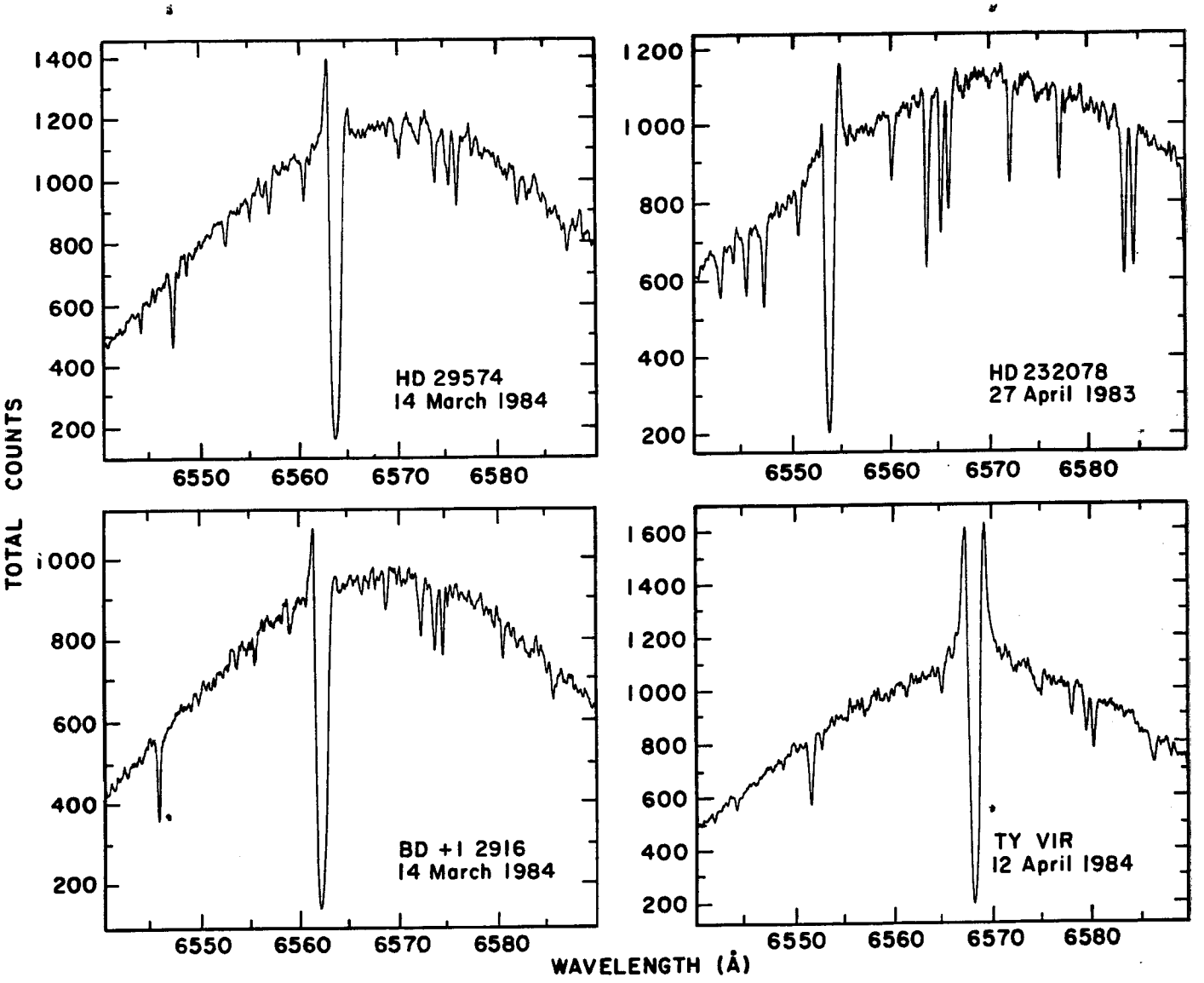

A. Dupree + G. H. Smith

Ca II Emission in Field Metal-Poor Giants

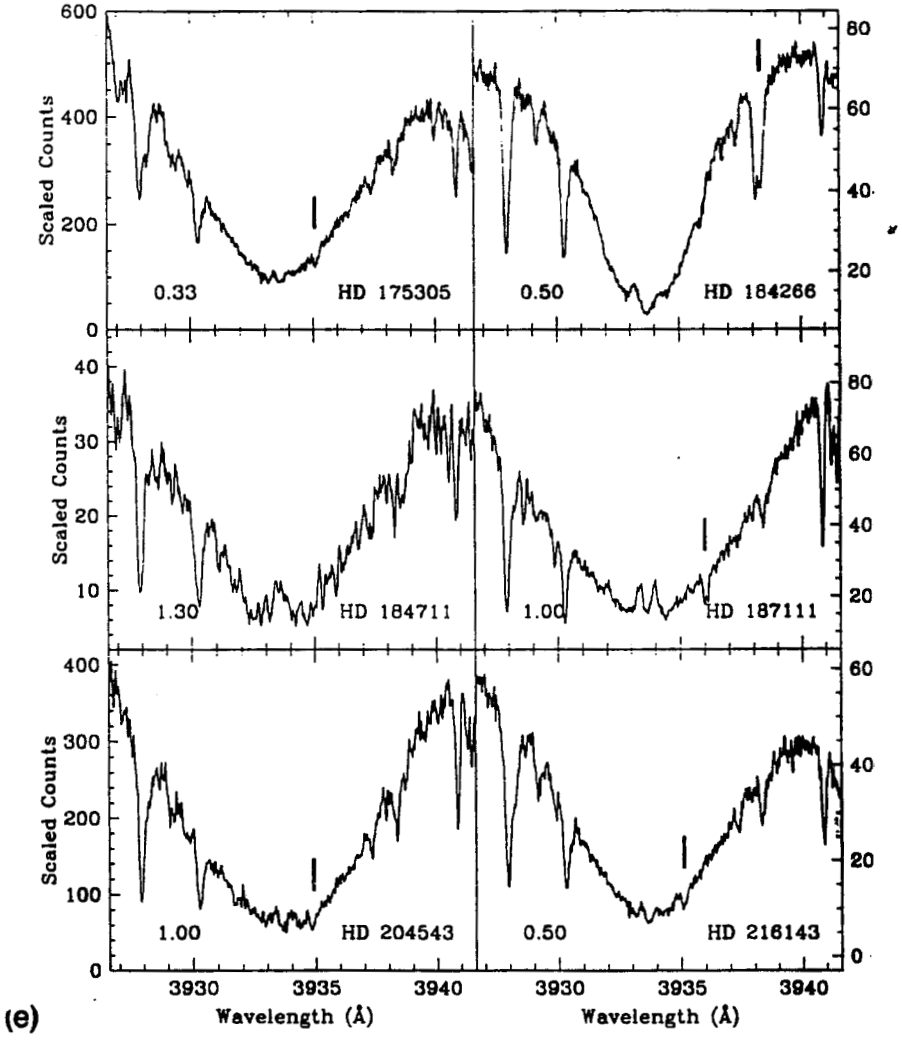

(e)

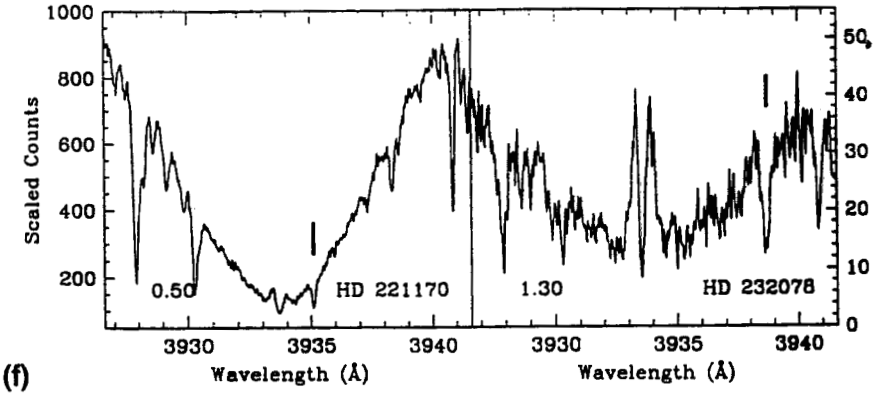

(f)

A. Dupree + G. H. Smith

Trends in Hα Emission

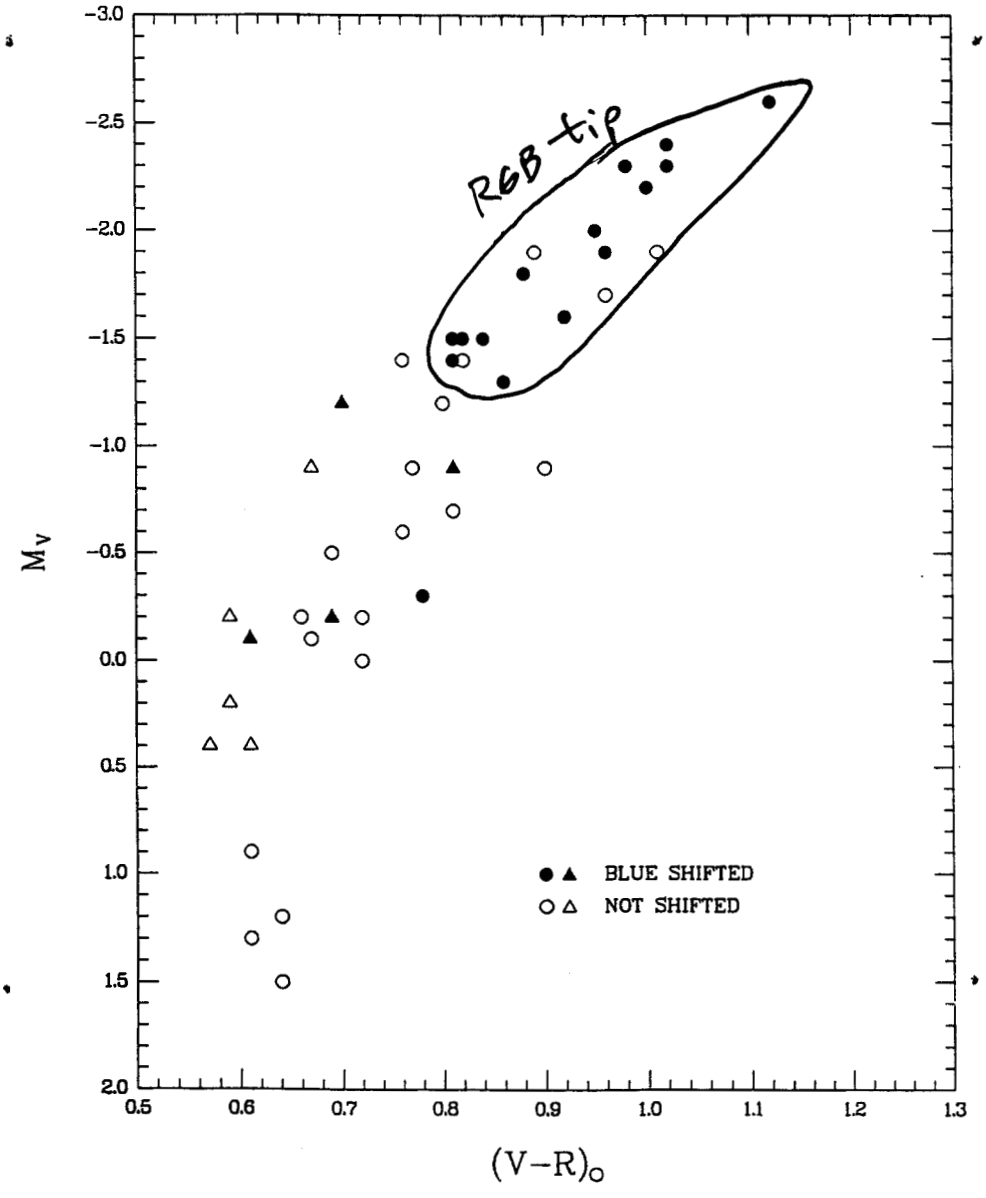

Cluster Color-Magnitude Diagrams

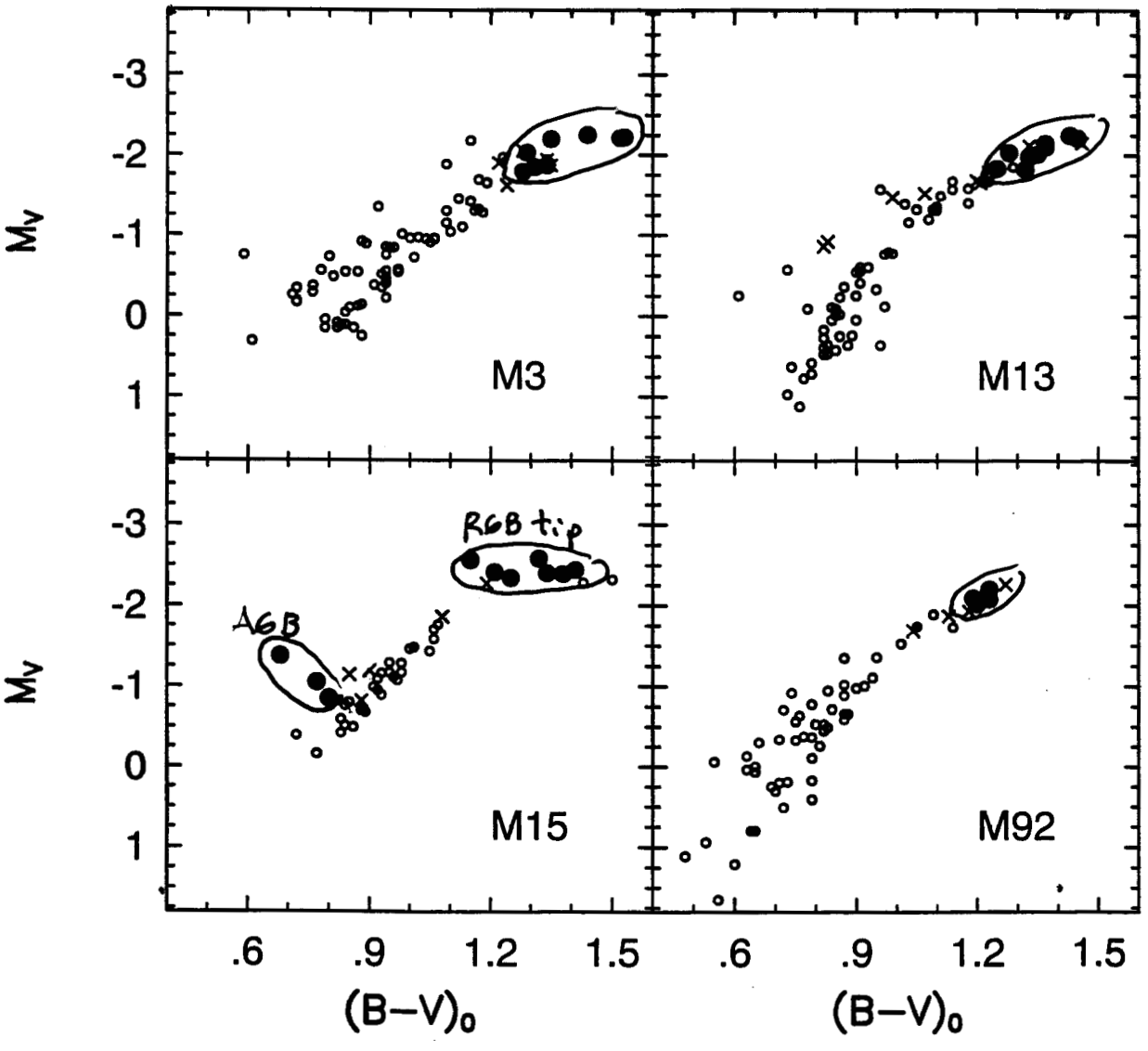

filled circles = stars with obvious Hα Emission
crosses = stars with incipient Hα Emission
open circles = stars with no Hα Emission

Pilachowski + Sneden
(in prep)

AGB and death of low mass ★

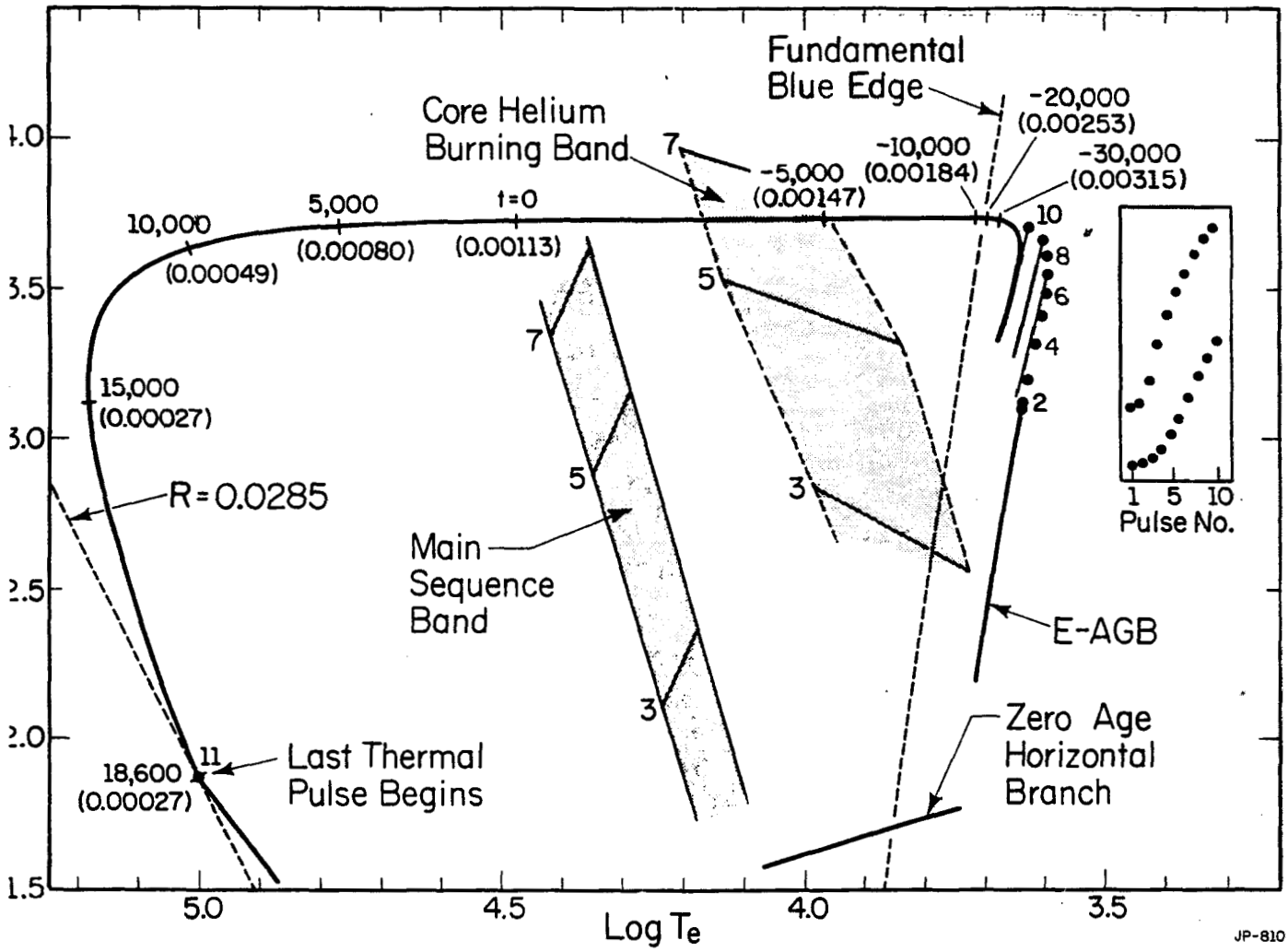

Figure 5 Evolutionary track in the H-R diagram of an AGB model of mass $0.6M_{\odot}$, initial composition $(Y, Z) = (0.25, 0.001)$. After burning helium in its core on the horizontal branch, the model arrives on the E-AGB to burn helium in a shell; the hydrogen-burning shell is extinguished. The E-AGB phase is terminated when hydrogen reignites and thermal pulsing begins. The location of the model at the start of each pulse is indicated by heavy dots. Excursions in the H-R diagram during the extended postflash dip and recovery period are shown for pulses 7, 9, and 10. Dots in the panel in the extreme right-hand portion of the diagram describe the excursion in luminosity during extended dips for all pulses that occur on the AGB. Evolution time ($t = 0$ when $T_e = 30{,}000$ K) and mass in the hydrogen-rich envelope (in parentheses) are shown at various points along the track leaving the AGB after the tenth pulse. Time is in yr, and M_e and R are in solar units. A line of constant radius passes through the location of the beginning of the eleventh pulse when the model has become a hot white dwarf. The dashed line is a blue edge for pulsation in the fundamental mode for a model of mass $0.6M_{\odot}$ and $(Y, Z) = (0.25, 0.001)$. Shown for orientation purposes are rough evolutionary tracks during core hydrogen- and core helium-burning phases for $(Y, Z) = (0.28, 0.001)$ and masses 3, 5, and $7M_{\odot}$.

Iben + Renzini 1983

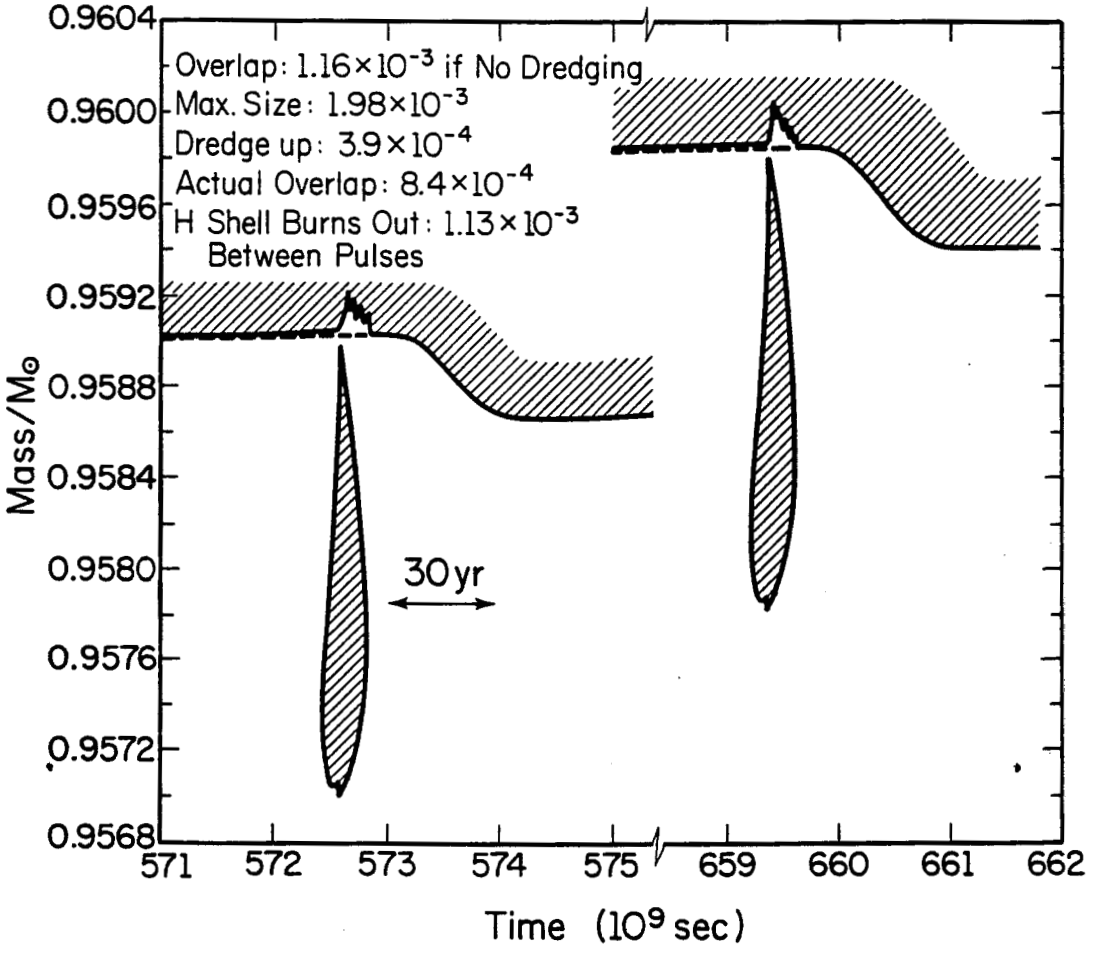

Figure 3 Convective regions during the fifteenth and sixteenth pulses in a model of mass $7M_{\odot}$ and initial composition $(Y, Z) = (0.28, 0.02)$. Shading indicates where convection occurs, and the dashed lines indicate the location of the hydrogen-helium interface before dredging up begins.

Iben + Renzini 1983

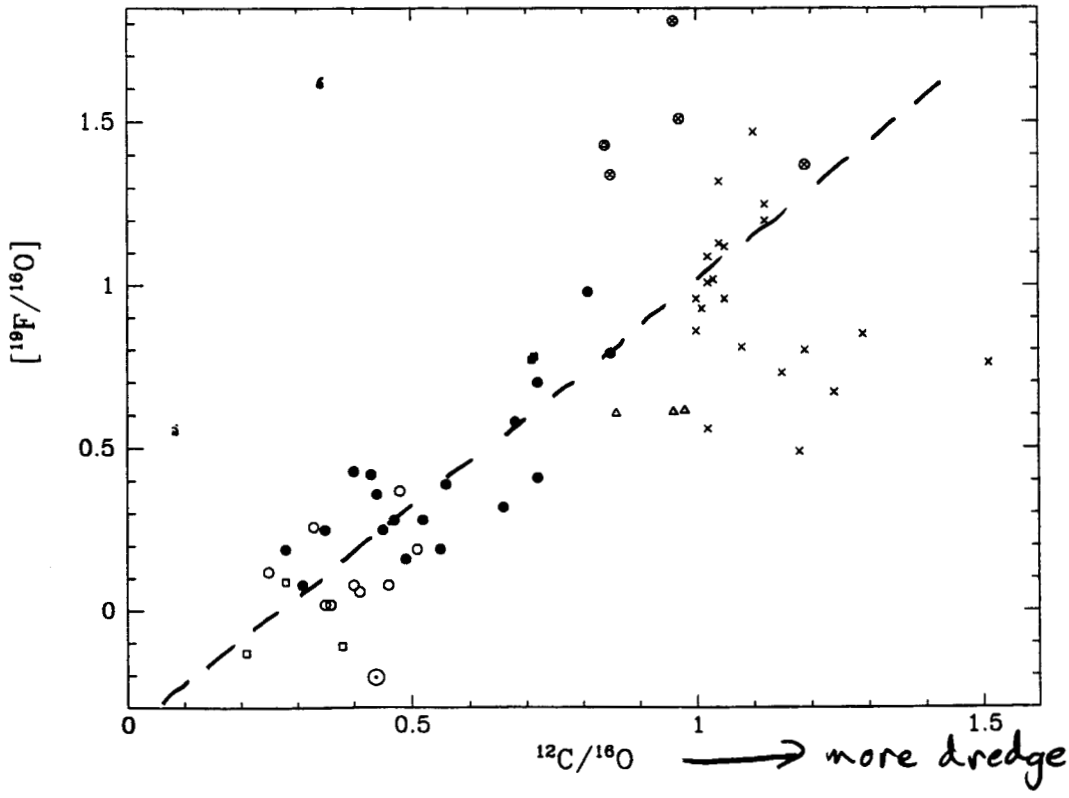

Jorissen et al. 1992

Fig. 6. The same as Fig. 5, with the abundances normalized by the ^{16}O abundance. Note that $[^{19}F/^{16}O] = (\log \varepsilon(^{19}F) - 4.69) - (\log \varepsilon(^{16}O) - \log \varepsilon_{\odot}(^{16}O))$ was not normalized by the solar system fluorine abundance ($\log \varepsilon_{\odot}(F) = 4.48$), but by the mean F abundance, $\log \varepsilon(F) = 4.69$, in K and M stars with $[Fe/H] \geq -0.20$

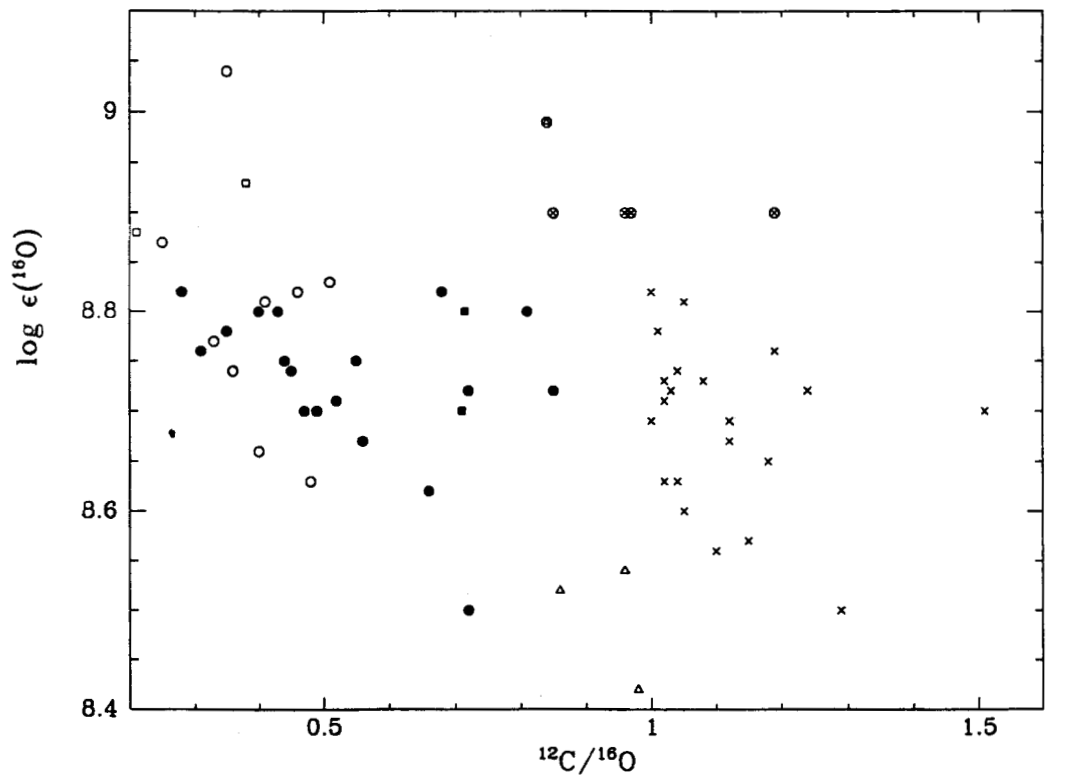

Fig. 7. Oxygen abundances in the various samples of red giants (see Fig. 3 for an explanation of the symbols) as a function of $^{12}C/^{16}O$. Since no large trend is apparent in the diagram, the normalization by ^{16}O cannot be responsible for the correlation ($[^{19}F/^{16}O]$, $^{12}C/^{16}O$) observed in Fig. 6

Lattanzio et al. 1997

⇒ with more and more pulses, more ^{12}C and ^{19}F will be produced

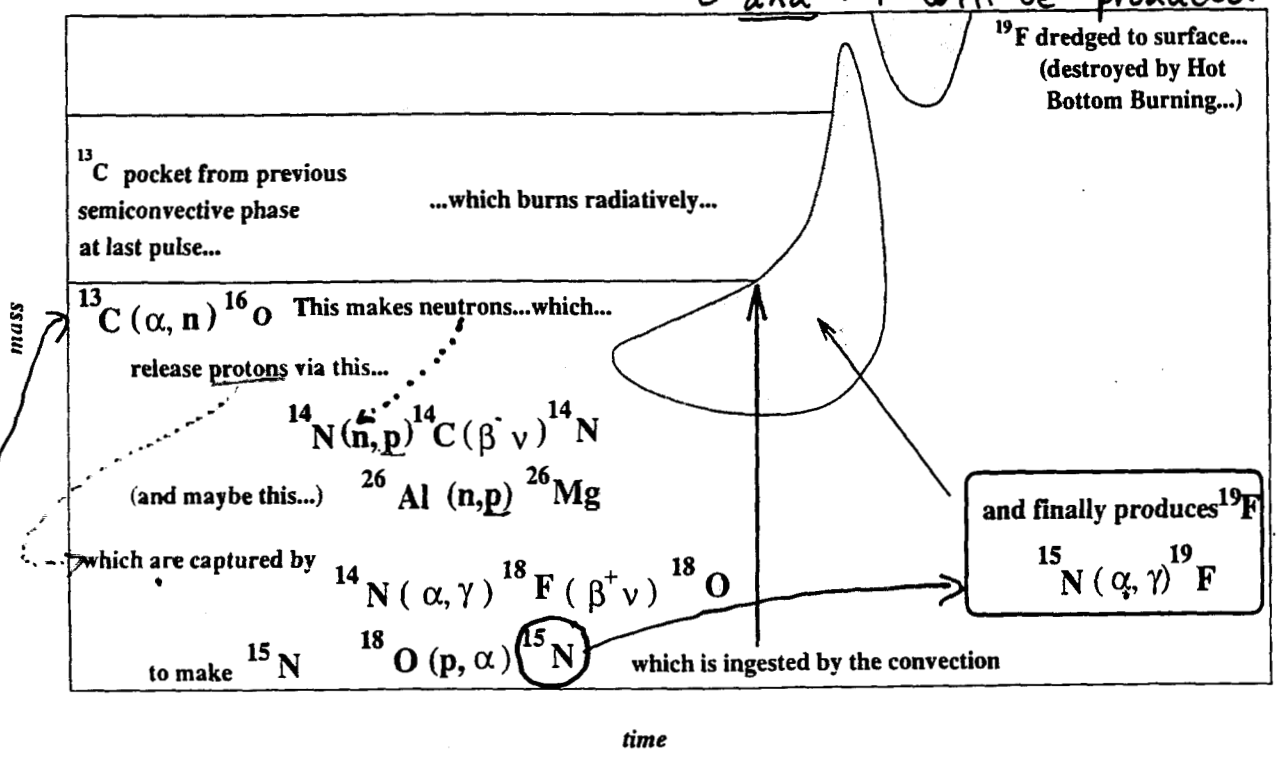

FIGURE 3. A schematic showing how ^{19}F is believed to be produced in AGB star interiors.

need to mix protons down to zones where $^{12}C + p \rightarrow {}^{13}N \rightarrow {}^{13}C$